CHALMERS
UNIVERSITY OF TECHNOLOGY

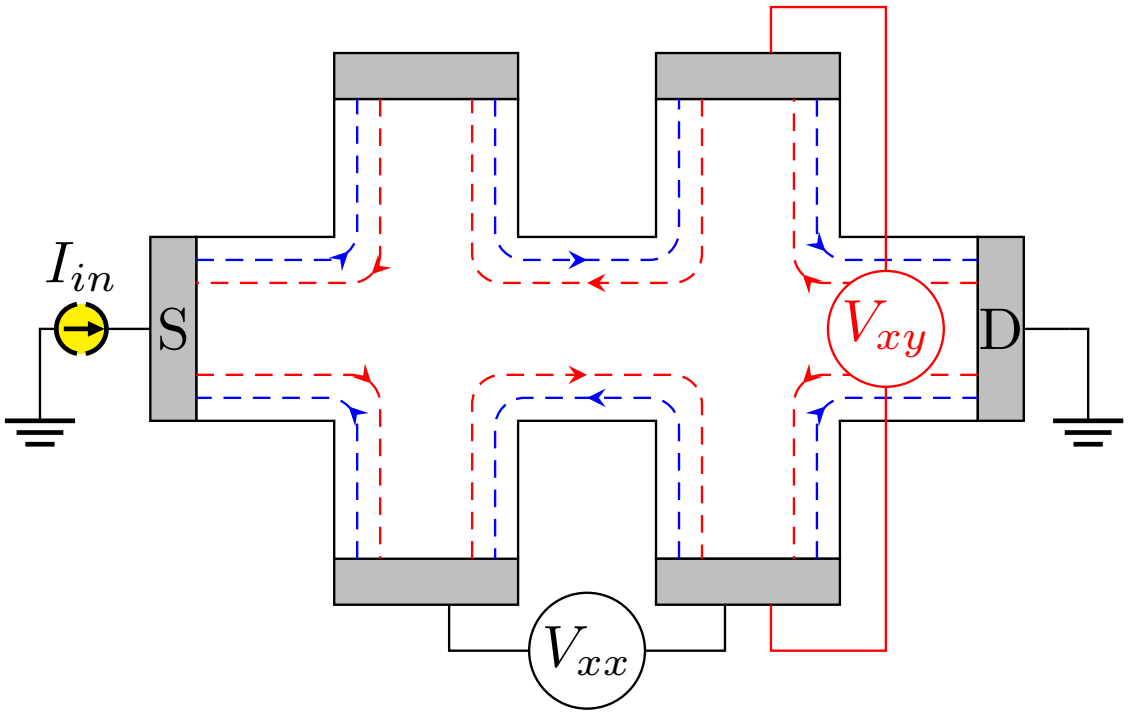

Impact of Equilibration on the Heat Conductance and Noise of non-Abelian fractional Quantum Hall Edges

Master thesis in Nanotechnology

Michael Hein

Applied Quantum Physics Laboratory
CHALMERS UNIVERSITY OF TECHNOLOGY
Gothenburg, Sweden 2022
www.chalmers.se

Master thesis 2022

Impact of Equilibration on the Heat Conductance and Noise of non-Abelian fractional Quantum Hall Edges

Michael Hein

CHALMERS
UNIVERSITY OF TECHNOLOGY

MC2 - Department of Microtechnology and Nanoscience
Applied Quantum Physics Laboratory
Chalmers University of Technology
Gothenburg, Sweden 2022

Impact of Equilibration on the Heat Conductance and Noise of non-Abelian fractional Quantum Hall Edges
Michael Hein

Supervisor: Christian Spånslätt, Applied Quantum Physics Laboratory
Examiner: Janine Splettstößer , Applied Quantum Physics Laboratory

Master Thesis 2022
Department of Microtechnology and Nanoscience
Applied Quantum Physics Laboratory
Chalmers University of Technology
SE-412 96 Gothenburg
Telephone +46 31 772 1000

Cover: Visualization of the *Hall-Bar* setup commonly used to observe the quantum Hall effect. It portrays the transport in counter propagating channels (blue and red) at the edge of quantum Hall systems.

Typeset in LaTeX
Printed by Chalmers Reproservice
Gothenburg, Sweden 2022

Impact of Equilibration on the Heat Conductance and Noise of non-Abelian fractional Quantum Hall Edges
Michael Hein
Department of Microtechnology and Nanoscience
Chalmers University of Technology

Abstract

Performing resistance measurements in a cold 2D electron gas allows to observe the quantum Hall effect. It comes along with a quantized transverse and simultaneously vanishing longitudinal resistance as well as transport along the edge in chiral channels. Some of the discovered fractional quantum Hall states are predicted to host non-Abelian quasi particles that obey exotic exchange statistics with potential use for quantum computation. An essential step towards the manipulation of these particles is to uncover the edge structure of the underlying state and thus verifying the usability of their non-Abelian properties. Recently, a novel method to distinguish between potential candidates for the fractional quantum Hall edge at filling 5/2 has been established using a combination of heat transport and noise arguments.

In this thesis, the role of equilibration between counter-propagating edge modes on the heat conductance and the generation of noise at the 5/2 edge is investigated theoretically. This includes an analysis of potential structures describing the 5/2 edge within a common transport scheme and a comparison to experimental results. It is furthermore shown that the heat conductance of the most promising candidate is expected to be quantized to different values of the quantum of heat $\kappa_0 = \pi^2 k_B^2/(3h)$ depending on the degree of thermal equilibration between the involved modes. Performing experiments with controlled thermal equilibration are therefore predicted to uncover even more details of the underlying structure.

Keywords: Topological Quantum Matter, Condensed Matter Physics, Fractional Quantum Hall

Acknowledgements

First of all I'd like to thank my supervisors Christian and Janine for giving me the opportunity to work on this topic, for encouraging and inspiring me to look even further into the field of theoretical physics, for their great guidance throughout the entire time of working on this project and also for their support when I applied for PhD positions. It was an amazing experience for me - Thank you! Furthermore I'd like to thank all of the other AQP members as well as my colleagues from MPNAT for supporting me and also giving me the opportunity to learn about their research. Finally I'd also like to thank my friends and family for bearing with me and having an open ear whenever I had to get something off my chest.

Thanks also to Deutsche Bahn for always taking me to Gothenburg (atleast eventually) - this thesis project would have neither started nor ended without you.

Michael Hein, Gothenburg, June 2022

List of Acronyms

Ch.	chapter
Fig.	figure
Sec.	section
Tab.	table
Eq.	equation
EOM	equation of motion
QHE	quantum Hall effect
IQH	integer quantum Hall
FQH	fractional quantum Hall
QSH	quantum Spin Hall
2DEG	two dimensional electron gas
LL	Landau level
LLL	lowest Landau level
GS	ground state
BZ	Brillouin zone
LBF	Landauer - Büttiker formalism
CFT	conformal field theory
OPE	operator product expansion
phPf	particle-hole Pfaffian
aPf	anti-Pfaffian
Pf	Pfaffian

Contents

1 Introduction

With Max Planck postulating the discrete nature of energy emission and absorption in 1900 [1], the foundation for a quantized description of the energy in physical systems had been set. The concept of quantum mechanics started to develop in the following decades and is still being finalized today. In combination with classical field theory and special relativity, quantum field theory was further introduced [2]. Together with theories about electromagnetism, statistical physics and principles such as symmetry breaking and topological matter it builds the base of modern condensed matter physics. The entirety of concepts that is available within this frame allows to describe very specific phenomena on some length scale without the need to fit it into a more general model. Therefore it becomes possible to examine systems beyond the standard model and to describe new exotic particles [3]. One effect that is thought to have such peculiar properties is the fractional quantum Hall effect which is in the focus of this thesis. To understand the rich physics underlying this effect, its conceptual description is built up starting from the classical Hall effect followed by a comparison to the integer quantum Hall effect and an extension to the fractional quantum Hall effect.

1.1 Classical Hall Effect

The classical Hall effect can be understood from the transport characteristics of free charge carriers subject to an applied electric $\vec{E} = (E_x, 0, 0)^T$ and magnetic field $\vec{B} = (0, 0, B)^T$ in a solid sample. In such a setup the Lorentz force deflects charge carriers from their path along the $\hat{x}$-direction. According to the charge and the direction of the magnetic field, they will accumulate at the edges of the sample, building up an electrical field E_y perpendicular to the applied E_x as depicted in figure (Fig.) 1.1a.

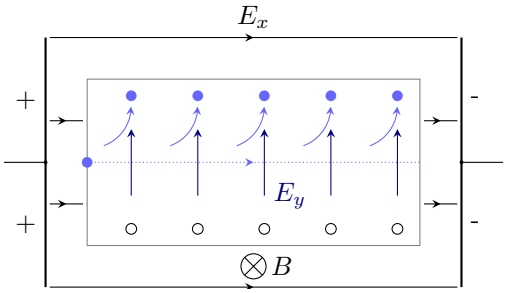

(a) Setup of a sample with free electrons subject to an electrical field in $\hat{x}$ and a magnetic field in $\hat{z}$ direction. The dotted blue line denotes the undeflected path.

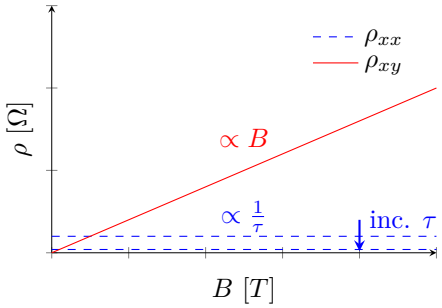

(b) Plot of ρ_{xx} and ρ_{xy} in dependence of the magnetic field strength B. As the scattering time τ increases, ρ_{xy} remains unchanged, whereas ρ_{xx} decreases.

At a certain magnitude of the perpendicular electric field E_y, the effect of the $\vec{B}$-field is compensated for, leading to no further deflection in $\hat{y}$-direction and all charges being transported in the $\hat{x}$-direction. An explanation to this effect is given by the *Drude-model* taking collisions between free electrons and impurities in the underlying lattice into account [4]. In linear response to the electric field, the current density $\vec{j}$ in the (x, y)-plane is described by the matrix equation

$$\vec{j} = \frac{mnq^2}{m^2 + q^2B^2\tau^2} \begin{pmatrix} \tau & -qB\tau^2 \\ qB\tau^2 & \tau \end{pmatrix} \begin{pmatrix} E_x \\ E_y \end{pmatrix} \xrightarrow{\tau \to \infty} \frac{1}{B} \begin{pmatrix} 0 & -nq \\ nq & 0 \end{pmatrix} \begin{pmatrix} E_x \\ E_y \end{pmatrix}$$

with n denoting the number density of charge carriers with charge q and mass m. The current in $\hat{y}$ is therefore only caused by the $\vec{B}$ field acting on the charge carriers. This manifests in the possibility to define a transverse resistivity ρ_{xy}, called *Hall resistivity* in the 2D system which depends linearly on the magnetic field strength B

$$\rho_{xy} = \frac{E_y}{j_x} = \frac{B}{qn}$$

The longitudinal resistivity ρ_{xx} is found to be independent of B and vanishing for large scattering times $\tau \to \infty$ (compare Fig. 1.1b). The latter property was to be expected since infinite scattering times correspond to the case of no collisions and thus no resistance. As will be seen later, the quantum version of the Hall effect is quite different from this description. It is worth noting that the definitions of resistance R and resistivity ρ coincide in (2+1) D since a homogeneous geometry of unit cross-sectional area in d dimensions leads to the resistivity [5]

$$R = \rho \frac{L}{A} = \rho \frac{L}{L^{d-1}} = \rho L^{2-d} \overset{d=2}{=} \rho$$

For later convenience rotational invariance around $\hat{z}$ is assumed and the relation between conductivity and resistivity therefore takes the general form

$$\boldsymbol{\sigma} = \begin{pmatrix} \sigma_{xx} & \sigma_{xy} \\ -\sigma_{xy} & \sigma_{xx} \end{pmatrix} \qquad \text{with} \qquad \sigma_{xx} = \frac{\rho_{xx}}{\rho_{xx}^2 + \rho_{xy}^2} \qquad \sigma_{xy} = \frac{-\rho_{xy}}{\rho_{xx}^2 + \rho_{xy}^2}$$

Where the negative sign in σ_{xy} depends on the direction of the magnetic field. These relations furthermore indicate that the distinction between an insulator and a conductor is not straight forward in the presence of a $\vec{B}$-field since it is possible to simultaneously have $\sigma_{ij} = \rho_{ij} = 0$ with $i, j \in \{x, y\}$.

1.2 Integer Quantum Hall Effect in 2D

Performing the experiment from section (Sec.) 1.1 using a cold two dimensional electron system and high magnetic field strengths, the integer quantum Hall (IQH) effect and the fractional quantum Hall (FQH) effect are observed depending on the degree of disorder in the sample [6]. They result from a quantized energy spectrum of the underlying bulk system. This quantization manifests in the transverse resistivity ρ_{xy} now showing plateaus persisting over a range of magnetic field strengths with quite sharp transitions between neighbouring plateaus. Whenever ρ_{xy} is on a plateau, the longitudinal resistivity ρ_{xx} becomes negligibly small. The description of the individual states has been in the focus of research for many years and until today not all of the observed states have been explained[1].

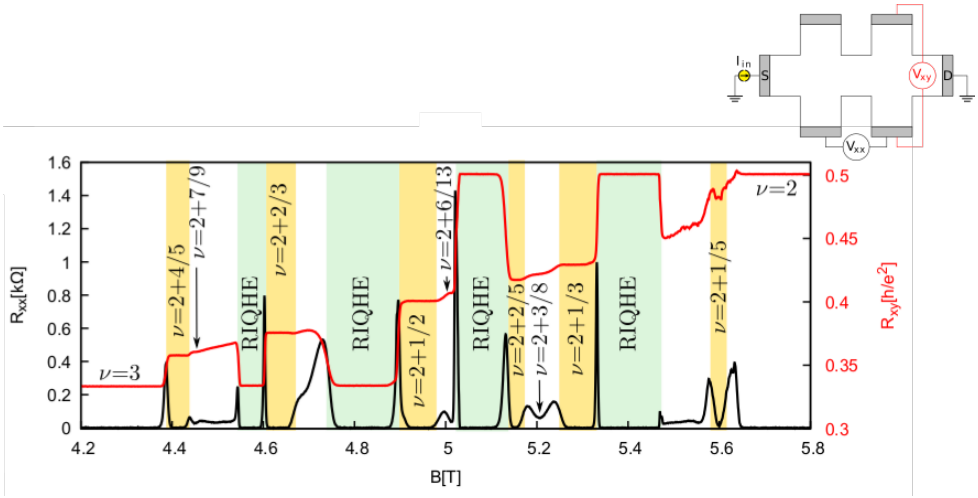

Figure 1.2: Plot of the longitudinal and transverse resistance R_{xx} and R_{xy} using the measurement setup indicated in the top right corner. Amongst many fractional states, the integer states at filling $\nu = 2$ and $\nu = 3$ are visualized. (Fig. from Ref. [8])

[1] I highly recommend to read the lecture notes of David Tong [7] for a great introduction into the effect.

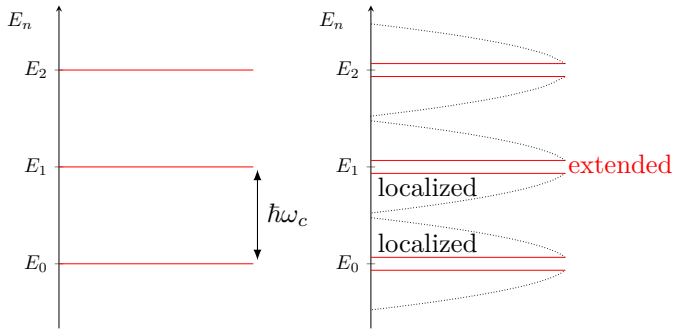

Figure 1.3: Visualisation of the energy spectrum for the gapped bulk energy states without disorder (left) and with disorder (right).

The integer states are described by the filling of bulk Landau levels (LLs). Depending on how many of these energy levels are filled, different states can be observed. To describe the number of filled LLs, the *filling factor* $\nu \in \mathbb{Z}^+$ is commonly used. According to this definition, the transverse resistivity is quantized to $1/\nu$ times the *von Klitzing* constant h/e^2 [9].

The density required to observe the ν^{th} plateau $n = \frac{B}{\Phi_0}\nu$, with $\Phi_0 = \frac{h}{e}$ the flux quantum, is defined to be the density needed to fill exactly ν LLs. In order to occupy the next higher LL, an energy gap $\hbar\omega_c$ has to be overcome which is big enough to exclude thermal occupation of higher LLs as long as $k_B T \ll \hbar\omega_c$. Applying a small electric field to the system thus leads in no electron transport and $\rho_{xx} = 0$ since there are no empty states available for the electrons to scatter into. Looking at a fixed electron density, a decrease in the magnetic field strength $B < \frac{n\Phi_0}{\nu}$ results in a partially filled LL $\nu + 1$ which now has accessible states to scatter into. Thus ρ_{xx} would be non-vanishing and ρ_{xy} non-quantized looking at a range of B values around the plateau. This ambiguity has been resolved by taking the effect of disorder into account. Weak disorder[2] broadens the δ-peaks of the discrete energy spectrum to some finite width [10] as visualized in Fig. 1.3. This allows electrons to localize in close vicinity to the sites of disorder (impurities) in states that lie within the energy gap of the former discrete spectrum. Only around the center of the broadened peaks there exist extended states that contribute to transport across the sample. Decreasing B with a fixed density n now first leads to population of the localized states[3]. Since these do not contribute to the transport, a decrease in B results in a stagnating ρ_{xy} until all localized states are filled. Further decrease of B then leads to partial population of the next LL and thus to a changing in ρ_{xy} and some finite ρ_{xx}. Therefore, disorder explains the persistence of the plateaus over a range of B as long as a mobility gap exists between localized and extended states. Revisiting the argument for the precise value of the quantization, it was assumed that all states contribute to the transport. With disorder being present in the sample it is not obvious anymore why this quantization should still be obtained. In section 2.2 an argument taking into account topological aspects is used to remove any doubts about the proper quantization [11].

It is this connection to topological aspects that also gives rise to the occurrence of chiral *edge channels* (or *edge "modes"*) by the so called *Bulk-boundary correspondence*. The existence of conducting edge states can already be seen in a semi-classical picture visualized in figure 1.4. Electrons that are subject to an external $\vec{B}$-field are forced into an orbital motion. In the bulk, the Lorentz force leads to electrons moving on well defined orbits explaining the bulk insulating behaviour. Looking at the region close to the edge of the sample[4], the motion is disturbed and the electrons need to perform a *chiral skipping orbit motion* directed by the magnetic field. In contradiction to the insulating behaviour of the bulk, the edges now carry a chiral current. Quantum mechanically the transport at the edge[5] is explained by the bending of the LLs in response to the steep potential confining the electrons at the border of the sample. Close to the edge the LLs thus cross the Fermi-energy E_F resulting in one chiral edge channel for every filled LL in the bulk. These edge states are robust against disruption by weak disorder at the edge if

[2] The potential associated with the disorder obeys $V \ll \hbar\omega_c$
[3] Which are randomly distributed in the sample at locations of impurities.
[4] Visually, looking at the region within the distance of the orbits' radius from the edge.
[5] In general, this picture holds only for integer fillings.

the corresponding potential varies smoothly along the edge [11, 12]. The chirality also protects electrons from back scattering since the entire sample would have to be crossed to change direction. The picture of edge channel transport has been extended for the FQH effect by several authors such as X.G. Wen [13] and will play an important role throughout this thesis, especially in a Landauer-Büttiker scheme.

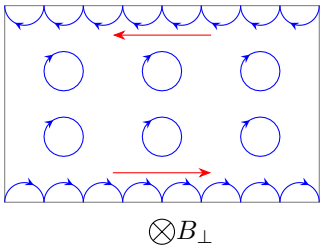

Figure 1.4: Visualization of the electrons motion on cyclotron orbits in the bulk and the disturbed nature of that motion close to the edge.

1.3 Fractional Quantum Hall Effect in 2D

For samples with less disorder than in case of the IQH effect, additional plateaus at fractional values of $1/\nu$ appear in the graph of ρ_{xy} (also shown in Fig. 1.2). The explanation to why these plateaus occur is related to the arguments from before but with some caveats. Arguing like in the IQH effect, one finds that these plateaus occur at fractional fillings of the LLs. Why should those configurations lead to quantized behaviour? The answer lies in how the electron system is modelled. Instead of having non-interacting electrons as in the IQH effect, electron-electron interactions play a major role in the FQH effect. These strong interactions allow for the occurrence of fractionally charged quasi-particles. To describe the electrons at the edge, the *Tomonaga - Luttinger liquid* is used [14]. It has been shown to have exact solutions for the low energy excitations of a 1D system by using the technique of *bosonization* [15]. As for the IQH effect, the existence of gapless edge excitations plays a major role in why systems in the FQH regime conduct in first place. Particularly interesting in the fractional quantum Hall regime is that the different states represent different phases of topological matter with excitations called *anyons*[6]. They can be divided into states with odd denominator[16], described by Abelian anyons [17–19] and states with an even denominator that are predicted to host non-Abelian anyons [20, 21] with potential use for quantum computation [22–24]. Contrary to the description of the integer analogue, the channels at the edge of some fractional quantum Hall systems are predicted to be counter-propagating, also allowing for length dependent transport behaviour if the channels interact somehow. A brief introduction to the mathematical modelling of the edge theory in the fractional quantum Hall effect is given in sections 2.4 and 2.5.

[6] Anyons are quasi particles that are neither fermions ($\varphi = \pi$) nor bosons ($\varphi = 0$). They are defined by being able to pick up *any* phase in the wave function when exchanged, hence the name *any-on*.

1.4 Recent Experimental Results and Goal of Thesis

Above, the theory of the quantum Hall effects (QHEs) has been introduced based on the transport of charges. Intuitively, the edge transport of charged particles also gives the opportunity to the quantized transport of energy (heat). In quantum Hall systems the mechanisms by which heat and charges are transported along the edge have been found to be uncoupled [25–28]. Therefore measurements of the heat transport are expected to give further insights about the underlying system, in particular about the edge structure of more complex states. In this context, the existence of non-Abelian Majorana edge modes has been justified by measuring half integer quantized thermal conductance for several bulk states [29]. Therefore, the experimental observation of the thermal conductance of the $\nu = 5/2$ state being quantized to $5/2$[7] points towards the existence of an odd number of Majorana modes at the edge [30]. Because of the relevance of Majorana modes for topological quantum computation, the determination of the actual edge structure has been in the focus of research for some time [22, 24, 31]. In 2022 a paper [32] has been published describing the experimental implementation of a novel method to distinguish between several theories for FQH states. It is based on interfacing fractional and integer states to isolate the dynamics of the interesting non-Abelian parts. The results of above mentioned works provide a mix of charge, heat and noise transport measurements at various interfaces of $\nu = 5/2$ with counter-propagating integer modes posing a great basis to distinguish between theoretical proposals.

The main goal of this thesis is to describe and to visualize a suiting theory, recovering experimental results as well as proposing further measurements for consolidation. To achieve this, I give a brief introduction into theoretical aspects of the topic in chapter (Ch.) 2 starting from the description of the bulk and finishing with the theory for the edge state transport. In chapter Ch. 3 the introduced description of the edge is used in phenomenological models to describe mesoscopic transport properties. Using the defined tools, the transport at the 5/2 edge is described in Ch. 4. The results of this thesis are summarized in Ch. 5 and a short outlook for future work is given in Ch. 6.

[7] The quantization of heat is in terms of the heat conductance quantum $\kappa_0 T$.

2

Theory Toolbox

In this chapter, the theoretical description of quantum Hall systems is explained exemplary for the integer quantum Hall effect since the theory of the fractional quantum Hall effect is based on it. Whenever it is possible, implications on the fractional quantum Hall effect are made and the corresponding publications are referenced.

2.1 Quantum Mechanical Treatment of the Bulk States

In this section the insulating bulk states, called LL will be given a mathematical description. Starting from the classical description of a particle with mass M and charge e in the presence of a magnetic field $\vec{B} = \nabla \times \vec{A} = B\vec{e}_z$, with $\vec{A}$ being a gauge field to be specified, the Lagrangian takes the form

$$L = \frac{1}{2}M\dot{\vec{x}}^2 - e\dot{\vec{x}} \cdot \vec{A}. \tag{2.1}$$

with the canonical momentum $\vec{p} = M\dot{\vec{x}} - e\vec{A}$ differing from the mechanical momentum by a term including the gauge. The Poisson brackets of interest are

$$\{x_i, p_j\} = \delta_{ij} \quad \{x_i, x_j\} = \{p_i, p_j\} = 0 \quad \{M\dot{x}_i, M\dot{x}_j\} = -e\left(\frac{\partial A_j}{\partial x^i} - \frac{\partial A_i}{\partial x^j}\right) = -e\epsilon_{ijk}B_k \tag{2.2}$$

The quantized theory can be constructed by using canonical quantization with the given Poisson brackets replaced by commutators as

$$[\hat{x}_i, \hat{p}_j] = i\hbar\delta_{ij} \quad [\hat{x}_i, \hat{x}_j] = [\hat{p}_i, \hat{p}_j] = 0 \quad [\hat{\pi}_x, \hat{\pi}_y] = -ie\hbar B, \tag{2.3}$$

where $\hat{\pi} \equiv m\dot{\hat{\vec{x}}}$ is the mechanical momentum. Dropping the hat notation of operators, the quantized Hamiltonian takes the form

$$H = \frac{1}{2M}(\vec{p} + e\vec{A})^2 = \frac{1}{2M}\vec{\pi} \cdot \vec{\pi}. \tag{2.4}$$

Resubstituting the canonical momentum operator, the Hamiltonian takes the gauge-independent form on the right side of the equation. The energy spectrum to this Hamiltonian is found by introducing creation and annihilation operators $a^\dagger$ and a arising from the mechanical momentum with commutator in Eq. (2.3)

$$a^\dagger = \frac{l_B}{\sqrt{2}\hbar}(\pi_x + i\pi_y) \quad a = \frac{l_B}{\sqrt{2}\hbar}(\pi_x - i\pi_y) \quad \text{obeying} \quad [a, a^\dagger] = 1, \tag{2.5}$$

with $l_B = \sqrt{\frac{\hbar}{eB}}$ the magnetic length. The Hamiltonian thus takes the form of a harmonic oscillator, with eigenenergies E_n called LLs

$$E_n = \hbar\omega_c\left(a^\dagger a + \frac{1}{2}\right) \quad \text{with} \quad \omega_c = \frac{|e|B}{M}. \tag{2.6}$$

As for the general harmonic oscillator, the Hilbert space is constructed by filling up states starting from a ground state $|0\rangle$, fulfilling $a|0\rangle = 0$ and number states $|n\rangle$ by

$$a^\dagger|n\rangle = \sqrt{n+1}\,|n+1\rangle \quad \text{and} \quad a|n\rangle = \sqrt{n}\,|n-1\rangle\,. \tag{2.7}$$

To compute wave functions in position space and to visualize the state degeneracy, the symmetric gauge is used in the following. It is defined as

$$\vec{A} = -\frac{1}{2}\vec{r} \times \vec{B} = -\frac{By}{2}\vec{e}_x + \frac{Bx}{2}\vec{e}_y. \tag{2.8}$$

Within this gauge another momentum operator can be defined $\tilde{\vec{\pi}} = \vec{p} - e\vec{A}$. It obeys the commutation relations

$$[\tilde{\pi}_x, \tilde{\pi}_y] = ie\hbar B \quad \text{and} \quad [\pi_i, \tilde{\pi}_j] = 0. \tag{2.9}$$

The corresponding ladder operators b and $b^\dagger$ take the form

$$b = \frac{l_B}{\sqrt{2}\hbar}(\tilde{\pi}_x + i\tilde{\pi}_y) \quad b^\dagger = \frac{l_B}{\sqrt{2}\hbar}(\tilde{\pi}_x - i\tilde{\pi}_y) \quad \text{obeying} \quad [b, b^\dagger] = 1. \tag{2.10}$$

A general state $|n, m\rangle$ in the Hilbert space is now defined by applying both creation operators a number of times on the ground state $|0, 0\rangle$, leading to

$$|n, m\rangle = \frac{a^{\dagger n} b^{\dagger m}}{\sqrt{n!m!}} |0, 0\rangle \quad \text{with} \quad a|0, 0\rangle = b|0, 0\rangle = 0. \tag{2.11}$$

It can be seen that the states corresponding to an energy E_n are degenerate, described by the quantum number m. To compute wave functions in coordinate space, the chosen gauge is inserted in the Hamiltonian, resulting in

$$H = \frac{1}{2M}\left(-\hbar^2\nabla^2 + eB(xp_y - yp_x) + \frac{e^2B^2}{4}(x^2 + y^2)\right). \tag{2.12}$$

In this equation the canonical angular momentum operator in z-direction $L_z = xp_y - yp_x$ with eigenvalues m is identified. A transformation into polar coordinates $x = r\cos(\phi)$ and $y = r\sin(\phi)$, with $L_z = -i\hbar\partial_\phi$ leads to

$$H = -\frac{\hbar^2}{2M}\frac{1}{r}\frac{\partial}{\partial r}\left(r\frac{\partial}{\partial r}\right) + \frac{L_z^2}{2Mr^2} - \frac{\omega_c}{2}L_z + \frac{M}{8}\omega_c^2 r^2. \tag{2.13}$$

At this point it is important to notice that L_z is not gauge invariant and its eigenvalues m are no physical observables. In many textbooks this circumstance is not given much attention even though it could lead to some confusion about signs in the results for the wave function in coordinate space. The fact that L_z depends on the quantum number m reflects the symmetry of the Hamiltonian. This symmetry however depends on the choice of coordinate system and vector potential [33]. In order to make physical sense of it, the guiding center operators X and Y are introduced instead as proposed by [34]

$$X = x - \frac{\pi_y}{M\omega_c} \quad Y = y + \frac{\pi_x}{M\omega_c} \quad \text{obeying} \quad [X, H] = [Y, H] = 0 \quad \text{and} \quad [X, Y] = il_B^2. \tag{2.14}$$

It can be seen, that the guiding center coordinates are time-independent and don't commute. The latter property can be visualized by introducing a circle with radius R depicting the average distance of the guiding center from the origin. For a given eigen-state $|n, m\rangle$, the guiding center is uniformly distributed on this circle. With the definition of the guiding center, new ladder operators $c^\dagger$ and c are defined as

$$c^\dagger = \frac{X - iY}{l_B\sqrt{2}} \quad c = \frac{X + iY}{l_B\sqrt{2}} \quad \text{with} \quad [c, c^\dagger] = 1. \tag{2.15}$$

The eigenvalue value $k \in \mathbb{Z}^+$ of $c^\dagger c$, is given a physical meaning by noting the equation for a circle in

$$R^2 = X^2 + Y^2 = (2c^\dagger c + 1)l_B^2. \tag{2.16}$$

Therefore k can be related to the distance of the orbits center from the guiding center[1]. In symmetric gauge it furthermore holds that $c^\dagger c = b^\dagger b$. Therefore the wave functions derived in the literature (for example in [7, 35]) can be used with $m = k$. The small but important difference is that $m > 0$ is given a physical meaning by using the guiding center argument. The wave function for the LLL ($n = 0$) in symmetric gauge takes the final form [34]

$$\psi_{LLL} \sim r^m e^{im\phi} \exp\left(-\frac{r^2}{4l_B^2}\right). \tag{2.17}$$

Eq. (2.17) indicates that ψ_{LLL} is peaked around $r \approx \sqrt{2ml_B^2}$.

2.2 Elaboration on Laughlin's Argument

In preparation to explain why disorder does not change the nicely quantized value of ρ_{xy}, the argument published by Laughlin and reworked by Halperin is presented in the following [7, 12, 36]. It is based on the existence of a mobility gap between localized and extended states and the different effect of gauge transformations on them. Since the quantization of ρ_{xy} is a general feature and should thus be independent of the geometry, the system can be modelled as having any shape. To get another handle on the problem, the annulus[2] geometry shown in Fig. 2.1 is chosen and a magnetic flux Φ through its center is added replacing the applied voltage bias by Faraday's law[37]. The entire argument is presented in the Nobel lecture given by Laughlin [38].

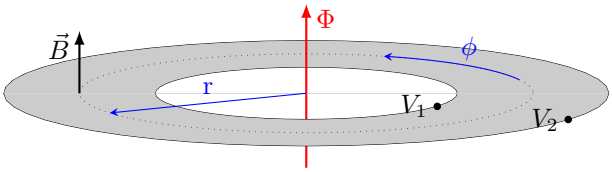

Figure 2.1: Visualization of the Corbino disk geometry setup with a virtual flux Φ in the center of the ring, a magnetic field $\vec{B}$ applied perpendicular to the surface and a voltage bias $\Delta V = V_1 - V_2$ across the ring.

To visualize this argument, a single quantum particle in the setup depicted in Fig. 2.1 is considered. Its' dynamics are described in polar coordinates $(r,\, \phi)$ by the Hamiltonian in symmetric gauge with an additional gauge term A_ϕ as

$$H = \frac{1}{2m}\left[\vec{p} + e\vec{A}\right]^2 = \frac{1}{2m}\left[-\frac{\hbar^2}{r}\partial_r(r\partial_r) + \left(\frac{\hbar}{r}\left(-i\partial_\phi + \frac{eBr^2}{2\hbar} + \frac{er}{\hbar}A_\phi\right)\right)^2\right] . \tag{2.18}$$

The eigenenergies corresponding to this Hamiltonian are degenerate in one quantum number as before (see Eq. (2.13) with $A_\phi = 0$). Due to the geometry of the disk, the magnetic flux Φ through its center can be identified with a constant gauge term A_ϕ in the corresponding vector potential adding to the background flux Br^2. In polar coordinates, A_ϕ is related to the flux Φ through the surface S by *Stokes' theorem*

$$\oint \vec{A} \cdot d\vec{r} = \int_S \vec{B} \cdot d\vec{S} = \Phi \ , \tag{2.19}$$

leading to $A_\phi = \frac{\Phi}{2\pi r}$ [12, 36]. For non-zero flux Φ it follows, that the spectrum of the system directly depends on the chosen gauge which might look confusing from a classical point of view. In quantum mechanics however, particles are sensitive to gauge fields by the *Aharonov-Bohm* effect that couples gauge fields to the phase of the particles [39].

In the following the Fermi energy E_F is placed between the first and second LL. If the particle is prepared in an eigenstate (choose LLL) of the Hamiltonian and the flux is increased $\Phi : \ 0 \to \Phi_0$ slowly within the time $t \gg \frac{1}{\omega_c}$, the *adiabatic theorem* [40] ensures that the entire set of eigenstates is restored. Individual states on the other hand are not necessarily mapped back onto themselves. This phenomenon, where individual states are non-invariant after being gauge transformed although they belong to a gauge equivalent Hamiltonian[3] is called *spectral flow* [3]. Recall the wave functions of the LLL from Eq. (2.17) corresponding to the Hamiltonian with $A_\phi = 0$. In this system they are slightly different as they are symmetrically centered around a center coordinate r_m. Adding the flux Φ_0 leads to a shift of the center coordinate by [3, 12]

$$r_m(\Phi + \Phi_0) = r_{m-1}(\Phi) \ . \tag{2.20}$$

It furthermore leads to one level being pushed above the Fermi-level E_F at the inner edge of the system whereas on the outer edge one level sinks below E_F. To reacquire thermal equilibrium

[2] Often called *Corbino disk*. It is homeomorphic to the originally proposed geometry of a ribbon.
[3] Meaning that $H_{\Phi=\Phi_0}$ can be mapped back onto $H_{\Phi=0}$ using a gauge transformation without altering the boundary conditions.

the system wants to react by transferring one electron from the inner to the outer edge. This is however only possible with the before mentioned caveat of taking disorder into account as it gives rise to the formation of localized and extended states [10, 12]. Using a gauge transformation to remove the gauge field dependence from the Hamiltonian, the states are transformed accordingly by

$$\psi(r,\phi) \to e^{-\frac{ie\Phi}{2\pi\hbar}\phi}\psi(r,\phi) \ .$$

Transforming localized states in this manner resembles no problem since they are only non zero in a finite region close to sites of disorder. Extended states on the other hand also have to remain single valued as they are taken around the annulus $\phi \to \phi + 2\pi$. This directly results in the requirement of Φ being an integer multiple of Φ_0. It furthermore implies that only the extended states undergo spectral flow as the magnetic flux is increased adiabatically. Therefore the conclusion from the case of no disorder still holds: If the extended states in ν LLs are filled, the adiabatic change of the flux $\Phi : 0 \to \Phi_0$ results in the transport of ν electrons from the inner to the outer edge. Noting that due to the confining potential there will always be at least two extended states present at the edges of the annulus, a radial current $I_r = \frac{\Delta E}{\Delta \Phi} = \nu \frac{e^2}{h}\Delta V$ is maintained by the voltage difference $\Delta V = V_1 - V_2$ between inner and outer edge. It is this current that recovers the expected value of $\rho_{xy} = \frac{\Delta V}{I_r} = \nu \frac{h}{e^2}$ in the presence of disorder[4].

2.3 Significance of Topology in Quantum Hall Effects

The introduced argument made by Laughlin can further be related to topological arguments in $\vec{k}$ space. Here, the focus lies on describing the topological effect on integer quantum Hall states[5]. [7, 41]

In general, the adiabatic evolution of eigenstates results in a phase shift consisting of a dynamical ϕ_t [6] and a geometrical component γ, also called *Berry-phase*[7]. Therefore a final state is defined up to a phase difference which depends on the shape of the momentum space of the underlying system. Using *Bloch's theorem*, the eigenfunctions in the Brillouin zone (BZ) are defined by planar waves fine-tuned with a periodic expression $u_{\vec{k}}(\vec{r})$

$$\psi_{\vec{k}}(\vec{r}) = e^{i\vec{k}\cdot\vec{r}} u_{\vec{k}}(\vec{r}). \tag{2.21}$$

The periodicity implied by the periodic boundary conditions of the BZ requires the momentum space to be a Torus $\mathcal{T}^2$ in 2D and an annulus $\mathcal{S}^1$ in 1D. Using that the final state has to obey the time-dependant Schrödinger equation, the Abelian Berry phase is obtained by integrating the *Berry connection* $\vec{\mathcal{A}}(\vec{k}) = -i \langle u_{\vec{k}} | \nabla_{\vec{k}} | u_{\vec{k}} \rangle$ over the path taken in momentum space. For a closed contour $\mathcal{C}$, the Berry phase takes the form

$$\gamma = \oint_{\mathcal{C}} \vec{\mathcal{A}}(\vec{k}) \cdot d\vec{k}. \tag{2.22}$$

Using Stokes' theorem, the integral over the closed path $\mathcal{C}$ in $\vec{k}$-space inscribing the surface $\mathcal{D}$ is translated into a surface integral of the curl of the Berry connection. The resulting tensor $\mathcal{F} = \nabla_{\vec{k}} \times \vec{\mathcal{A}}(\vec{k})$ is called *Berry curvature* and defines the Berry phase by

$$\gamma = \int_{\mathcal{D}} \mathcal{F}\, d\vec{k}. \tag{2.23}$$

By the *Gauss-Bonet* theorem the above integral is quantized in units of 2π whenever it is computed over a closed manifold $\mathcal{D}$. Noting the equivalence to the Euler characteristic, the topological invariant called *first Chern number* $C \in \mathbb{Z}$ is defined. As in the case of the Euler characteristic it is deeply connected to the genus of the enclosed manifold. In case of the Torus, the Chern number is computed by integrating the Berry curvature over the BZ

$$C = \frac{1}{2\pi} \int_{\mathcal{T}^2} \mathcal{F}_{xy}\, dk^2. \tag{2.24}$$

[4] Recall: Disorder also explains the persistence of the plateaus over a range of B values.
[5] This can be extended to the FQH effect using the non-Abelian Berry connection as shown in [7].
[6] It depends on the energy and the time T needed to complete a loop in parameter space $\varphi_t = \int_0^T E(t)\, dt$
[7] This component is only non-zero for a cyclical variation of the Hamiltonian. The *Aharonov-Bohm* phase can be seen as a "special" case of the Berry-phase.[39]

For a bulk insulator with a finite number of filled bands, one can assign a first Chern number to each band α. For non-interacting systems, like in case of the IQH effect, the TKNN (Thouless, Kohmoto, Nightingale, den-Nijs) formula [42] can then be used to connect the Hall conductivity to the Chern numbers by

$$\sigma_{xy} = \frac{e^2}{h} \sum_{\alpha} C_{\alpha}. \tag{2.25}$$

The Hall conductivity can thus be thought of as being a purely topological expression justifying the existence of gapless edge channels. Using the two band Dirac model and imposing translational symmetry in x-direction, the energy dispersion takes the form [43]

$$E(k_x) = \hbar v_F k_x \quad \text{with group velocity} \quad \frac{dE(k_x)}{dk_x} = \hbar v_F. \tag{2.26}$$

Since this energy dispersion implies the crossing of the Fermi-energy with a positive group velocity it is viewed as a right moving edge mode. If the Hamiltonian is changed close to the surface, the dispersion relation might be altered and the edge mode might cross the Fermi-energy E_F multiple times. The difference in crossings of E_F with positive and negative group velocity (N_R, N_L) however, has to remain constant and equal to the difference in Chern numbers ΔC at the interface of the valence and conduction band

$$N_R - N_L = \Delta C. \tag{2.27}$$

This relation gives a vivid picture of the before mentioned *bulk-boundary correspondence* as it relates the gapless edge excitations to the properties of the bulk insulator. [7, 43]

2.4 Bosonization

Having motivated the existence of gapless edge channels in quantum Hall systems, a model to describe the charge carriers at the edge of a strongly interacting electron system is needed to deduct transport characteristics for fractional quantum Hall systems. In this thesis the method of bosonization is used to describe charge carriers in 1D chiral edge channels. [15, 44, 45]

For weakly interacting electron systems in 1D at low energies, the mathematical procedure of bosonization is used to describe the fermionic system in terms of bosonic degrees of freedom. It is based on linearizing the low energy spectrum of the fermions around the two Fermi points $\pm k_F$[8]. The resulting V-shaped spectrum consists of two branches with opposite group velocity and needs to be unbound to allow for a proper definition of bosonic operators [44]. In order to avoid running into ultraviolet divergences, the final result is further regularized. In the following only the right moving branch ($v_F > 0$) with the normal ordered Hamiltonian H_0 is considered, where

$$H_0 = v_F \sum_k k : c_k^\dagger c_k : . \tag{2.28}$$

The fermionic creation and annihilation field operators are defined in a box of length L by assuming vanishing lattice spacing $a \to 0$ and thus an infinitely large BZ $\left(-\frac{\pi}{a}, \frac{\pi}{a}\right)$. For $x \in \left[-\frac{L}{2}, \frac{L}{2}\right]$ they take the form

$$\psi(x) = \frac{1}{\sqrt{L}} \sum_k e^{ikx} c_k \quad \text{and} \quad \psi^\dagger(x) = \frac{1}{\sqrt{L}} \sum_k e^{-ikx} c_k^\dagger \tag{2.29}$$

and obey the fermionic anti commutation relations

$$\{\psi(x), \psi(y)\} = \{\psi^\dagger(x), \psi^\dagger(y)\} = 0 \quad \text{and} \quad \{\psi(x), \psi^\dagger(y)\} = \delta(x-y). \tag{2.30}$$

[8] Therefore there is a built-in particle-hole symmetry in the theory. Amongst other effects (no energy dependent scatterer) this excludes the description of any thermo-electric effects in this model. To take them into account the low energy corrections to the linearized spectrum could be considered (not done here).[46]

To construct a finite Hilbert space, the difference between the total number of fermions and that of the vacuum state $|0\rangle_0$ (Dirac sea) is used. Therefore the normal ordering of the number operator $\hat{N}$ is of crucial importance to avoid diverging behaviour

$$\hat{N} = \sum_k : c_k^\dagger c_k := \sum_k \left[c_k^\dagger c_k - {}_0\langle 0| \, c_k^\dagger c_k \, |0\rangle_0 \right]. \tag{2.31}$$

Particle-hole excitations are created using the density operator $\rho(q)$ with $q \neq 0$

$$\rho(q) = \sum_k c_{k+q}^\dagger c_k \quad \text{obeying} \quad [\rho(p), \rho(q)] = -\frac{Lp}{2\pi}\delta_{p,-q}. \tag{2.32}$$

The commutation relation gives the possibility to define bosonic creation and annihilation operators $b_q^\dagger$ and b_q based on $\rho(q)$ by

$$b_q^\dagger = \sqrt{\frac{2\pi}{Lq}}\rho(q), \quad b_q = \sqrt{\frac{2\pi}{Lq}}\rho(-q) \quad \text{with} \quad [b_q^\dagger, b_{q'}^\dagger] = [b_q, b_{q'}] = 0 \quad \text{and} \quad [b_q, b_{q'}^\dagger] = \delta_{q,q'}. \tag{2.33}$$

In terms of the introduced bosonic operators, the fermionic density takes the form

$$: \psi^\dagger(x)\psi(x) := \frac{\hat{N}}{L} + \frac{1}{\sqrt{2\pi L}} \sum_{q>0} \sqrt{q} \left[e^{iqx} b_q + e^{-iqx} b_q^\dagger \right] . \tag{2.34}$$

Having a description of the interacting fermionic system in terms of non-interacting bosons, it remains to show that this description captures all excitations of the original system. At this point the discovery of Haldane [15] provides the essential piece to the puzzle. He showed that the N-particle Hilbert space spanned by all particle-hole excitations on top of the N-particle GS is also spanned by applying the bosonic creation operator $b_q^\dagger$ a number of times on this GS. He therefore showed that the bosonic representation of the Hilbert space is complete. To rewrite the final expression for the fermionic density, the bosonic fields $\varphi(x)$ and $\phi(x)$ are introduced

$$\varphi(x) = \frac{i}{\sqrt{L}} \sum_{q>0} \frac{e^{iqx}}{\sqrt{q}} e^{-b\frac{q}{2}} b_q \quad \text{and} \tag{2.35}$$

$$\phi(x) = \varphi(x) + \varphi^\dagger(x) = \frac{i}{\sqrt{L}} \sum_{q>0} e^{-b\frac{q}{2}} \left(e^{iqx} b_q - e^{-iqx} b_q^\dagger \right) . \tag{2.36}$$

The term $e^{-bq/2}$ acts as a regularization and has been introduced to ensure convergence at intermediate steps in the computation. Computational results should always be viewed with $b \to 0^+$. The fermionic annihilation operator takes the final form

$$\psi(x) = \frac{F}{\sqrt{2\pi b}} e^{i2\pi \hat{N}\frac{x}{L}} e^{-i\sqrt{2\pi}\phi(x)} , \tag{2.37}$$

where F denotes a *Klein factor* that is used to ensure fermionic commutation relation when Hilbert spaces of different particle numbers are connected. The important result of the entire bosonization process is that the linearized Hamiltonian H_0 is now expressed by

$$H_0 = v_F \int_{-\frac{L}{2}}^{\frac{L}{2}} dx : \psi^\dagger(x)(-i\partial_x)\psi(x) := \frac{v_F}{2} \int_{-\frac{L}{2}}^{\frac{L}{2}} dx : (\partial_x \phi)^2 : + \frac{\pi}{L} v_F \hat{N}(\hat{N}+1) . \tag{2.38}$$

The term $\frac{\pi}{L} v_F \hat{N}(\hat{N}+1)$ is neglected in the following since it becomes less important in the thermodynamic limit[9].
In combination with the topological argument, this result can now be used to define the action of chiral bosonized fermions at the edge of a fractional quantum Hall system.

[9] $\hat{N} \to \infty$, $L \to \infty$ and $\hat{N}/L = \text{const.}$

2.5 Edge State Transport

As argued before, the transport in the quantum Hall regime is carried out by chiral edge states. Using the bosonization result, the low energy excitations of the integer and the fractional quantum Hall effect can now be described by non-interacting bosons. While the IQH edges consist exclusively of co-propagating edge channels, this is only the case for the so called Laughlin-states of filling $\nu = \frac{1}{m}$ with $m \in \mathbb{Z}_{>0}$ in the FQH regime. Edge modes that are not Laughlin-states are assumed to consist of a multitude of counter-propagating channels. The low energy effective theory is thus described by various layers of incompressible quantum Hall fluids layered on top of each other. In the following I will introduce the theory used in this thesis closely following the descriptions of [13, 47, 48].

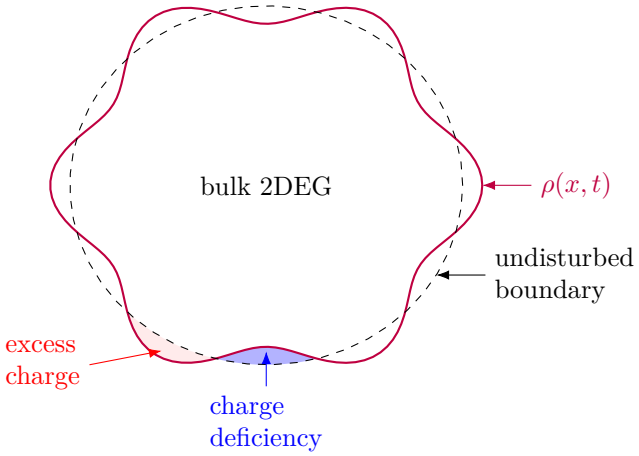

Figure 2.2: Illustration of the charge density wave $\rho(x,t)$ propagating along the surface of the bulk two dimensional electron gas (2DEG) system. According to the propagation of the wave, there will be regions of excess and deficient charge.

The fundamental concept of this theory is to think about the GS as resembling an incompressible disc shaped quantum Hall droplet. Excitations of this GS are thought to be deformations at the boundary resulting in chiral one dimensional charge density waves that propagate along the boundary of the droplet as illustrated in Fig. 2.2. By the effect of the *bulk-boundary correspondence* the edge "knows" about the bulk state properties and carries the correct amount of charge (heat). In order to combine the bosonization result for the Hamiltonian with the chiral nature of the edge wave, the action describing the edge state transport is derived from the equation of motion (EOM) of the density wave $\rho(x,t)$ propagating with velocity v. It has the general form

$$\partial_t \rho - v \partial_x \rho = 0 \ . \tag{2.39}$$

The bosonization result from before can now be used to rewrite the charge density ρ in terms of the bosonic field ϕ. The resulting action describing the dynamics at the edge of filling ν takes the form of the *Floreanini-Jackiw* action with ϕ a chiral compact bosonized fermion [13, 49, 50]

$$S = \frac{1}{4\pi\nu} \iint \partial_t \phi \partial_x \phi - v(\partial_x \phi)^2 \, dx \, dt \ . \tag{2.40}$$

The wave equation from before is recovered with $\rho = \frac{1}{2\pi}\partial_x \phi$ by minimizing this action (compare Sec. A.5.1). The quantization of the fields ρ and ϕ is done in momentum space with $k_n = \frac{2\pi n}{L}$, where L denotes the circumference of the disc that describes the 1D momentum space of the BZ.

It follows that

$$\phi(x,t) = \frac{1}{\sqrt{L}} \sum_{n=-\infty}^{\infty} \phi_n(t) e^{ik_n x} \quad \text{with} \quad k_n = \frac{2\pi n}{L} \quad \text{and} \tag{2.41}$$

$$\rho(x,t) = \frac{1}{\sqrt{L}} \sum_{n=-\infty}^{\infty} \rho_n(t) e^{ik_n x} \quad \text{and} \quad \rho_n(t) = \frac{ik_n}{2\pi} \phi_n(t) \ . \tag{2.42}$$

Discriminating between positive and negative n in the Fourier expansion of $\phi_n(t)$, the additional condition $\phi_{-n}(t) = \phi_n^*(t)$ is obtained (computation in Sec. A.5.2). Because the modes exist on a circle, $\phi_n(t)$ is furthermore symmetric. The action rewritten in terms of $\phi_n(t)$ becomes

$$S = -\frac{1}{2\pi\nu} \int_t \sum_{n=0}^{\infty} ik_n \dot{\phi}_n(t)\phi_{-n}(t) + vk_n^2 \phi_n(t)\phi_{-n}(t) \ , \tag{2.43}$$

with the corresponding conjugate momentum $\pi_n(t)$ given as

$$\pi_n(t) = -\frac{ik_n}{2\pi\nu} \phi_{-n}(t) = \frac{1}{\nu} \rho_{-n}(t) \ . \tag{2.44}$$

Having defined the conjugate variables $\phi_n(t)$ and $\pi_n(t)$, the commutation relations in Fourier space are

$$[\rho_n(t), \phi_{n'}(t)] = i\nu\delta_{n+n'} \quad [\phi_n(t), \phi_{n'}(t)] = \frac{2\pi\nu}{k_n}\delta_{n+n'} \quad [\rho_n(t), \rho_{n'}(t)] = \frac{k_n\nu}{2\pi}\delta_{n+n'} \tag{2.45}$$

These relations are an example of a $U(1)$ *Kac-Moody Algebra* and play an important role within the use of CFT in later parts of this thesis. Transforming back into coordinate space, the equal time commutation relations become[9]

$$[\phi(x), \phi(x')] = i\pi\nu \mathrm{sgn}(x-x') \quad [\rho(x), \phi(x')] = i\nu\delta(x-x') \quad [\rho(x), \rho(x')] = -\frac{i\nu}{2\pi}\partial_x\delta(x-x'). \tag{2.46}$$

Having introduced the theory for a density wave ρ of one type of liquid at the edge of the quantum Hall droplet, it remains to construct operators that create/annihilate particles in different fluids at the edge. Therefore electron Ψ_e and quasi particle Ψ_{qp} annihilation are defined by the normal ordered field operators

$$\Psi_e =: e^{im\phi} : \quad \Psi_{qp} =: e^{i\phi} : \ . \tag{2.47}$$

In Sec. A.5.3 it is shown that they indeed annihilate the correct charge in the corresponding channel. The non-interacting theory is thus completely described by the above introduced theory. For an edge consisting of multiple modes, the action is generalized to the *K-matrix-action* [13]

$$S = \frac{1}{4\pi} \iint \left[K_{ij} \partial_t \phi_i \partial_x \phi_j - V_{ij} \partial_x \phi_i \partial_x \phi_j \right] dt\, dx \ . \tag{2.48}$$

The matrix $\boldsymbol{K}$ describes the filling factors and chiralities of the edge modes, whereas $\boldsymbol{V}$ hosts the velocities of the modes. Therefore the off-diagonal elements of $\boldsymbol{V}$ describe Coulomb interactions between the modes. With disorder being present at the edge this system is sometimes exactly solvable at a random fixed point in the renormalization group sense [51, 52]. In the context of this thesis coulomb interactions are neglected since they only renormalize the inter mode tunneling conductances. When looking at the influence of reflections at the contacts however, it becomes necessary to take them into account [53–55]. Disorder furthermore breaks translational symmetry allowing for scattering events that give rise to inter channel equilibration by *tunneling interactions*.

[9] Here, $\mathrm{sgn}(x)$ is defined as $\mathrm{sgn}(0) = 1$ which leads to $\mathrm{sgn}(x) = 2\Theta(x) - 1$ and thus $\partial_x \mathrm{sgn}(x) = 2\delta(x)$.

3

Phenomenological Description of Edge State Transport

In this chapter, three semi-classical models are introduced to describe the transport along the edge consisting of channels that carry charge ν_i and heat n_i. The obtained transport characteristics are then used to draw conclusions about the models predictive power by comparing them to experimental results.

3.1 Landauer-Büttiker Description

Assuming that the edge of a system in the quantum Hall regime consists of a number of well defined channels, the Landauer - Büttiker formalism (LBF) is a useful approach to describe the transport along the edge [56, 57]. The channels transport energy according to the applied voltage ΔV and temperature bias ΔT in a chiral way. By convention, the transport is considered to be in the downstream direction if it follows the direction set by the magnetic field. Therefore the transport by co-propagating channels is always ballistic in downstream direction which is the case for integer and Laughlin edges [58]. The transport along more complex FQH edges is predicted to be carried out by counter-propagating channels [58, 59]. To describe the transport of the considered states within this thesis, three different types of edge channels are distinguished depending on their intrinsic properties

1. Bosonic channel with filling $\nu = 1$ and heat conductance $n = 1$
2. Bosonic channel with filling $\nu = 1/m$ and heat conductance $n = 1$
3. Majorana channel with filling $\nu = 0$ and heat conductance $n = 1/2$

The notion of counter-propagating channels becomes visible by (for example) looking at the transport characteristics of the $\nu = 2/3$ edge. In general, this edge could be modelled by two co-propagating channels, each with filling $\nu = 1/3$. Contradictory to the expected uniform transport characteristics, experimental results demonstrated properties that are not possible within this description [60]. To circumvent this objection, the edge is instead modelled by a downstream mode $\nu_+ = 1$ and an upstream mode with $\nu_- = 1/3$ giving the opportunity to explain all observed transport characteristics depending on degree of equilibration between the involved modes [52].
To show the influence of equilibration on the edge transport, the LBF is introduced first to describe the transport along edges of non-interacting[1] channels. Without interactions between the channels there is no possibility for channels to equilibrate as they propagate along the edge. The only possibility to achieve some equilibration at this edge is by inter channel mixing in macroscopic[2] contacts.
A chiral charge current $J_{e,i}$ emanating from contact i with voltage V_i is defined according to the chirality χ_j and filling factor ν_j of the j^{th} channel by

$$J_{e,i} = \chi_j \nu_j V_i \ . \tag{3.1}$$

Similarly, a chiral heat current is defined by the squared temperature T_i^2 at contact i

$$J_{Q,i} = \chi_j n_j \kappa_0 T_i^2 \ , \tag{3.2}$$

[1] The term interaction is used to describe scattering interactions between the channels. It does **not** refer to Coulomb interactions.
[2] I will refer to contacts that are connected to the edge in experiments as *macroscopic* to distinguish them from any virtual probe contacts.

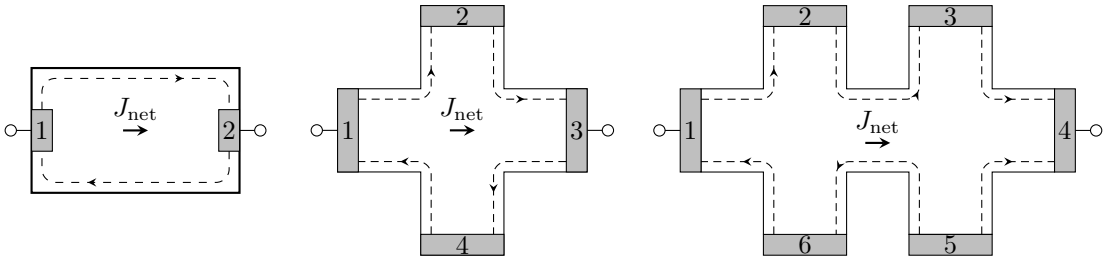

Figure 3.1: Visualization of transport in common measurement setups with two, four or six terminals (left to right) hosting one effective downstream channel.

where n_j denotes the channels' heat conductance. Multiple co-propagating channels at one edge are further merged into one effective channel of filling ν_j and heat conductance n_j. For N_d downstream and N_u propagating channels of individual ν_l and n_l this leads to effective downstream $\nu_d(n_d)$ and upstream parameters $\nu_u(n_u)$

$$\nu_d = \sum_{l=1}^{N_d} \nu_l \qquad n_d = \sum_{l=1}^{N_d} n_l \qquad \nu_u = \sum_{l=1}^{N_u} \nu_l \qquad n_u = \sum_{l=1}^{N_u} n_l$$

To compute transport properties that are observed in experiments such as conductances, the most common measurement setups: two terminal setup, four terminal setup (Hall-cross) and six terminal setup (Hall-Bar) (compare figure 3.1) are considered.
Looking at the charge transport by integer and Laughlin states in the the two terminal setup the edge is modelled as consisting of one channel with filling $\nu \in \{\nu, \frac{1}{m}\}$. Therefore, applying a bias in the chemical potential $\mu_L > \mu_R$[3] leads to the charge current J_e that can be referred to the two terminal charge conductance G_{2t}. Using the Fermi-distributions f_L, f_R at the left and the right contact, the charge current evaluates to

$$J_e = \nu \frac{e}{h} \int_0^\infty dE \big[f_L(E, \mu_L, T) - f_R(E, \mu_R, T) \big]. \tag{3.3}$$

At low temperatures, the Sommerfeld expansion can be used to simplify this expression by relating the statistical average of a function $H(E)$ to the problem. With the inverse temperature $\beta = (k_B T)^{-1}$, this expansion provides approximate solutions to problems that are described by integrals of the form [61]

$$\int_{-\infty}^{\infty} \frac{H(E)}{e^{\beta(E-\mu)} + 1} \, dE = \int_{-\infty}^{\mu} H(E) \, dE + \frac{\pi^2}{6} \left(\frac{1}{\beta} \right)^2 H'(\mu) + \mathcal{O}\left(\frac{1}{\beta\mu} \right)^4. \tag{3.4}$$

Using this formalism with $H_L(E) = H_R(E) = 1$ and thus $H'_L(E) = H'_R(E) = 0$, the charge current J_e results in the charge conductance G_{2t}

$$J_e = \nu \frac{e}{h} \Big[\int_0^{\mu_L} 1 dE - \int_0^{\mu_R} 1 dE \Big] = \nu \frac{e}{h} (\mu_L - \mu_R) = \nu \frac{e}{h} \Delta\mu \tag{3.5}$$

$$G_{2t} = \frac{J_e}{\Delta V} = \frac{e J_e}{\Delta \mu} = \nu \frac{e^2}{h}. \tag{3.6}$$

The charge conductance of $G_{2t} = \{\nu, \frac{1}{m}\}$ thus takes the expected form for integer and Laughlin states in units of the charge conductance quantum $g_0 = \frac{e^2}{h}$. Applying a temperature gradient $T_L > T_R$, the heat current J_Q associated with transport in one channel of heat conductance n evaluates to

$$J_Q = \frac{n}{h} \int_0^\infty dE E \big[f_L(E, \mu, T_L) - f_R(E, \mu, T_R) \big]. \tag{3.7}$$

[3] By applying a voltage bias $V_L > V_R$

Using the Sommerfeld-expansion with $H_L(E) = H_R(E) = E$ and thus $H'_L(E) = H'_R(E) = 1$ it follows for the heat current after some steps

$$J_Q = n\frac{\pi^2 k_B^2}{6h}(T_L^2 - T_R^2) \approx n\frac{\pi^2 k_B^2}{3h} T\Delta T. \tag{3.8}$$

In the second part of this equation, the heat current has been expanded for small biases ΔT with $T_L = T_0 + \Delta T$ and $T_R = T_0$. Using the definition of the heat conductance G^Q_{2t}, one arrives at the final result

$$G^Q_{2t} = \frac{dJ^Q}{d\Delta T} = n\frac{\pi^2 k_B^2}{3h} T_0 = n\kappa_0 T_0 \ , \tag{3.9}$$

with the heat conductance quantum $\kappa_0 := \frac{\pi^2 k_B^2}{3h}$. An edge consisting of one channel with intrinsic heat conductance n will thus show a quantized two terminal heat conductance of $G^Q_{2t} = n\kappa$, with $\kappa := \kappa_0 T$ the adjusted heat conductance quantum. The quantization of heat has been shown in experiments in 2000 [62] and more recently also in quantum Hall states [27–30]. Unless stated otherwise the expressions derived in this thesis are given in units of the charge and heat conductance quantum g_0 and κ. The computation of the one channel case for the Hall-cross and the six terminal setup are not carried out explicitly in this thesis[4].

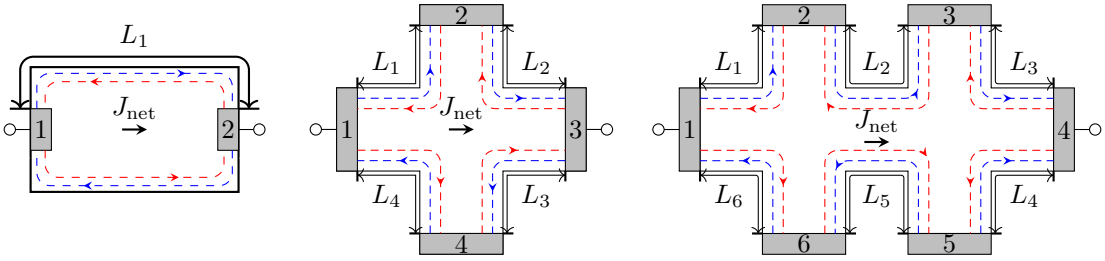

Figure 3.2: Counter-propagating modes in common measurement setups with effective filling factors of ν_+ in the downstream and ν_- in the upstream direction.

Looking at channels of opposite chirality in the considered setups visualized for two channels in Fig. 3.2, the character of the LBF becomes visible. Additionally to the two terminal conductance G_{2t}, the setups with more than two macroscopic contacts allow to compute the Hall-conductance G_H between contacts of different edges and the longitudinal conductance G_L between neighbouring contacts at the same edge. The additional macroscopic contacts are modelled as voltage probes leading to the local conservation law $J^{in} = J^{out}$. The charge transport in linear response to a voltage is described by the matrix equation $\vec{I} = \boldsymbol{G}\vec{V}$ and the conductance matrices $\boldsymbol{G}$ have to be circulant. They are defined for the setups shown in Fig. 3.2 using the permutation matrix $\boldsymbol{P} = (p_{ij}) \in \mathbb{R}^{n\times n}$ corresponding to the permutation

$$\pi_n = \begin{pmatrix} 1 & 2 & 3 & \dots & n \\ n & 1 & 2 & \dots & n-1 \end{pmatrix} \in S_n \quad \text{and} \quad p_{ij} = \begin{cases} 1 & \text{if } \pi(i) = j \\ 0 & \text{else} \end{cases}, \tag{3.10}$$

where n is the number of contacts and takes the values $n \in \{2, 4, 6\}$ for Two Terminal setup, Hall-Cross and Hall-Bar correspondingly. Accordingly, $\boldsymbol{G}_n$ takes the general form

$$\boldsymbol{G}_n = (\nu_+ + \nu_-)\mathbf{1}_n - \nu_+ \boldsymbol{P}_n - \nu_- \boldsymbol{P}_n^{n-1}. \tag{3.11}$$

The so found $\boldsymbol{G}_n$ are singular and $\vec{I} = \boldsymbol{G}\vec{V}$ cannot be solved for the voltages in this form. Assuming the injected current I between source (left) and drain (right) is conserved and by imposing gauge invariance of the system, the conductance matrix is reduced to a non-singular matrix. The system of equations is then solved for the various voltages defining the conductances shown in table (Tab.) 3.1. Using the introduced matrices for the setups these conductances are computed depending on the effective filling factors ν_+ and ν_-. The results of this computation are shown

[4] They can be deduced from the upcoming theory for counter-propagating channels by setting upstream transport properties to zero.

Table 3.1: Definition of the charge Hall-conductance G_H, the two terminal charge conductance G_{2t} as well as the longitudinal charge conductance G_L in the considered setups. The longitudinal conductance for the Hall-bar is defined according to the convention used in many experiments.

	G_{2t}	G_H	G_L
Two terminal setup	$\frac{I}{V_1 - V_2}$	x	x
Hall-cross	$\frac{I}{V_1 - V_3}$	$\frac{I}{V_2 - V_4}$	see Sec. A.2
Hall-bar	$\frac{I}{V_1 - V_4}$	$\frac{I}{V_2 - V_6} = \frac{I}{V_3 - V_5}$	$\frac{I}{V_2 - V_3} = \frac{I}{V_5 - V_6}$

below in Tab. 3.2. The heat transport in the different setups is described using a chiral heat current. With the modes' individual heat conductances, the heat conductance matrices are deduced from the charge conductance matrices by exchanging $\nu_i \to \kappa_0 n_i$. Using gauge invariance to analyze this system is more complicated this time. But since the transport is assumed to be free of dissipation, the system is directly solved for the heat current in terms of the difference of squared temperatures at source (L) and drain (R) $T_L^2 - T_R^2$. The heat conductances G_{2t}^Q, G_H^Q and G_L^Q are then computed to the expressions shown in Tab. 3.2.

At this point one should be confused by the values of the conductances in the different measurement setups - especially by the non-uniqueness of the Hall conductance which is the key characteristic of the QHEs. This is a consequence of the LBF not taking interactions between the channels into account. However, increasing the number of macroscopic contacts at the edge, the two terminal charge(heat) conductance seems to approach the expected unique value of $G_{2t}^{(Q)} = |\nu_+(n_+) - \nu_-(n_-)|$. This observation is further investigated in the following by looking at mixing of edge channels in macroscopic contacts.

Table 3.2: Values of measurable charge conductances (in units e^2/h) in the considered setups depending on the effective filling factors of the downstream ν_+ and upstream ν_- propagating modes as well as the heat conductances (in units of κ) depending on the effective heat conductances of the downstream n_+ and upstream n_- propagating modes.

	G_{2t}	G_H	G_L
Two terminal setup	$\nu_+ + \nu_-$	x	x
Hall-cross	$\frac{\nu_+^2 + \nu_-^2}{\nu_+ + \nu_-}$	$\frac{\nu_+^2 + \nu_-^2}{\nu_+ - \nu_-}$	see Sec. A.2
Hall-bar	$\frac{\nu_+^3 + \nu_-^3}{\nu_+^2 + \nu_+\nu_- + \nu_-^2}$	$\frac{\nu_+^2 - \nu_+\nu_- + \nu_-^2}{\nu_+ - \nu_-}$	$\frac{\nu_+^3 + \nu_-^3}{\nu_+\nu_-}$
	G_{2t}^Q	G_H^Q	G_L^Q
Two terminal setup	$n_+ + n_-$	x	x
Hall-cross	$\frac{n_+^2 + n_-^2}{n_+ + n_-}$	$\frac{n_+^2 + n_-^2}{n_+ - n_-}$	see Sec. A.2
Hall-bar	$\frac{n_+^3 + n_-^3}{n_+^2 + n_+n_- + n_-^2}$	$\frac{n_+^2 - n_+n_- + n_-^2}{n_+ - n_-}$	$\frac{n_+^3 + n_-^3}{n_+n_-}$

3.2 Mixing Model

To verify, that the conductances approach a unique value for $\nu_+(n_+) \neq \nu_-(n_-)$, an alternative model taking a deeper look into the nature of mixing in macroscopic contacts is introduced in the following. Therefore the local conservation law at each contact is viewed as resembling a mixing of channels that emanate from different neighbouring contacts. Generalizing this thought for an arbitrary number of contacts m attached to one edge[5] leads to the notion of a recurrence relation.
For N_d downstream channels with ν_j and N_u upstream channels with ν_l, the recurrence relation for the charge transport becomes

$$V_n = \frac{\sum_{j=1}^{N_d} \nu_j}{\sum_{i=1}^{N_c} \nu_i} V_{n-1} + \frac{\sum_{l=1}^{N_u} \nu_l}{\sum_{i=1}^{N_c} \nu_i} V_{n+1}. \tag{3.12}$$

The voltage V_n at contact n is now described as the result of the weighted average between the voltages of the neighbouring contacts V_{n+1} and V_{n-1}. Summarizing channels propagating in the same direction into one effective downstream channel with ν_d and one effective upstream channel of ν_u, the mixing behaviour becomes even more vivid

$$V_n = \frac{\nu_d}{\nu_d + \nu_u} V_{n-1} + \frac{\nu_u}{\nu_d + \nu_u} V_{n+1}. \tag{3.13}$$

Applying a voltage bias between contact $n = 0$ (left) and $n = m$ (right) and imposing the corresponding boundary conditions for the top and bottom edge, the voltage at contact n of the top(bottom) edge becomes for $\nu_+ \neq \nu_-$

$$V_n^{top(bot)} = \frac{V_{L(R)} \left(\frac{\nu_+}{\nu_-}\right)^m - V_{L(R)} \left(\frac{\nu_+}{\nu_-}\right)^n + V_{R(L)} \left(\frac{\nu_+}{\nu_-}\right)^n - V_{R(L)}}{\left(\frac{\nu_+}{\nu_-}\right)^m - 1}. \tag{3.14}$$

The corresponding two terminal charge conductance is obtained by computing the net current at the top (bottom) $I^{top(bot)}$ edge and takes the form

$$G_{2t} = \frac{I^{top} - I^{bot}}{V_L - V_R} = (\nu_+ - \nu_-) \frac{\left(\frac{\nu_+}{\nu_-}\right)^m + 1}{\left(\frac{\nu_+}{\nu_-}\right)^m - 1}. \tag{3.15}$$

In the limits of having no mixing between the channels ($m = 1$) and having well mixed channels $m \to \infty$, the two terminal charge conductance approaches the values:

$$G_{2t} \overset{m=1}{=} \nu_+ + \nu_- \qquad\qquad G_{2t} \overset{m\to\infty}{\to} \nu_+ - \nu_- \tag{3.16}$$

Not only does this model reproduce the result of the LBF computation for the two terminal setup with $m = 1$, it also shows that the quantized value of the conductance is obtained for the limit of well-mixed channels $G_{2t} \overset{m\to\infty}{\longrightarrow} \nu_+ - \nu_-$. Physically this refers to equilibration between two edge modes of opposite chirality just by mixing in a large number of macroscopic contacts connected to the edge. In Fig. 3.3b the voltage drop along the top and bottom edges are visualized. It can be seen that the voltage drop occurs in the vicinity of the right contact at $n = m$. Since a voltage drop leads to Joule-heating, this region is referred to as the *hotspot* in the following. Even though the result might look promising, this model does not explain real setups where only a finite amount of macroscopic contacts is connected to the edge. Therefore this already implies that the assumption of non-interacting channels might not be suitable to describe the transport by fractional quantum Hall edges.
In QSH systems on the other hand, where interactions between the channels are negligible due to the energy required to flip the spin, the mixing model might be useful to predict charge and heat conductances [63, 64]. With $\nu_+ = \nu_-$, the discrete voltage profiles for top(bottom) edge now take the form

$$V^{top(bot)} = V_{L(R)} - \frac{n}{m} V_{L(R)} + \frac{n}{m} V_{R(L)}. \tag{3.17}$$

[5] Thus the total number of contacts attached to the system is $N = 2m$.

Computing the two terminal charge conductance as before, it follows for the limits of interest

$$G_{2t} = \frac{2\nu}{m} \qquad G_{2t} \overset{m=1}{=} 2\nu \qquad G_{2t} \overset{m\to\infty}{\longrightarrow} 0 \tag{3.18}$$

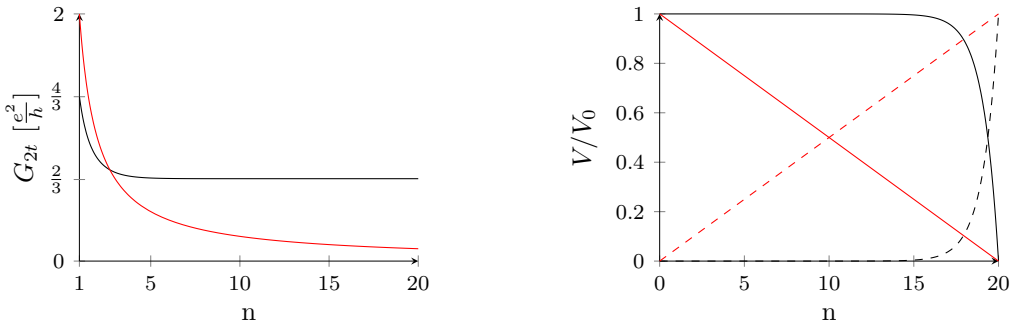

(a) **(b)**

Figure 3.3: Visualization of the two terminal charge conductance G_{2t} on the left and the corresponding voltage drop along the top (solid lines) and the bottom edge (dashed lines) with $\nu_+ = 1$, $\nu_- = \frac{1}{3}$ and $\nu_+ = \nu_- = 1$ for an increasing number of probe contacts n.

In this scenario the net charge transport is computed to be vanishing in the well mixed limit $m \to \infty$ since the channels carry the same amount of charge in opposite direction (compare Fig. 3.3a). The transport of charges is therefore referred to as being *diffusive*. This is underlined taking a look at the recurrence relation of such a system

$$V_n = \frac{1}{2}V_{n-1} + \frac{1}{2}V_{n+1}. \tag{3.19}$$

Each macroscopic contact is influenced equally strong from its two neighbours, indicating a random walk of charges and thus a linear voltage drop across the system as depicted in Fig. 3.3b.
Introducing a conserved heat current in the probe contacts, the formalism is also applicable to look into mixing of heat along the edge. The recurrence relation for $n_+ \neq n_-$ becomes

$$T_n^2 = \frac{n_+}{n_+ + n_-}T_{n-1}^2 + \frac{n_-}{n_+ + n_-}T_{n+1}^2. \tag{3.20}$$

To compute the heat conductance, the heat currents on top and bottom edge used to define the net heat current across the sample $J_{Q,net} = J_Q^{top} - J_Q^{bot}$ by

$$J_Q^{top(bot)} = \frac{\kappa_0}{2}(n_+ T_{0,top(bot)}^2 - n_- T_{1,top(bot)}^2). \tag{3.21}$$

Biasing the system by $T_L = T_0 + \Delta T$ and $T_R = T_0$ and expanding the net heat current small ΔT up to $\mathcal{O}(\Delta T)$ the heat conductance is computed. In the relevant limits of no ($m = 1$) and very well mixing ($m \to \infty$) it takes the form

$$G_{2t}^Q = (n_+ - n_-)\frac{\left(\frac{n_+}{n_-}\right)^m + 1}{\left(\frac{n_+}{n_-}\right)^m - 1} \qquad G_{2t}^Q \overset{m\to 1}{\longrightarrow} n_+ + n_- \qquad G_{2t}^Q \overset{m\to\infty}{\longrightarrow} n_+ - n_- \tag{3.22}$$

Applying the same formalism for $n_+ = n_- = n$, depicting heat transport without a preferred direction (diffusion), the heat conductance becomes

$$G_{2t}^Q = \frac{2n}{m} \qquad G_{2t}^Q \overset{m\to 1}{\longrightarrow} 2n \qquad G_{2t}^Q \overset{m\to\infty}{\longrightarrow} 0 \tag{3.23}$$

As in the charge transport case, the heat conductance exponentially approaches its equilibrium value for $n_+ \neq n_-$ and vanishes diffusively for $n_+ = n-$. Up to this point the unique nature

of the charge and heat conductances has been recovered under the constraint of having an infinite number of perfect macroscopic contacts attached to the edge. Since this is not given in common measurement setups, the mixing model is used best to compute the conductances of systems with non-interacting channels for a finite number of probes. On the other hand there has to be an explanation for the uniqueness of the conductances in the fractional quantum Hall regime. Therefore it seems crucial to take interactions between the modes on one edge into account.

3.3 Incoherent Tunneling Model

In the incoherent tunneling model, the already mentioned interactions between the two channels are taken into account. Due to a large amount of disorder at the edge, tunneling between the channels is allowed at a point contact. Assuming local equilibrium conditions in the channels, it is possible to associate local voltages V and temperatures T to the channels before and after the interaction site. A tunneling current at the point contact is then caused by the difference in local V and T between the involved channels. Schematically, the edge is visualized in Fig. 3.4 for two counter propagating modes. [65–69]

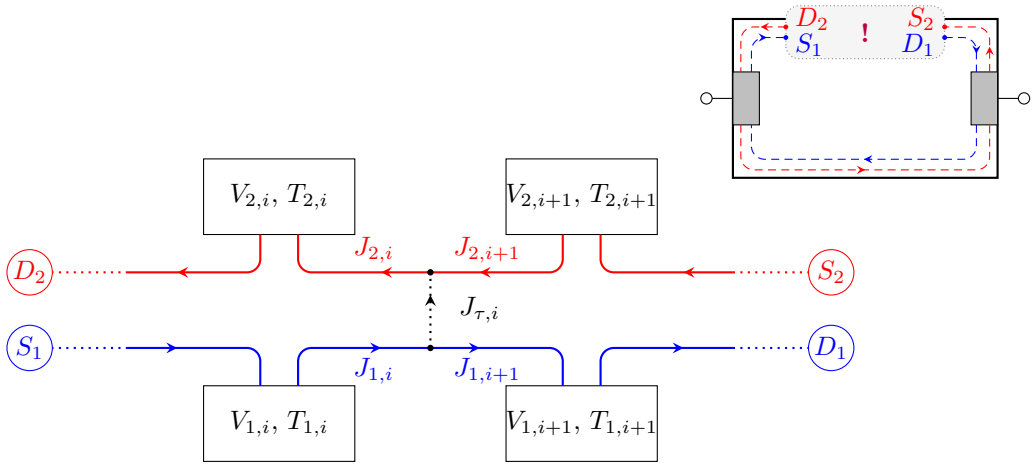

Figure 3.4: Schematic drawing of the incoherent tunneling model described by two channels 1, 2 interacting at a point contact between two neighbouring virtual probes. It describes interactions along a single edge segment as indicated in the top right corner.

To describe the transport properties resulting from this edge description it is assumed that two adjacent tunneling points are located within a distance a larger than the coherence length of the modes. Therefore any effect of quantum interference becomes negligible. Assuming that no charge (heat) is dissipated at the disorder sites, the charge and energy current obey a local conservation law given by

$$\chi_1 I_{1,i+1} = \chi_1 I_{1,i} - I_{\tau,i} \qquad \text{and} \qquad \chi_2 I_{2,i+1} = \chi_2 I_{2,i} + I_{\tau,i} \quad . \tag{3.24}$$

In general, the tunneling current depends on the chiralities of the two channels but to first order the difference between the two cases $\chi_1 = +(-)$ and $\chi_2 = -(+)$ vanishes. The chiral currents $I_{k,i}$ of the k^{th} channel ($k \in \{1, 2\}$) at the i^{th} probe as well as the tunneling current between two channels $I_{\tau,i}$ are defined by

$$I_{k,i} = \nu_k V_{k,i} \qquad \text{and} \qquad I_{\tau,i} = g(V_{1,i} - V_{2,i+1}) \quad . \tag{3.25}$$

where g describes the probability amplitude of the tunneling (interaction) process. Restructuring the system of equations, the discrete description of the voltages is obtained as

$$\begin{pmatrix} V_{1,i+1} \\ V_{2,i+1} \end{pmatrix} = \begin{pmatrix} -\frac{g\nu_2\chi_2}{g\nu_1\chi_1+\nu_1\chi_2\nu_2} & \frac{g\nu_2\chi_2}{g\nu_1\chi_1+\nu_1\chi_2\nu_2} \\ \frac{g}{g+\chi_2\nu_2} & -\frac{g}{g+\chi_2\nu_2} \end{pmatrix} \begin{pmatrix} V_{1,i} \\ V_{2,i} \end{pmatrix} \quad . \tag{3.26}$$

Taking the continuum limit for small tunneling amplitudes $g \to 0$, vanishing $a \to 0$ and by introducing a constant length $\frac{a}{g} = l$, the continuous version of this equation is obtained. For an infinite number of virtual probes along the edge, it takes the form

$$\partial_x \vec{V}(x) = \frac{1}{l} \begin{pmatrix} -\frac{1}{\chi_1 \nu_1} & \frac{1}{\chi_1 \nu_1} \\ \frac{1}{\chi_2 \nu_2} & -\frac{1}{\chi_2 \nu_2} \end{pmatrix} \vec{V}(x) \ . \tag{3.27}$$

Imposing the boundary conditions $V_1^{top}(0) = V_0$, $V_2^{top}(L) = 0$ for a setup biased by $\Delta V = V_0$, the voltage profiles of the top edge are obtained as

$$V_1^{top}(x) = V_0 \ \frac{\nu_1 - \nu_2 e^{\frac{x-L}{l_{eq}^C}}}{\nu_1 - \nu_2 e^{-\frac{L}{l_{eq}^C}}} \qquad \text{and} \qquad V_2^{top}(x) = V_0 \nu_1 \ \frac{1 - e^{\frac{x-L}{l_{eq}^C}}}{\nu_1 - \nu_2 e^{-\frac{L}{l_{eq}^C}}} \ . \tag{3.28}$$

Here, a new constant charge equilibration length $l_{eq}^C = l \frac{\nu_1 \nu_2}{\nu_1 - \nu_2}$ has been introduced. Imposing the boundary conditions for the bottom edge, the corresponding voltage profiles take the form

$$V_1^{bot}(x) = V_0 \nu_2 \ \frac{e^{-\frac{L}{l_{eq}^C}} + e^{\frac{x-L}{l_{eq}^C}}}{\nu_1 - \nu_2 e^{-\frac{L}{l_{eq}^C}}} \qquad \text{and} \qquad V_2^{bot}(x) = V_0 \ \frac{\nu_2 - \nu_1 e^{\frac{x-L}{l_{eq}^C}}}{\nu_2 - \nu_1 e^{-\frac{L}{l_{eq}^C}}} \ . \tag{3.29}$$

In Fig. 3.5, the voltage profiles of the top and bottom edge are visualized for the $\nu = 2/3$ state consisting of counter propagating channels with filling $\nu_1 = 1$ and $\nu_2 = \frac{1}{3}$. Similar to the results for the mixing model, the voltage drop occurs within a small region, in vicinity to the downstream contact at $x = L$ indicating the position of the *hotspot* in that region. Based on the voltages, the length dependent behaviour of the charge conductances between the different channels' source and drain contacts is computed. The "downstream" conductances are defined by the conductance between the source of channel one S_1 and the drains D_1 and D_2

$$G_{S_1 D_1} = \frac{I_1^{top}(L)}{V_0} = \frac{\nu_1 V_1^{top}(L)}{V_0} \qquad \text{and} \qquad G_{S_1 D_2} = \left| \frac{I_2^{top}(0)}{V_0} \right| = \left| \frac{\nu_2 V_2^{top}(0)}{V_0} \right| \ . \tag{3.30}$$

Similarly, the "upstream" conductances become

$$G_{S_2 D_1} = \left| \frac{I_1^{bot}(L)}{V_0} \right| = \left| \frac{\nu_1 V_1^{bot}(L)}{V_0} \right| \qquad \text{and} \qquad G_{S_2 D_2} = \frac{I_2^{bot}(0)}{V_0} = \frac{\nu_2 V_2^{bot}(0)}{V_0} \ . \tag{3.31}$$

In the limit $L \gg l_{eq}^C$, where the charge transport between the two channels is fully equilibrated, the conductances take the values:

$$\begin{aligned} G_{S_1 D_1} &\overset{L \gg l_{eq}^C}{\longrightarrow} \nu_1 - \nu_2 & G_{S_1 D_2} &\overset{L \gg l_{eq}^C}{\longrightarrow} \nu_2 \\ G_{S_2 D_1} &\overset{L \gg l_{eq}^C}{\longrightarrow} \nu_2 & G_{S_2 D_2} &\overset{L \gg l_{eq}^C}{\longrightarrow} 0 \end{aligned} \tag{3.32}$$

In the regime where the charge transport is not fully equilibrated, the charge conductances show non unique behaviour as visualized in Fig. 3.5 for $0 \leq L/l_{eq}^C \leq 10$.

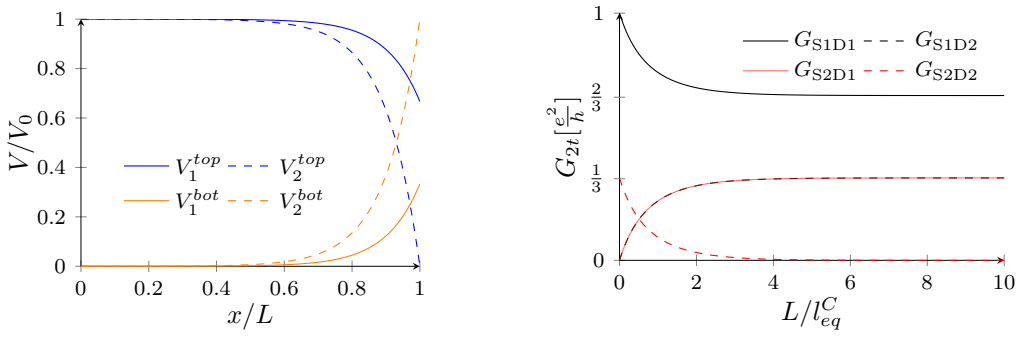

Figure 3.5: Visualization of the voltage profiles of the channels at top and bottom edge with $\nu_1 = 1$, $\nu_2 = \frac{1}{3}$ and $l_{eq}^C = 0.1L$ on the left and the channel length dependent behaviour of the conductances on the right.

With the hand waving picture of particles being transported along the edge, it comes with no surprise that there is also energy transported along the edge allowing to look into heat transport characteristics. The heat transport equation is obtained by using the local conservation of energy at the i^{th} probe. It follows that

$$\chi_1 J_{1,i+1} = \chi_1 J_{1,i} - J_{\tau,i} \qquad \text{and} \qquad \chi_2 J_{2,i+1} = \chi_2 J_{2,i} + J_{\tau,i} \ . \tag{3.33}$$

The chiral energy currents are furthermore described by the local constitution relation of the k^{th} mode at contact i

$$J_{k,i} = \nu_k \frac{e^2}{2h} V_{k,i}^2 + n_k \frac{\kappa_0}{2} T_{k,i}^2 \ , \tag{3.34}$$

where ν_k and n_k are the filling factor and the heat conductance of the k^{th} channel. Similarly to the case of charge transport, an interaction energy current $J_{\tau,i}$ is defined. It has the form

$$J_{\tau,i} = g\frac{e^2}{2h}(V_{1,i}^2 - V_{2,i+1}^2) + \frac{g\gamma\kappa_0}{2}(T_{1,i}^2 - T_{2,i+1}^2) \ , \tag{3.35}$$

where γ denotes the deviation from the Wiedemann-Franz law. Using the result from the charge transport, the terms $V_{1,i+1}$ and $V_{2,i+1}$ are replaced by $V_{1,i}$ and $V_{2,i}$. Expanding for small g up to $\mathcal{O}(g)$, setting $x = ia$, introducing an infinite number of probes $n \to \infty$ and taking the continuum limit $a \to 0$ by leaving $\frac{g}{a} = \frac{1}{l} = \text{const}$, the continuous energy transport is given by the equation

$$\partial_x \begin{pmatrix} T_1^2(x) \\ T_2^2(x) \end{pmatrix} = \frac{\gamma}{l} \begin{pmatrix} -\chi_1 n_2 & \chi_1 n_2 \\ \chi_2 n_1 & -\chi_2 n_1 \end{pmatrix} \begin{pmatrix} T_1^2(x) \\ T_2^2(x) \end{pmatrix} + \frac{e^2}{lh\kappa_0} \begin{pmatrix} 1 \\ -1 \end{pmatrix} (V_1(x) - V_2(x))^2 \ . \tag{3.36}$$

In the final heat transport equation the heat-wise equilibration between pairs of channels is taken into account (first term) as well as a contribution from Joule-heating (second term). This model describes only weak tunneling. Other transport regimes are described in [54].
For a system of length L with two counter-propagating channels ($\chi_1 = +$, $\chi_2 = -$) biased by a temperature gradient ΔT, the two terminal heat conductance G_{2t}^Q is found by solving the heat transport equation. Following the same algorithm as before (see Eq. (3.9)), the heat conductance becomes for $n_1 \neq n_2$

$$G_{2t}^Q = \frac{(n_1 - n_2)\left(n_1 + n_2 e^{-\frac{L}{l_{eq}^Q}}\right)}{n_1 - n_2 e^{-\frac{L}{l_{eq}^Q}}} \overset{L \gg l_{eq}^Q}{\longrightarrow} n_1 - n_2 \ . \tag{3.37}$$

The above introduced heat equilibration length $l_{eq}^Q = \frac{l}{\gamma(n_1 - n_2)}$ is in general quite different from the charge equilibration length l_{eq}^C allowing to view the transport of charge and heat on different characteristic length scales. In the limit $L \gg l_{eq}^Q$, the unique quantization of the heat transport expected from experiments is recovered [30]. In case of $n_1 = n_2 = n$, the heat conductance evaluates to the diffusive conductance

$$G_{2t}^Q = 2n \frac{l_{eq}^Q}{l_{eq}^Q + Ln\gamma} \overset{L \gg l_{eq}^Q}{\longrightarrow} 0 \ . \tag{3.38}$$

In the trivial case of co-propagating channels with n_1 and n_2, the heat conductance is independent of l_{eq}^Q and evaluates to

$$G_{2t}^Q = n_1 + n_2 \ . \tag{3.39}$$

Anticipating the prerequisites for following chapters, the above transport relations are generalized to an arbitrary number of channels N by the matrix equations [67]:

$$\partial_x \vec{V}(x) = M_V \vec{V}(x) \quad \text{and} \quad \partial_x \overrightarrow{T^2}(x) = M_T \overrightarrow{T^2}(x) + \Delta \overrightarrow{V^2}(x) \ . \tag{3.40}$$

In general, the matrices M_V and M_T become for an edge consisting of N channels [67]

$$M_V = \begin{pmatrix} -\frac{\sum_{k\neq 1} l_{1,k}^{-1}}{\chi_1\nu_1} & \frac{l_{1,2}^{-1}}{\chi_1\nu_1} & \cdots & \frac{l_{1,N}^{-1}}{\chi_1\nu_1} \\ \frac{l_{2,1}^{-1}}{\chi_2\nu_2} & -\frac{\sum_{k\neq 2} l_{2,k}^{-1}}{\chi_2\nu_2} & \cdots & \frac{l_{2,N}^{-1}}{\chi_2\nu_2} \\ \vdots & \vdots & \ddots & \vdots \\ \frac{l_{N,1}^{-1}}{\chi_N\nu_N} & \frac{l_{N,2}^{-1}}{\chi_N\nu_N} & \cdots & -\frac{\sum_{k\neq N} l_{N,k}^{-1}}{\chi_N\nu_N} \end{pmatrix} \quad \text{and} \tag{3.41}$$

$$M_T = \begin{pmatrix} -\frac{\sum_{k\neq 1} \tilde{l}_{1,k}^{-1}}{\chi_1 n_1} & \frac{\tilde{l}_{1,2}^{-1}}{\chi_1 n_1} & \cdots & \frac{\tilde{l}_{1,N}^{-1}}{\chi_1 n_1} \\ \frac{\tilde{l}_{2,1}^{-1}}{\chi_2 n_2} & -\frac{\sum_{k\neq 2} \tilde{l}_{2,k}^{-1}}{\chi_2 n_2} & \cdots & \frac{\tilde{l}_{2,N}^{-1}}{\chi_2 n_2} \\ \vdots & \vdots & \ddots & \vdots \\ \frac{\tilde{l}_{N,1}^{-1}}{\chi_N n_N} & \frac{\tilde{l}_{N,2}^{-1}}{\chi_N n_N} & \cdots & -\frac{\sum_{k\neq N} \tilde{l}_{N,k}^{-1}}{\chi_N n_N} \end{pmatrix}, \tag{3.42}$$

where the lengths $\tilde{l}_{m,n} = \frac{l_{m,n}}{\gamma_{m,n}}$ and $l_{m,n} = l_{n,m} = l_{m,n}^C$ resemble the heat and charge equilibration lengths corresponding to channel pairs (m,n). The Joule-heating contribution $\Delta\overrightarrow{V^2}(x)$ furthermore generalizes to

$$\Delta\overrightarrow{V^2}(x) = \frac{e^2}{h\kappa_0}\sum_{n=1}^{N}\left(\frac{(V_1(x)-V_n(x))^2}{l_{1,n}^C\chi_1},\ldots,\frac{(V_N(x)-V_n(x))^2}{l_{N,n}^C\chi_N}\right)^T . \tag{3.43}$$

In the following, the introduced model is applied to compute length dependent conductances for the measurement setups shown in Fig. 3.2. According to the length dependence of the equilibration mechanisms, three different regimes for counter-propagating modes of filling factors ν_+, ν_- and heat conductances n_+, n_- are distinguished

1. The *fully equilibrated regime* where the channel length is much bigger than the equilibration lengths $L \gg l_{eq}^{C(Q)}$.
2. The *intermediate regime*, where $L \approx l_{eq}^{C(Q)}$ and the conductances are length dependent.
3. The *fully non-equilibrated regime* where $L \ll l_{eq}^{C(Q)}$.

Since the incoherent tunneling model describes the transport between two macroscopic contacts, it is possible to define a *downstream* $G_+^{C(Q)}$ and *upstream* $G_-^{C(Q)}$ charge (heat) conductance for an edge segment that serve as *"new filling factors"* in a Landauer-Büttiker approach. In general the conductances for one edge segment are defined by:

$$G_{i,+} = \nu_+\frac{\nu_+-\nu_-}{\nu_+-\nu_-e^{-\frac{L_i}{l_{eq,i}^C}}} \quad \text{and} \quad G_{i,-} = \nu_-\frac{\nu_+-\nu_-}{\nu_+-\nu_-e^{-\frac{L_i}{l_{eq,i}^C}}} . \tag{3.44}$$

The equivalent heat conductances defined by relating the channels' heat currents at the drain to a corresponding conductance by

$$G_{i,+}^Q = \frac{d}{d\Delta T}J_{+,top}(L) \quad \text{and} \quad G_{i,-}^Q = \frac{d}{d\Delta T}J_{-,bot}(0) . \tag{3.45}$$

To simplify the expressions, symmetrical(homogeneous) properties of the segments are assumed leading to $L_i = L$ and $l_{eq,i}^{C(Q)} = l_{eq}^{C(Q)}$. The adjusted conductance matrices for charge(heat) transport $\boldsymbol{G}^{(Q)}(L)$ become

$$\boldsymbol{G}_n^{(Q)} = (G_+^{(Q)}+G_-^{(Q)})\mathbb{1}_n - G_+^{(Q)}\boldsymbol{P}_n - G_-^{(Q)}\boldsymbol{P}_n^{n-1} . \tag{3.46}$$

The charge conductances defined in Tab. 3.1 are summarized for transport in fractional quantum Hall edges in the considered setups and the different regimes below. Since measuring heat conductances is not as simple as measuring charge conductances, only the two terminal heat conductance G_{2t}^Q is considered in the heat regime[6]. The diffusive regime is covered in A.3.

[6] The temperatures needed to compute them are usually deduced from noise measurements.

$\nu_+ \neq \nu_-$		
Two terminal setup		
$G_{2t} = G_+ + G_-$	$G_{2t} \overset{L\gg l_{eq}^C}{\longrightarrow} \nu_+ - \nu_-$	$G_{2t} \overset{L\ll l_{eq}^C}{\longrightarrow} \nu_+ + \nu_-$
Hall-cross		
$G_{2t} = \dfrac{G_+^2 + G_-^2}{G_+ + G_-}$	$G_{2t} \overset{L\gg l_{eq}^C}{\longrightarrow} \nu_+ - \nu_-$	$G_{2t} \overset{L\ll l_{eq}^C}{\longrightarrow} \dfrac{\nu_+^2 + \nu_-^2}{\nu_+ + \nu_-}$
$G_H = -\dfrac{G_+^2 + G_-^2}{G_- G_+}$	$G_H \overset{L\gg l_{eq}^C}{\longrightarrow} \nu_+ - \nu_-$	$G_H \overset{L\ll l_{eq}^C}{\longrightarrow} \dfrac{\nu_+^2 + \nu_-^2}{\nu_+ - \nu_-}$
Hall-bar		
$G_{2t} = \dfrac{G_+^3 + G_-^3}{G_+^2 + G_+G_- + G_-^2}$	$G_{2t} \overset{L\gg l_{eq}^C}{\longrightarrow} \nu_+ - \nu_-$	$G_{2t} \overset{L\ll l_{eq}^C}{\longrightarrow} \dfrac{\nu_+^3 + \nu_-^3}{\nu_+^2 + \nu_+\nu_- + \nu_-^2}$
$G_H = -\dfrac{G_+^2 - G_+G_- + G_-^2}{G_-^2 - G_+^2}$	$G_H \overset{L\gg l_{eq}^C}{\longrightarrow} \nu_+ - \nu_-$	$G_H \overset{L\ll l_{eq}^C}{\longrightarrow} \dfrac{\nu_+^2 - \nu_1\nu_2 + \nu_-^2}{\nu_+ - \nu_-}$
$G_L = \pm\dfrac{G_+^3 + G_-^3}{G_+G_-}$	$G_L \overset{L\gg l_{eq}^C}{\longrightarrow} -\infty$	$G_L \overset{L\ll l_{eq}^C}{\longrightarrow} \pm\dfrac{\nu_+^3 + \nu_-^3}{\nu_+\nu_-}$
$n_+ \neq n_-$		
Two terminal setup		
$G_{2t}^Q = G_+^Q + G_-^Q$	$G_{2t}^Q \overset{L\gg l_{eq}^Q}{\longrightarrow} n_+ - n_-$	$G_{2t} \overset{L\ll l_{eq}^Q}{\longrightarrow} n_+ + n_-$
Hall-cross		
$G_{2t}^Q = \dfrac{G_{+,\mathrm{Q}}^2 + G_{-,\mathrm{Q}}^2}{G_{+,\mathrm{Q}} + G_{-,\mathrm{Q}}}$	$G_{2t}^Q \overset{L\gg l_{eq}^Q}{\longrightarrow} n_+ - n_-$	$G_{2t}^Q \overset{L\ll l_{eq}^Q}{\longrightarrow} \dfrac{n_+^2 + n_-^2}{n_+ + n_-}$
Hall-bar		
$G_{2t}^Q = \dfrac{G_{+,\mathrm{Q}}^3 + G_{-,\mathrm{Q}}^3}{G_{+,\mathrm{Q}}^2 + G_{+,\mathrm{Q}}G_{-,\mathrm{Q}} + G_{-,\mathrm{Q}}^2}$	$G_{2t}^Q \overset{L\gg l_{eq}^Q}{\longrightarrow} n_+ - n_-$	$G_{2t}^Q \overset{L\ll l_{eq}^Q}{\longrightarrow} \dfrac{n_+^3 + n_-^3}{n_+^2 + n_+n_- + n_-^2}$

The conductances are found to agree to the ones obtained for the mixing model in the limit of absent equilibration $L \ll l_{eq}^{C(Q)}$. Even though mixing in macroscopic contacts and equilibration along the edge seems to result in a similar effect, only the latter one is able to describe the transport in realistic setups. This is consolidated by the conductances of all setups approaching a unique value in the limit of full equilibration $L \gg l_{eq}^{C(Q)}$ as visualized in Fig. 3.6 for an example.

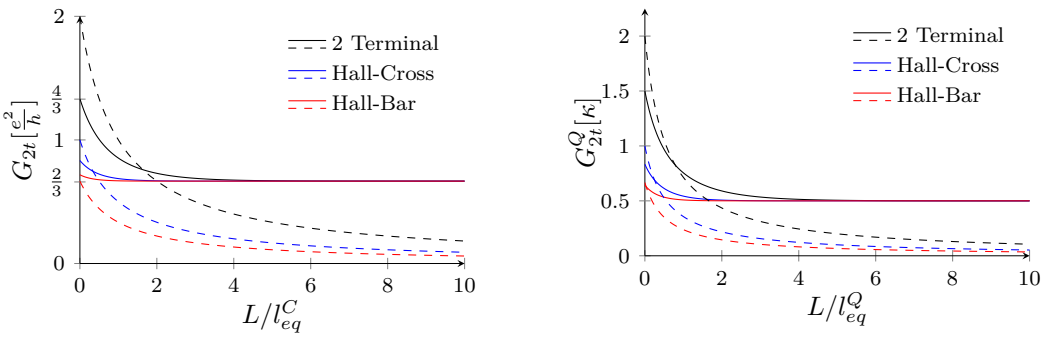

Figure 3.6: Comparison of the setups' charge conductance for $\nu_+ = 1$, $\nu_- = \frac{1}{3}$ (solid) and $\nu_+ = \nu_- = 1$ (dashed) on the left and their heat conductance for $n_+ = 1$, $n_- = \frac{1}{2}$ (solid) and $n_+ = n_- = 1$ (dashed) on the right, in terms of $L/l_{eq}^{C(Q)}$.

3.4 Noise Generation at the Edge

Whenever there are multiple channels carrying charge in opposite directions on one edge, charge partition noise (shot noise) can be measured. The partitioning mainly takes place within a distance l_{eq}^{C} of the contacts where full equilibration between counter-propagating modes is not given. This region is from now on referred to as the *noise spot*. The partitioning is enhanced for an increased temperature at the corresponding contact. This leads to interesting scenarios in the FQH regime where upstream heat transport from the *hotspot* to the *noise spot* is allowed resulting in an increased noise. In the following the incoherent tunneling model is used to describe the dependency of the noise on the channels temperature profiles along the channels. [66, 67, 69]

Using a similar approach as above for two counter propagating modes of filling $\nu_1 > \nu_2$, fluctuations in the charge current are computed. By convention the chiralities of the channels are set to $\chi_1 = +$ and $\chi_2 = -$. The total fluctuations of the tunneling current $\delta I_{\tau,j}$ is split into $\delta I_{\tau,j}^{int}$ describing the intrinsic temperature dependant fluctuations at the junction and $\delta I_{\tau,j}^{tr}$ representing the transmitted fluctuations in the virtual probes. While the intrinsic fluctuations cannot be defined in general since they depend on the applied biases as well as the edge structure of interest, the transmitted fluctuations are defined by

$$\delta I_{\tau,j}^{tr} = g\left(\delta V_{2,j+1} - \delta V_{1,j}\right) = g\left(\frac{\delta I_{2,j+1}}{\nu_2} - \frac{\delta I_{1,j}}{\nu_1}\right) . \tag{3.47}$$

Therefore the discrete transport model for the charge fluctuations becomes in matrix form

$$\vec{\delta I}_{j+1} = \boldsymbol{M}\vec{\delta I}_j + \vec{v}\delta I_{\tau,j}^{int} . \tag{3.48}$$

Imposing charge conservation, the matrix $\boldsymbol{M}$ and the vector $\vec{v}$are obtained by expanding for small tunneling probabilities g up to $\mathcal{O}(g)$. Introducing the total number of tunneling events N between the contacts, the model is used to compute the fluctuations at the drain ($j = N{+}1$). This is done by noting that charges undergo $N{+}1$ transitions between virtual probes and N tunneling events as they are transported from source to drain. Since the charge current fluctuation at an intermediate virtual probe j is influenced by the summed up effect of all previous tunneling events, the solution takes the form

$$\begin{pmatrix}\delta I_{1,N+1}\\ \delta I_{2,N+1}\end{pmatrix} = \boldsymbol{M}^{N+1}\begin{pmatrix}\delta I_{1,0}\\ \delta I_{2,0}\end{pmatrix} + \sum_{j=0}^{N}\boldsymbol{M}^{N-j}\vec{v}\delta I_{\tau,j}^{int} . \tag{3.49}$$

Introducing the dimensionless parameter $\alpha = \frac{\nu_2(g-\nu_1)}{\nu_1(g-\nu_2)}$, the problem simplifies to

$$\begin{pmatrix}\delta I_{1,N+1}\\ \delta I_{2,N+1}\end{pmatrix} = \begin{pmatrix}\frac{\nu_1-\nu_2\alpha^{N+1}}{\nu_1-\nu_2}\delta I_{1,0} + \frac{-\nu_1+\nu_1\alpha^{N+1}}{\nu_1-\nu_2}\delta I_{2,0} + \sum_{j=0}^{N}\alpha^{N-j}\delta I_{\tau,j}^{int}\\ \frac{\nu_2-\nu_2\alpha^{N+1}}{\nu_1-\nu_2}\delta I_{1,0} + \frac{-\nu_2+\nu_1\alpha^{N+1}}{\nu_1-\nu_2}\delta I_{2,0} + \sum_{j=0}^{N}\alpha^{N-j}\delta I_{\tau,j}^{int}\end{pmatrix} . \tag{3.50}$$

The fluctuation $\delta I_{2,0}$ at the source of channel two becomes

$$\delta I_{2,0} = \frac{\nu_1-\nu_2}{\nu_1\alpha^{N+1}-\nu_2}\delta I_{2,N+1} - \frac{\nu_2-\nu_2\alpha^{N+1}}{\nu_1\alpha^{N+1}-\nu_2}\delta I_{1,0} - \sum_{j=0}^{N}\frac{(\nu_1-\nu_2)\alpha^{N-j}}{\nu_1\alpha^{N+1}-\nu_2}\delta I_{\tau,j}^{int} . \tag{3.51}$$

The total fluctuation at contact two is defined by contributions from both channels by

$$\delta I_2 = \delta I_{1,N+1} - \delta I_{2,N+1} . \tag{3.52}$$

Inserting (3.51) into (3.50), δI_2 evaluates to

$$\delta I_2 = -\frac{\nu_1-\nu_2}{\nu_1\alpha^{N+1}-\nu_2}\delta I_{2,N+1} + \left(1 + \frac{\nu_2-\nu_2\alpha^{N+1}}{\nu_1\alpha^{N+1}-\nu_2}\right)\delta I_{1,0} + \sum_{j=0}^{N}\frac{(\nu_1-\nu_2)\alpha^{N-j}}{\nu_1\alpha^{N+1}-\nu_2}\delta I_{\tau,j}^{int} . \tag{3.53}$$

The noise corresponding to this fluctuation is defined by the average of the square of the fluctuations and takes in general the form

$$S_2 = \overline{\delta I_2^2} = \tilde{A}\overline{(\delta I_{2,N+1})^2} + \tilde{B}\overline{\delta I_{2,N+1}\delta I_{1,0}} + \sum_j \tilde{C}\overline{\delta I_{2,N+1}\delta I_{\tau,j}^{int}} + \tilde{D}\overline{(\delta I_{1,0})^2} + \sum_j \tilde{E}\overline{\delta I_{1,0}\delta I_{\tau,j}^{int}} + \sum_j \tilde{F}\overline{(\delta I_{\tau,j}^{int})^2} \ . \tag{3.54}$$

This equation now consists of different noise contributions. Terms one and four describe the noise originating from the macroscopic contacts two and one respectively. In the following they are renamed to $S_{2,R}$ and $S_{1,L}$. The second term describes the noise at the source of channel one influenced by the current fluctuations at the source of channel two and is neglected in the following. Terms three and five describe the connection of the noise at the tunneling junctions to the contacts and will be called $S_{2,x/R}$, $S_{1,x/L}$ respectively. The intrinsic noise at each junction is described by term six. Because the intrinsic noise is assumed to depend on the local temperature at the tunneling junction it is defined by a local noise kernel $\Lambda(x)$ that has to be defined by microscopic computations. The coefficients $\{\tilde{A}\dots\tilde{F}\}\setminus\tilde{B}$ are defined according to Eq. (3.54). Taking the continuum limit $N\to\infty$ by introducing $\Delta x_j = \frac{L}{N+1}$, the summations can be transformed into integrals by using Riemann's definition of integrals. Defining the equilibration length $l_{eq}^C = \frac{2L}{N\ln\alpha}$ [66] and $x = j\frac{L}{N}$, the continuous version of eq. (3.54) is found by expanding l_{eq}^C for small g to obtain

$$S_2 \approx \frac{2\nu_1\nu_2}{g l_{eq}^C(\nu_1-\nu_2)}\left[(AS_{2,R}+DS_{1,L}) + \int_0^L (CS_{2,x/R}+ES_{1,x/L})\,dx + 2g\int_0^L F\Lambda(x)\,dx\right] . \tag{3.55}$$

Where $\{A\dots F\}$ are the adjusted coefficients of the according contributions to the discrete noise in eq (3.54). They are obtained by $\{A\dots F\} = \lim_{N\to\infty}\{\tilde{A}\dots\tilde{F}\}$. In particular they take the values defined in Sec. A.4. It remains to define the expressions for the noise at the boundaries of the channel ($S_{2,R}$, $S_{1,L}$, $S_{2,x/R}$, $S_{1,x/L}$) as well as the noise kernel $\Lambda(x)$. Assuming local equilibrium at the tunnel junctions, the principle of detailed balance gives the opportunity to use thermal noise relations of the Johnson-Nyqvist form [70, 71]. Unfortunately, the assumption of local equilibrium noise doesn't hold in general and the channels' temperatures might be very different. In that case the non-equilibrium situation has too be investigated further. By neglecting the noise contributions from the contacts, the excess noise at contact two[8] S_2^{exc} is defined. For non-diffusive charge transport with $\nu_1 > \nu_2$, it becomes

$$S_2^{exc} = \frac{4\nu_1\nu_2(\nu_1-\nu_2)}{l_{eq}^C\left(\nu_1-\nu_2 e^{-\frac{2L}{l_{eq}^C}}\right)^2}\int_0^L \Lambda(x)e^{-\frac{4x}{l_{eq}^C}}\,dx \ . \tag{3.56}$$

In case of full (very efficient) charge equilibration and thus $L \gg l_{eq}^C$, it simplifies to

$$S_2^{exc} = \frac{4\nu_2}{\nu_1 l_{eq}^C}(\nu_1-\nu_2)\int_0^L \Lambda(x)e^{-\frac{4x}{l_{eq}^C}}\,dx \ . \tag{3.57}$$

In case of $\nu_1 = \nu_2 = \nu$ (diffusive charge transport) and by using the above approach with the equilibration length $l_{eq} = \frac{L(1-g)}{(N+1)g}$ [66], the noise at contact two takes the form

$$S_2 = \frac{1-g}{g l_{eq}}\left[(aS_{2,R}+dS_{1,L}) + \int_0^L (cS_{2,x/R}+eS_{1,x/L})\,dx + 2g\int_0^L f\Lambda(x)\,dx\right] . \tag{3.58}$$

The corresponding prefactors follow from the charge transport equation in the diffusive charge transport regime. They become

$$a = d = \frac{l_{eq}^2}{l_{eq}^2+L^2} \qquad c = -e = -\frac{l_{eq}^2}{(1-g)(l_{eq}+L)^2} \qquad f = \frac{l_{eq}^2}{(1-g)^2(l_{eq}+L)^2} \ . \tag{3.59}$$

Specifying the terms of interest for the case of interest as well as plugging in all of the necessary prefactors, S_2 is found by expanding the obtained expression for small g up to $\mathcal{O}(g)$.

[8] The excess noise at contact one and two are identical.

The obtained expressions for charge, temperature and noise transport at the edge of fractional quantum Hall systems are used to investigate the structure of different edges for different noise scenarios. The scenarios arise from charge and heat transport being decoupled in the FQH regime. In general there exist three different cases depending on the amount of heat transported in the upstream direction that are characterized by a new quantum number $\nu_Q = n_+ - n_-$ [67]. It resembles the heat analogue to the equilibrated filling factor $\nu = \nu_+ - \nu_-$ and similarly reveals intrinsic details of the edge.

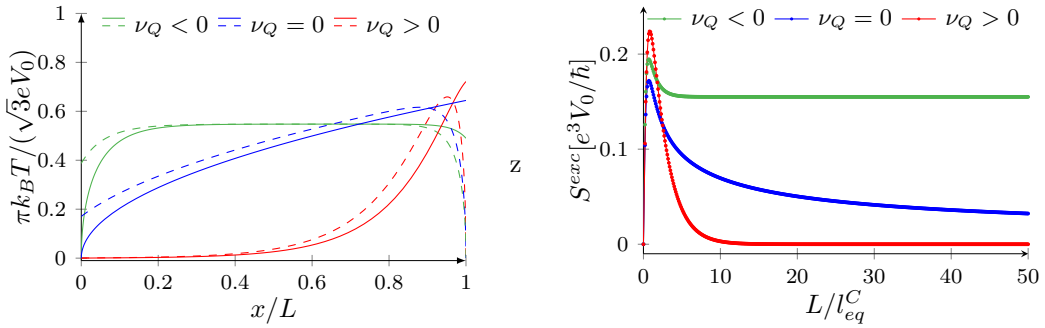

Figure 3.7: Plot of the temperature profiles (left) of channel one (solid) and two (dashed) for an applied voltage bias V_0 as well as the resulting excess noise (right) in terms of L/l_{eq}^C for $\nu_1 = 1$, $\nu_2 = \frac{1}{3}$, $n_1 = n_2 = 1$, $\nu_1 = 2$, $\nu_2 = \frac{1}{3}$, $n_1 = 2$, $n_2 = 1$ and $\nu_1 = 1$, $\nu_2 = \frac{2}{5}$, $n_1 = 1$, $n_2 = 2$

In case of equilibrated upstream heat transport $\nu_Q < 0$, the temperatures of the channels are non-zero basically over the entire channel length. Therefore tunneling will be enhanced leading to a constant noise independent of the channel length. For diffusive heat transport $\nu_Q = 0$, the temperature decays over the channel length from the hot spot close to $x/L = 1$ to the noise spot $x/L = 0$ leading to a vanishing noise for long channels. Equilibrated downstream heat transport on the other hand leads to an even lower increase in the temperature at the noise spot for channels much longer than the charge equilibration length. The noise is expected to decay exponentially over the channel length in this scenario. The ν_Q dependent behaviour of the noise is summarized according to [67] by[9]

$\nu_Q > 0$: Ballistic downstream heat transport $\Rightarrow S^{exc} \simeq e^{-L/l_{eq}^C}$

$\nu_Q = 0$: Diffusive heat transport $\Rightarrow S^{exc} \simeq \sqrt{L/l_{eq}^C}$

$\nu_Q < 0$: Ballistic upstream heat transport $\Rightarrow S \simeq$ const. for $L/l_{eq}^C \gg 1$

Having defined the transport characteristics as well as the generation of noise within the incoherent tunneling model, the theoretical insights are used in the following to compare the implications of different trial structures for the edge at filling 5/2 to experimental results.

[9] One can also view this in analogy to a fish school. If the majority of the fishes swims from left to right, one individual fish wont get very far swimming right to left without getting carried away by the rest. Therefore all fishes will eventually end up at the right position. Similarly, the net number of fishes ending up at the left position will be zero (diffusive) for two equally sized groups of fishes. In case of the majority of fishes going from right to left (ballistic upstream) all fishes will end up at the left position. To make the connection to the actual problem, the fishes resemble heat carriers.

4

Transport at the 5/2 Edge

In this chapter the incoherent tunneling model is used to describe the transport characteristics at the edge of filling 5/2 using various candidate edge theories. The obtained expressions for the heat conductance and noise of each candidate are then compared to recent experimental results to identify the theory describing the 5/2 edge best [30, 32]. This edge is of particular interest since it has been predicted to host non-Abelian anyons [31, 72–74] with potential use for quantum computation [22, 24].

4.1 Candidates for the 5/2 Edge

Since the edge structure of the 5/2 state is nothing that can be defined bottom up, one is restricted to compare experimental results probing specific features of this edge to trial theories. In this thesis the comparison is based on transport features of the edge. The considered trial theories are the particle-hole Pfaffian (phPf) [75–78], anti-Pfaffian (aPf) [79, 80] and Pfaffian (Pf) [72] structures which have been identified as potential candidates for the 5/2 edge before. They consist of a combination of bosonic channels and a Majorana channel[1] to recover the expected charge conductance of $G_{2t} = 5/2$. To get more evidence about the underlying edge structure, a method to distinguish between different candidates has been used in experiments [30, 32]. It is based on interfacing the 5/2 edge with different counter propagating integer channels in order to expose the exotic nature of the edge. The transport characteristics of the interfaced edges are then used to compare theoretical predictions of the candidates to experimental observations. In Fig. 4.1 the interfaced edges of interest are visualized using an arrow scheme that encodes the transport properties of the involved channels.
Whenever there are counter-propagating channels with identical transport characteristics, they become irrelevant for the transport[2]. Therefore pairs of counter propagating integer states between the candidates and $\nu \in \{2, 3\}$ can be removed from the description. This results in different reduced edge structures, visualized in Fig. 4.1).
An edge structure consisting of more than two channels after interfacing is called an intermediate model. It requires multiple steps to reach full charge and/or heat equilibration depending on the possible interactions between pairs of the involved channels. For the considered interfaces there exist only intermediate models in the heat transport regime since the Majorana does not carry charges on its own. Using the incoherent tunneling model (compare Sec. 3.3) for pairwise heat equilibration between multiple channels without an applied voltage, the heat conductance is obtained by solving the system of heat transport equations for the corresponding boundary conditions.

$$\overrightarrow{T^2}_{top(bot)}(L) = e^{LM_T}\overrightarrow{T^2}_{top(bot)}(0) \ . \tag{4.1}$$

In case of the phPf-3, the matrix M_T consists of the sum of pairwise heat interaction matrices between pairs of counter-propagating[3] channels

$$M_T = \frac{1}{l_{12}}M_T^1 + \frac{1}{l_{23}}M_T^2 \ . \tag{4.2}$$

[1] The existence of a Majorana mode was shown by measuring half-integer quantized heat conductance [29].
[2] For strong interactions (caused by large degree of disorder) this is due to "true" localization [10]. For weak interactions they still don't contribute to the transport for $L \gg l_{eq}^{C(Q)}$ due to their diffusive nature.
[3] In general, there also exists a matrix corresponding to interactions between the co-propagating ϕ and ψ. It is omitted since it doesn't change the heat conductance.

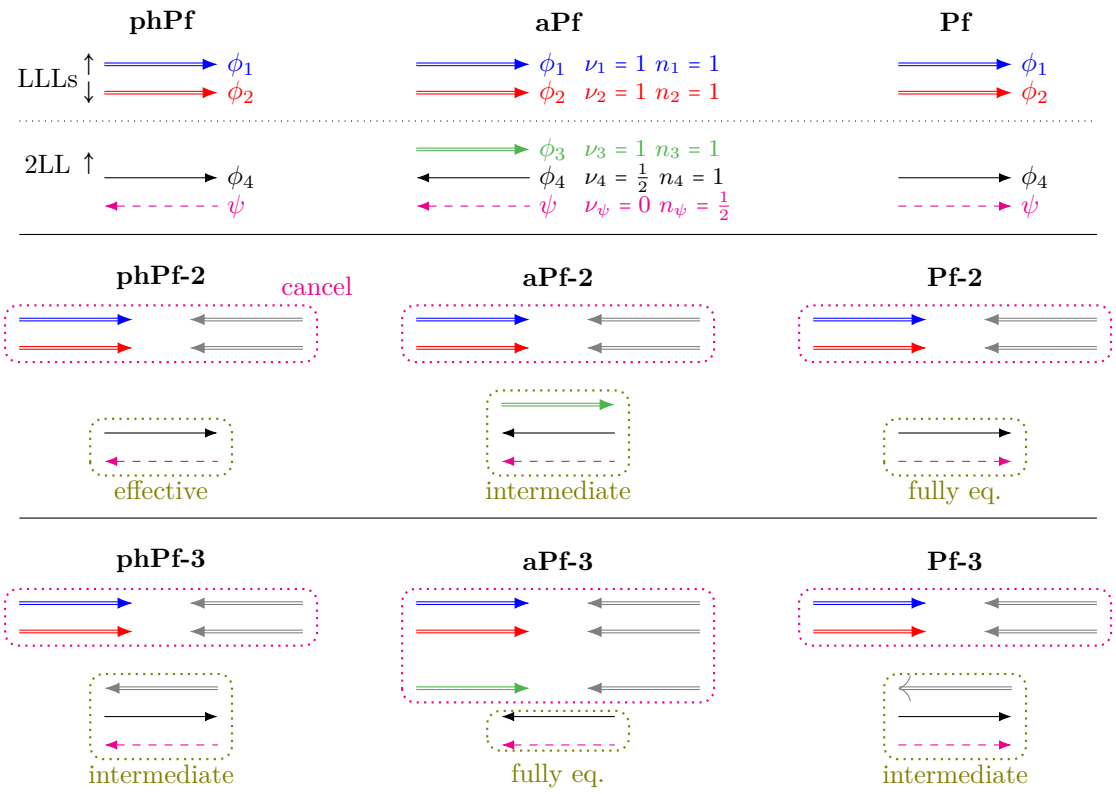

Figure 4.1: Interface between phPf, aPf and the Pf and counter-propagating $\nu \in \{0, 2, 3\}$ edges (gray). The chirality of the channels is defined by the arrows direction (positive: left to right).

They correspond to the equilibration interaction between the following pairs channels

$$M_T^1 \widehat{=} (\phi, \phi_4) \quad \text{and} \quad M_T^2 \widehat{=} (\phi_4, \psi) \ . \tag{4.3}$$

They furthermore depend on the equilibration lengths l_{ij} given by the interactions between the involved modes i and j [4]. The two terminal heat conductances of the interfaces are computed using the channels heat conductances n_1, n_2, n_3 and imposing the boundary conditions corresponding to the channels' chiralities. Throughout the following computations, the direction corresponding to positive chirality on the top edge is defined as "left to right" and biases are applied accordingly.
An edge structure is called to be an effective one if interfacing the candidate with $\nu \in \{2, 3\}$ leads to an edge structure of two counter-propagating modes. Therefore the results of the two channel transport model introduced in Sec. 3.3 can be used directly and only one step is needed to achieve full equilibration.
A fully equilibrated model on the other hand consists of co-propagating modes, leading to no further equilibration.
The difference between an intermediate and an effective model becomes visible when computing the length dependent two terminal heat conductance $G_{2t}^Q(L)$ shown in Fig. 4.2. Whereas the effective model (phPf$-$2) shows only one transition, the intermediate models (aPf$-$2, Pf$-$3 and phPf$-$3) show two transitions at different length scales I and II representing the different length dependencies of the underlying mechanisms of equilibration. In these plots it is furthermore indicated that the two transitions in the intermediate model are only possible to be resolved if the length scales for I and II are very different. The closer l_{eq}^I gets to l_{eq}^{II} the less distinct the plateau at $G_{2t}^Q = 3/2$ becomes. These plots were created using a self-written module for Mathematica presented in Sec. A.9.
The existence of transport in opposite directions also gives the opportunity to look into noise characteristics at the edges. Upstream heat transport allows for some finite increase in the

[4] Interactions involving the Majorana mode ψ can not be explained by electron tunneling into (out of) the Majorana channel.

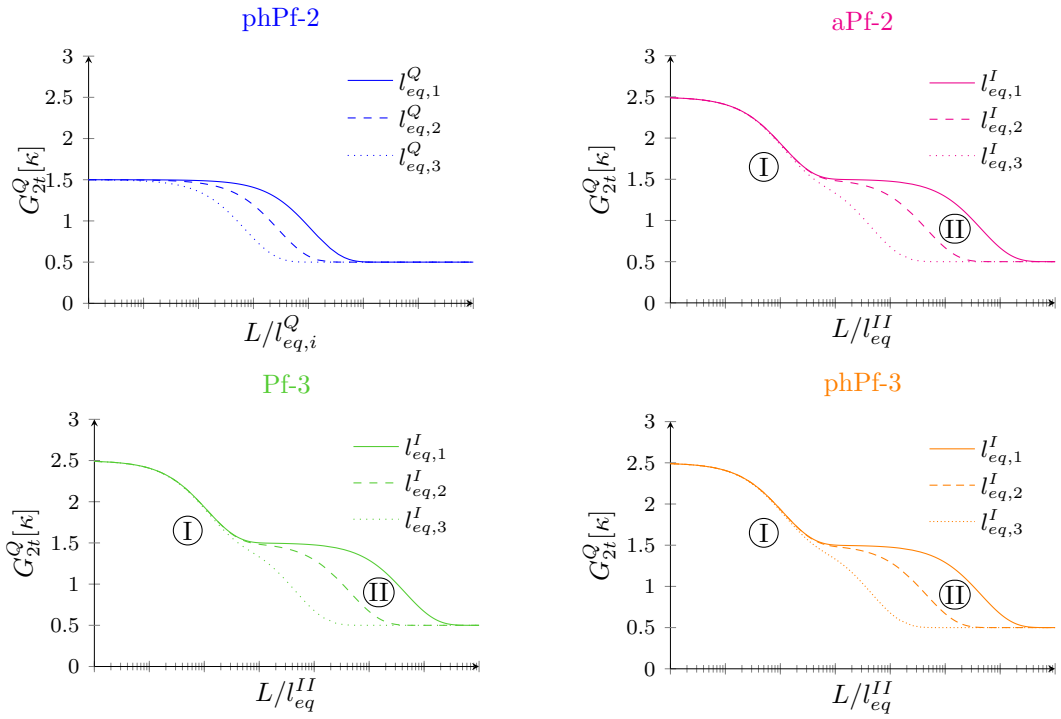

Figure 4.2: Visualization of the two terminal heat conductance in dependency of the degree of thermal equilibration between the involved modes. The graphs are obtained for different thermal equilibration lengths $L/l^I_{eq,i} \in 8 \cdot \{10^2, 10^3, 10^4\}$ (solid, dashed, dotted) and $L/l^{II}_{eq,1} = 10^5$.

temperature at the upstream contact which is measured by increased thermal noise. The magnitude of the noise depends heavily on how well the channels at the interface equilibrate and thus how much heat arrives at the upstream contact. Therefore an intricate relation between charge, heat and noise transport exists depending on the specific length scales for charge and heat transport.

Depending on the considered length scale, the structures are expected to show well-defined transport and noise behaviour. Considering the case of $L \ll l^{C(Q)}_{eq}$, all of the edge structures are assumed to show non-uniform charge and heat transport properties. Within this regime the cancellation of the interfaced integer modes is not given and noise is expected for all of the edge structures. Even though this length scale might not be resolvable in experiments, it might explain some "left over" noise at the edges of structures that are not expected to show noise in first place. The non-universal values describing the transport on different length scales vary between the fully equilibrated (G^Q_{eq}, G^C_{eq}) and fully non-equilibrated (G^Q_{neq}, G^C_{neq}) values. They are calculated by:

$$G^C_{neq} = \sum_i \nu_i \ , \qquad G^C_{eq} = \sum_i \chi_i \nu_i \ , \qquad G^Q_{neq} = \sum_i n_i \quad \text{and} \quad G^Q_{eq} = \sum_i \chi_i n_i \ . \tag{4.4}$$

For the edge structures of interest the corresponding values are shown in Tab. 4.1. Unless stated otherwise the cancellation of the integer channels is assumed to take place on a length scale much smaller than the smallest length of interest in the following. This leads to the notion of noise only in the intermediate and effective models since the fully eq. models don't allow for upstream heat transport.[5]

Assuming that only one edge structure describes the 5/2 edge over all length scales, the phPf is predicted to describe the edge transport best. This prediction is based on measurements of the heat conductance for the bare 5/2 structure and at the interface 5/2-3 which showed values of 5/2 and 1/2 respectively. Since this is not agreeing with the aPf and Pf edges [30], the phPf edge poses the best candidate and is therefore in the focus of computations.

To connect the phenomenological model to microscopic insights, the charge (heat) currents at the edge are computed using CFT in the upcoming sections. Therefore, the unperturbed dynamics

[5] In the intermediate models one can furthermore think about the noise as being due to partitioning of charges.

Table 4.1: Comparison of the different edge structures' heat (G^Q) and charge (G^C) conductance in the fully non-equilibrated (neq) and the fully equilibrated (eq) limit. Measurements in an experiment may take values within these limits. Only absolute values are considered.

	phPf	aPf	Pf	phPf-2	aPf-2	Pf-2	phPf-3	aPf-3	Pf-3
G^Q_{neq}	3.5	4.5	3.5	5.5	6.5	5.5	6.5	7.5	6.5
G^Q_{eq}	2.5	1.5	3.5	0.5	0.5	1.5	0.5	1.5	0.5
G^C_{neq}	2.5	3.5	2.5	4.5	5.5	4.5	5.5	6.5	5.5
G^C_{eq}	2.5	2.5	2.5	0.5	0.5	0.5	0.5	-0.5	0.5

of the bosonic and Majorana edge channels are defined by the K-matrix action S_ϕ (compare Sec. 2.5) and the action for a Majorana fermion S_ψ by [81]

$$S_\phi = -\frac{1}{4\pi\nu}\iint \left[\chi_\phi \partial_t\phi\partial_x\phi + v(\partial_x\phi)^2\right] dx\,dt \quad \text{and} \tag{4.5}$$

$$S_\psi = -\iint \left[\chi_\psi \psi i\partial_t\psi + u\psi i\partial_x\psi\right] dx\,dt\ . \tag{4.6}$$

Interactions and thus the effect of equilibration between the channels are modelled by perturbations of the modes' actions and depend on the type of involved channels. Charge equilibration between channels of opposite chirality is achieved by tunneling processes between the channels. At each of the tunneling points charge is conserved locally meaning that an electron is annihilated in the initial channel i and created in the final channel f. In terms of electron operators the perturbation is described by the action

$$S_\tau = -\frac{\Gamma_0}{2\pi b}\iint \left[f(x)\Psi^\dagger_{e,f}\Psi_{e,i} + \text{h.c.}\right] dx\,dt = -\frac{\Gamma_0}{2\pi b}\iint \left[f(x)e^{i\left(\frac{\phi_f}{\nu_f}+\frac{\phi_i}{\nu_i}\right)} + \text{h.c.}\right] dx\,dt\ . \tag{4.7}$$

In some scenarios it is more efficient to think about the tunneling of quasiparticles. The tunneling of one electron then corresponds to the tunneling of ν^{-1} quasiparticles of charge $e^* = \nu e$ from an initial to a final channel. According to the definition of creation and annihilation operators of quasiparticles and the commutation relations (compare Sec. 2.5), the tunneling action for pairwise interactions takes the form

$$S_\tau = -\frac{\Gamma_0}{2\pi b}\iint \left[f(x)\Psi^\dagger_{qp,f}\Psi_{qp,i} + \text{h.c.}\right] dx\,dt = -\frac{\Gamma_0}{2\pi b}\iint \left[f(x)e^{i(\phi_f+\phi_i)} + \text{h.c.}\right] dx\,dt\ . \tag{4.8}$$

Above, the cut off b from the bosonization procedure has been re-introduced for the electron and quasiparticle description. The function $f(x)$ can be adjusted to cover the cases of point contact tunneling $f(x) = \delta(x)$ and random Gaussian correlated tunneling $f(x) = \xi(x)$, with $\langle\xi^a(x)\xi^b(x')\rangle = W\delta_{a,b}\delta(x-x')$. For processes that cannot be described by the tunneling of an electron such as between a charged bosonic and a neutral Majorana mode this interaction term cannot be used. Instead the simplest possible interaction term between these modes is used [82]

$$S' = -\Gamma_0\iint \delta(x)\partial_x\phi\psi i\partial_x\psi\,dx\,dt\ . \tag{4.9}$$

To understand the impact of different perturbations on the bare modes actions, the operators of allowed perturbations are analyzed from a scaling dimension perspective in the following.

4.2 Scaling Dimension Analysis of viable Perturbations

In general, the scaling dimension analysis is used to describe the rescaling properties of a local operator under spacetime dilations $x^\mu \to \lambda x^\mu$ [83]. It therefore gives a more intuitive way of looking at the renormalization of a viewed theory. For a scale invariant theory each operator rescales by a factor of λ^Δ under spacetime dilations, where Δ describes the scaling dimension of

the operator. This furthermore means that the two point-correlation function depends on the square of the distance by

$$\langle O(x,0)O^\dagger(0,0)\rangle \sim x^{-2\Delta} \tag{4.10}$$

For a bosonic mode with filling $\nu = \frac{1}{m}$, the Luttinger liquid propagator [14, 44] is furthermore used to obtain

$$\langle e^{im_j\phi_j(x,0)}e^{-im_j\phi_j(0,0)}\rangle = e^{m^2\langle\phi(x,0)\phi(0,0)\rangle} \sim x^{-m^2\nu} \tag{4.11}$$

which further implies that the scaling dimension for electron tunneling in the Luttinger liquid becomes

$$\Delta = \frac{m^2\nu}{2} \overset{\text{el. tun.}}{=} \frac{m}{2} \tag{4.12}$$

In the following the scaling dimension analysis is used to describe the temperature dependence of the heat equilibration length l_{eq}^Q in the conformally invariant theory of the 5/2 - ν edge. By assigning scaling dimensions Δ_- and Δ_+ to the operators corresponding to the left and right moving fields accordingly, the overall scaling dimension of the perturbation is obtained by the total scaling dimension $\Delta = \Delta_+ + \Delta_-$. To assign some temperature scaling corresponding to Δ, the following constraints are imposed to have a properly defined theory:

1. The action S has to be dimensionless.
2. The heat conductance G has to be dimensionless in 1D.

The latter one is visualised by noting that the conductivity has length dimension -1 in 1D. Therefore the heat conductance is required to have length dimension zero. Imposing the first requirement leads to

$$[S] \overset{!}{=} 0 \quad \Rightarrow \quad [\Gamma_0] = 1 - \Delta \tag{4.13}$$

Therefore the dimension of Γ_0 depends on the scaling dimension of the perturbation. In order to have $[G] \overset{!}{=} 0$, the external influence on the heat conductance [6] has to balance the dimension of Γ_0. Depending on the experimental setup this might be a voltage or a temperature. In the following only the case of a temperature dependence is considered since it will be mostly used to describe the temperature scaling of the heat equilibration length l_{eq}^Q. Using Fermi's golden rule it follows [7]

$$G \overset{eV \ll k_BT}{\sim} |\Gamma_0|^2 T^\alpha \quad \Rightarrow \quad \alpha = 2(\Delta - 1) \tag{4.14}$$

Where the scaling exponent of the temperature α directly depends on the scaling dimension of the operator. To find the proper value of Δ for the different edge structures, the most relevant perturbation operators O' have to be defined. The most relevant operators for the different edge structures are summarized in Tab. 4.2.

Table 4.2: Overview of the scaling dimensions Δ for the most relevant perturbation operators of the previously introduced interfaces shown in Fig. 4.1. The deduced temperature scaling exponent α, defined by $l_{eq,Q} \sim 1/g \sim 1/G \sim T^{-\alpha}$, is shown in the last column.

Interface	operator	Δ	α
phPf-2 (effective)	$\partial_x\phi_4 i\psi\partial_x\psi$	3	4
phPf-3 (intermediate)	$\psi e^{i(2\phi_4+\phi_3)}$	2	2
phPf-3 (effective)	$\partial_x\phi_4 i\psi\partial_x\psi$	3	4
aPf-2 (intermediate)	$\psi e^{i(2\phi_4+\phi_3)}$	2	2
aPf-2 (effective)	$\partial_x\phi i\psi\partial_x\psi$	3	4
Pf-3 (intermediate)	$\psi e^{i(2\phi_4+\phi_3)}$	2	2
Pf-3 (effective)	$\partial_x\phi_4 i\psi\partial_x\psi$	3	4

[6] The heat conductance is connected to the incoherent tunneling model by $G = g\kappa$.

4.3 Heat Conductance of the effective phPf-3 Edge

To uncover microscopic insights about the heat equilibration at the edge of the effective phPf-3 interface, a perturbative approach is used to describe the adjacent heat interaction. The intermediate phPf-3 is predicted to equilibrate at first charge wise and then heat wise[7], leading to a schematic path of equilibration as shown below in Fig. 4.3.

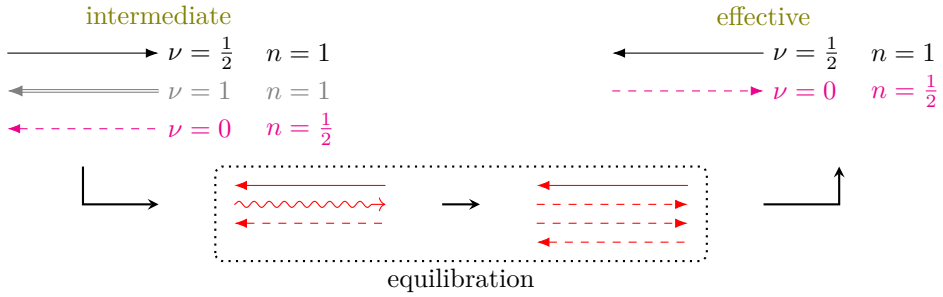

Figure 4.3: Phenomenological visualization of the equilibration from the intermediate model to the effective model of the phPf-3 edge by tunneling charges between the bosonic modes (solid arrows) and subsequent heat equilibration between neutral (curly arrow) and Majorana modes (dashed arrow). The so obtained effective model describes transition II in Fig. 4.2.

Starting from the non-interacting quadratic theory $S_0 = S_\phi + S_\psi$, defined by the bosonic K-matrix action S_ϕ and the Majorana action S_ψ (Eq. (4.5) and (4.6)), a small perturbation is added to account for a heat wise interaction between the modes. The perturbation of interest is the one with the smallest possible scaling dimension for the interaction of a bosonic and a Majorana mode. In the following a point interaction term at the interaction site $x = 0$ as defined in Eq. (4.9) is considered.
To simplify the following calculation, the field operators are separated into right (+) and left (-) moving ones. Products of field operators are further merged into a single field operator. The convention used in the computation is given by

$$T_- = (\partial_x \phi)^2 \ , \quad T_+ = \psi i \partial_x \psi \quad \text{and } O_- = \partial_x \phi \qquad O_+ = T_+ \tag{4.15}$$

where $T_{+(-)}$ resemble the energy density of the channel with corresponding chirality +(-). Rewriting the velocities $v_+ = \sqrt{2\pi}u$ and $v_- = v$, the Hamiltonians take the form

$$H_0 = \hbar \int dx \Big[\frac{v_+}{\sqrt{2\pi}} T_+ + \frac{v_-}{2\pi} T_- \Big] \qquad H' = \Gamma_0 O_-(0) O_+(0) \ . \tag{4.16}$$

To start the perturbative approach, the ground state energy (heat) current corresponding to the Hamiltonians at the drain is defined according to [84]

$$J_+^{(0)}(d,t) = \hbar \frac{v_+^2}{2\pi} T_+(\tilde{t}) \qquad J_-^{(0)}(d,t) = \hbar \frac{v_-^2}{2\pi} T_-(\tilde{t}) \ , \tag{4.17}$$

where $\tilde{t} = t - \frac{d}{v_i}$ is a shifted time referring to the transport of energy from source to drain by modes having some velocity. The average heat current is computed on top of the ground state energy current by using the Kubo formula in the interaction picture

$$\langle J_Q(t) \rangle = \langle \mathcal{T} e^{\frac{i}{\hbar} \int_t H'(t)} J_Q^{(0)}(\tilde{t}) e^{-\frac{i}{\hbar} \int_t H'(t)} \rangle \ , \tag{4.18}$$

[7] It is based on the experimental results of [30] indicating that the charge transport is equilibrated while the heat transport is not yet fully equilibrated.

with $\mathcal{T}$ denoting time ordering of the following operators. The operators including the time evolution are expanded for small tunneling amplitudes up to $\mathcal{O}(\Gamma_0^2)$ by using the identity of time-ordering Eq. (A.1). Collecting terms corresponding to the same order in Γ_0, the first and second order correction to the heat current become

$$J_Q^{(1)}(t) = \frac{i}{\hbar}\int_{-\infty}^{t} dt'[H'(t'), J_Q^{(0)}(\tilde{t})] \quad \text{and} \tag{4.19}$$

$$J_Q^{(2)}(t) = \frac{i^2}{\hbar^2}\int_{-\infty}^{t} dt' \int_{-\infty}^{t'} dt''[H'(t''), [H'(t'), J_Q^{(0)}(\tilde{t})]] \ . \tag{4.20}$$

Imposing conservation of energy only the left-moving part of the chiral energy current is considered in the following. The simplified expressions for the corrections to the heat current are obtained by applying the tools of CFT. After some computational steps including the OPE fields (carried out in Sec. A.6), the final result is obtained. For the first order correction to the heat current it follows that $\langle J_Q^{(1)}\rangle = 0$. Thus, only the second order contribution to the heat current gives rise to equilibration between ϕ and ψ. Visually, this means that $\langle J_{Q,-}^{(2)}\rangle$ can be associated with the total interaction current between the two modes. The total heat current thus takes the form

$$\langle J_{Q,-}\rangle = \langle J_{Q,-}^{(0)}\rangle + \langle J_{Q,-}^{(1)}\rangle + \langle J_{Q,-}^{(2)}\rangle = \langle J_{Q,-}^{(0)}\rangle + \langle J_{Q,-}^{(2)}\rangle \ . \tag{4.21}$$

Since conservation of energy has already been imposed, these expressions are related to the chiral energy currents and the heat interaction current following the visualization in Fig. 4.4 at the point contact

$$\langle J_{Q,-}^{out}\rangle = \langle J_{Q,-}^{in}\rangle + \langle J_{Q,-}^{int}\rangle \ . \tag{4.22}$$

By comparison, it follows that

$$\langle J_{Q,-}^{in}\rangle \equiv \langle J_{Q,-}^{(0)}\rangle \qquad \langle J_{Q,-}^{out}\rangle \equiv \langle J_{Q,-}\rangle \qquad \langle J_{Q,-}^{int}\rangle \equiv \langle J_{Q,-}^{(2)}\rangle \ . \tag{4.23}$$

Following the computational steps carried out in Sec. A.7, the heat interaction current thus evaluates to

$$\langle J_Q^{(2)}\rangle = \frac{32b^2k_B^6\pi^7\Gamma_0^2 c\nu}{105\hbar^7 v_-^2 v_+^4}T^5\Delta T \ . \tag{4.24}$$

Therefore the resulting heat conductance at the junction becomes with the central charge of the fermionic Majorana mode $c = 1/2$ and the filling fraction of the bosonic mode $\nu = 1/2$

$$G_{int}^Q = \frac{d}{d\Delta T}\langle J_Q^{(2)}\rangle = \frac{8b^2k_B^4\pi^5\Gamma_0^2}{35\hbar^6 v_-^2 v_+^4}T^4\kappa \ . \tag{4.25}$$

The so defined heat conductance should be thought of as a "*heat interaction conductance*" since the underlying interaction is not based on tunneling mechanisms. As expected, this result recovers the temperature scaling of the scaling dimension argument in Sec. 4.2. Referring to the phenomenological description of the edge, the interaction heat conductance G_{int}^Q is associated to the unit less parameter g which is furthermore connected to the lengths defined within the incoherent tunnelling model l and l_{eq}^Q by

$$l_{eq}^Q = \frac{l}{\gamma(n_\phi - n_\psi)} = \frac{2a}{g\gamma} = \frac{2a\kappa}{G_{int}^Q\gamma} \sim \frac{1}{T^4} \ , \tag{4.26}$$

where γ denotes the deviation from the Wiedemann-Franz law. Therefore the computation makes it possible to connect microscopic properties of the edge to the temperature scaling of the heat equilibration length and thus the heat conductance which is a macroscopic observable.

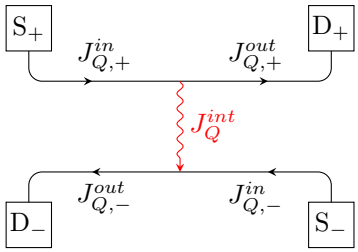

Figure 4.4: Phenomenological description of the point contact interaction with channels $+(-)$ emanating from source $S_{+(-)}$.

4.4 Noise at the intermediate phPf-3 Edge

Following the approach in [32], the noise generated at the interface by injecting a source current I_{in} in the source contact S is computed in the following. A schematic view of the experimental setup is given in Fig. 4.5. The authors of [32] indicate that the experiments took place in the regime of fully equilibrated charge but not fully equilibrated heat transport. This leads to the constraint on the charge conductance $G_{2t} = \left|\nu_{eq,5/2} - \nu_{eq,Int}\right|$. In the considered case of $5/2 - 3$ this means that $G_{2t} = 0.5$. To ensure this value in the incoherent tunneling model, the dependence of the charge conductance on δ is examined for different $\delta \in \{0.01, 0.1, 0.15\}$, where δ is defined by

$$\delta = l^C_{eq}/L \ . \tag{4.27}$$

For $\delta = 0.01$, the deviation from the expected value becomes immeasurable small which indicates it to be a good choice for further usage within the regime of full charge equilibration. For $\delta = 0.1$, the deviation is $\approx 0.005\%$ and therefore still in a reasonable range. The measured charge conductance furthermore indicates that the integer channels of the edges cancel on very small length scales.

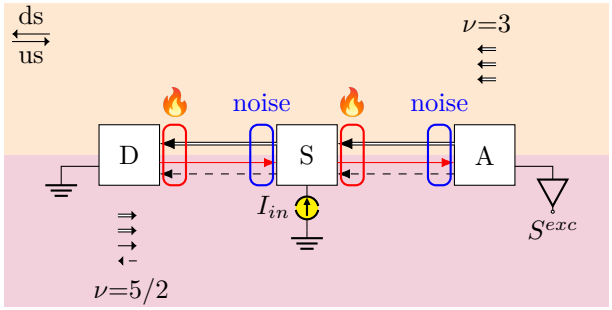

Figure 4.5: Schematic drawing of the experimental setup used to measure the excess noise S^{exc} at the interface of 5/2 and 3 by injecting a current I_{in} at the source S and measuring the noise at the amplifier A [32]. Using the predicted phPf edge, the majority of the charge and heat is transported downstream (ds) from S to drain D. For not fully equilibrated thermal transport it is possible to observe noise at the upstream (us) amplifier by the red channel transporting heat upstream.

At the interface, the edge is resembled by the intermediate phPf-3. Injecting a current into this interface[8] leads to voltage drop along the edge that is visualized in Fig. 4.6 for the considered values of δ. The characteristic drop of the voltage in the region close to $x/L = 0$ leads to the formation of a *hotspot* denoted by fire symbols in Fig. 4.5. The generated heat is then transported away from the *hotspot* by the channels at the interface. In the case of the phPf-3 edge, the channel marked in red (ϕ_2) in Fig. 4.5 allows for heat transport in the upstream direction leading to an increased temperature at the amplifier contact (A) measured by an increased excess noise S^{exc} in general. Depending on the degree of thermal equilibration between the channels at the edge, the measured S^{exc} is expected to take different values. In case of very good thermal

[8] Which is equivalent to applying a voltage bias between source and drain.

equilibration, the majority of the heat is transported downstream and the temperature at the upstream contact is only slightly altered. Imposing very good charge equilibration this leads to vanishing noise at contact A. In case of absent thermal equilibration on the other hand, the heat equilibration length $l_{eq}^{Q} \to \infty$ implies $M_T \to 0$ in the incoherent tunneling model. Therefore the channels' temperatures are constant upon leaving the *hotspot*. The corresponding noise is expected to be constant and independent of the channel length L, similar to the case $\nu_Q < 0$ in the phenomenological model for two channels (see Sec. 3.4). To compute the noise in the various cases, the incoherent tunneling model is supplemented with a microscopical description of the noise kernel $\Lambda(x)$ [30].
The edge dynamics of the intermediate PHPf-3 are defined in the bosonized language of the chiral Luttinger liquid according to the adjacent modes (see Sec. 4.1). The most relevant perturbation in this scenario is the point contact tunneling with amplitude Γ_0 at $x = 0$, given by the Hamiltonian

$$H_\tau = \frac{\Gamma_0}{2\pi b} \int \delta(x) \left(\psi e^{i(\phi_1 + 2\phi_2)} + \text{h.c} \right) dx \ . \tag{4.28}$$

With the definition of the excess noise in the incoherent tunneling model (see Eq. (3.57)), it remains to compute the noise kernel $\Lambda(x)$ in terms of the local temperatures $T_{+(-)}(x)$ of the downstream (+) and upstream channels (−) as well as the voltage difference $\Delta V(x)$ by [55][85]

$$\Lambda(x) = \frac{\hbar S^{loc}(\Delta V(x), T_+(x), T_-(x))}{2 g^{loc}(\Delta V(x), T_+(x), T_-(x))} \ , \tag{4.29}$$

where $S^{loc}(x)$ and $g^{loc}(x)$ denote the local noise and charge conductance. Starting from a perturbative approach in the interaction picture, the tunneling current I_τ, its' deviation from the average and thus the noise are obtained. Therefore the resulting terms for S^{loc} and g^{loc}, expressed by the operator O of the tunneling Hamiltonian H_τ take the form [55]

$$S^{loc}(x) = 4 \int_{-\infty}^{\infty} \cos\left(\frac{e\Delta V(x)\tau}{\hbar} \right) \langle O(\tau, 0) O^\dagger(0, 0) \rangle \, d\tau \quad \text{and} \tag{4.30}$$

$$g^{loc}(x) = 2i \int_{-\infty}^{\infty} \tau \langle O(\tau, 0) O^\dagger(0, 0) \rangle \, d\tau \ . \tag{4.31}$$

To compute these expressions, the modes' Greens' functions are used to rewrite the correlator of interest. It takes the form

$$\langle O(\tau, 0) O^\dagger(0, 0) \rangle = \frac{\Gamma_0^2}{(2\pi b)^2} G_\psi(\tau, 0) G_{\phi_1}(\tau, 0) G_{\phi_2}(\tau, 0) \ , \tag{4.32}$$

with b being a cut-off introduced in the bosonization procedure. Since this expression depends on the individual modes temperatures which are in general quite different, some assumptions on these temperatures have to be made to solve for the noise kernel. In case **(i)** of all channels being at the same temperature T, the case of very good heat equilibration and thus very short thermal equilibration lengths between the involved modes l_{ij} is viewed first. Performing the computation (see Sec. A.8), the resulting noise kernel evaluates to the expected equilibrium Johnson-Nyqvist form [70, 71]

$$\Lambda_i(x) = 2 k_B T(x) \ . \tag{4.33}$$

To simplify the description of the degree of thermal equilibration, the dimensionless parameters α and β are introduced to describe the equilibration behaviour depending on the pairwise equilibration between the involved modes[9] by

$$\alpha = \frac{l_{12}}{L} \quad \text{and} \quad \beta = \frac{l_{23}}{L} \ . \tag{4.34}$$

Here, the subscripts 1,2 and 3 refer to the channels ϕ_1, ϕ_2 and ψ respectively. The temperature profiles of the three channels are visualized in Fig. 4.6 for an applied voltage bias of $\Delta V = V_0$.

[9] The equilibration process between the co-propagating channels 1 and 3 is neglected since it has very low impact in general.

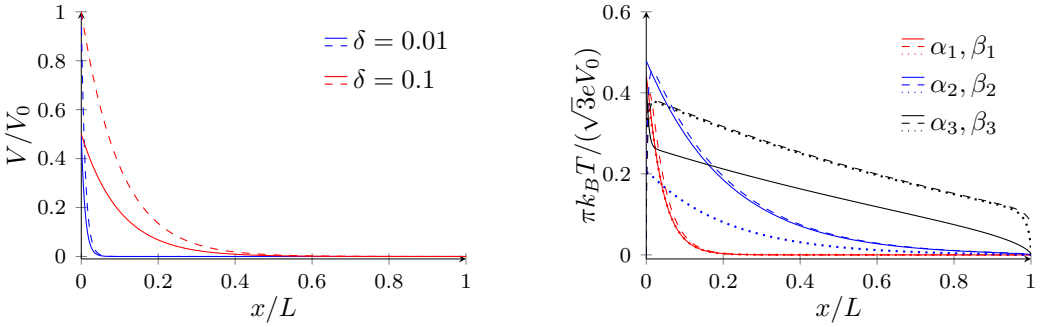

Figure 4.6: Visualization of the voltage profiles in terms of the charge equilibration coefficient δ (left) and the temperature profiles of ϕ_1 (solid), ϕ_2 (dashed) and ψ(dotted) for $(\alpha_i, \beta_i) \in \{(0.01, 0.01), (0.01, 0.5), (0.5, 0.01)\}$ and $\delta = 0.01$.

They justify the assumption of case **(i)** to hold for very short thermal equilibration lengths $\alpha \approx \beta \ll 1$. Since the temperatures drop very fast to zero, noise is expected to be exponentially suppressed as in the case of $\nu_Q > 0$ for the two channel analogue. In the slightly different cases of **(ii,1)** defined by $\alpha \ll \beta < 1$ and **(ii,2)** defined by $1 > \alpha \gg \beta$, two of the channels are at very similar temperatures. Thus, it looks intuitive to use an adjusted thermal equilibration, where only two temperatures are equal and the remaining one is within some range of them. Depending on the viewed case, the ratio $\kappa_{1j}(x) = \frac{T_1(x)}{T_{j\in\{2,3\}}(x)}$ is defined for $j \in \{2, 3\}$. The noise kernels are then computed for small deviations of $\kappa_j(x)$ from the equilibrium value $\kappa_j(x) = 1$. They take an adjusted Nyqvist form[10] (derivation in Sec. A.8)

$$\alpha \ll \beta < 1 \quad \Rightarrow \quad T_1(x) \approx T_2(x) \quad \Rightarrow \quad \Lambda_{ii,1}(x) = \frac{3\kappa_{13}(x) - 7}{\kappa_{13}(x) - 3} k_B T_1(x) \tag{4.35}$$

$$1 > \alpha \gg \beta \quad \Rightarrow \quad T_2(x) \approx T_3(x) \quad \Rightarrow \quad \Lambda_{ii,2}(x) = \frac{9\kappa_{12}(x) - 13}{3\kappa_{12}(x) - 5} k_B T_1(x) \tag{4.36}$$

The noise in those cases is expected to be again exponentially suppressed in the channel length. So far, it has been assumed that thermal equilibration plays a major role in the edge dynamics. **(iii)** In case of no thermal equilibration along the edge and therefore $l_{ij} = l_{eq}^Q \to \infty$, the heat transport is described by

$$\partial_x \overrightarrow{T^2}(x) = \frac{e^2}{hl\kappa_0} \Delta \overrightarrow{V^2}(x) \ . \tag{4.37}$$

The resulting temperature profiles are visualized for reasonable values of δ in Fig. 4.7 (left) using the incoherent tunneling model. The Majorana mode is thus found to stay at zero temperature in absence of thermal equilibration since it only interacts by thermal equilibration processes with the other modes. Because it is unreasonable that the Majorana is not influenced by the heating at the *hotspot*, the model is adjusted to account for some heating of the Majorana. One intuitive way to do this is by thinking about how the total power P dissipated at the *hotspot* ($x = l_{eq}^C$) is transported along the edge. In general P is computed by integrating the Joule-heating contribution over the channel length L, resulting in

$$P = \frac{e^2 V_0^2}{h l_{eq}^C} \int_0^L \Delta V^2(x)\, dx \overset{L \gg l_{eq}^C}{\longrightarrow} \frac{e^2 V_0^2}{2h} \frac{\nu_u(\nu_d - \nu_u)}{\nu_d} \ . \tag{4.38}$$

[10] As expected from the assumption of two channels being at the same temperature and the third one deviating only slightly from it.

For the viewed case $\nu_d = 1$ and $\nu_u = 1/2$, this expression simplifies to $P = \frac{e^2 V_0^2}{8h}$ in the limits of full charge equilibration. The so generated power is transported away from the *hotspot* by the modes according to their ability to transfer heat. This behaviour is described by a heat divider between upstream and downstream transport with $n_d = n_2$ and $n_u = n_1 + n_3$ and a subsequent divider between the two upstream transporting modes which leads to the effective heat currents J_i, defined as

$$J_1 = \frac{\kappa_0}{2}\overline{T}_1^2 = \frac{n_1}{n_1+n_3}\frac{n_u}{n_d+n_u}P = \frac{2}{5}P\ , \tag{4.39}$$

$$J_2 = \frac{\kappa_0}{2}\overline{T}_2^2 = \qquad\quad \frac{n_d}{n_d+n_u}P = \frac{2}{5}P \quad \text{and} \tag{4.40}$$

$$J_3 = \frac{\kappa_0}{2}\overline{T}_3^2 = \frac{n_3}{n_1+n_3}\frac{n_u}{n_d+n_u}P = \frac{1}{5}P\ . \tag{4.41}$$

Thereby after leaving the *hotspot*, the three channels can be associated with effective temperatures, defined as $\overline{T}_1 = \overline{T}_2 = \sqrt{2}\ \overline{T}_3 = \sqrt{\frac{e^2V_0^2}{10h\kappa_0}}$. In absence of thermal equilibration, the so defined temperature profiles become with the unit step function $\sigma(x)$ and the dimensionless parameter δ

$$T_1 = \sqrt{2}T_3 = \sigma\left(-\left(\frac{x}{L}-\delta\right)\right)\sqrt{\frac{e^2V_0^2}{10h\kappa_0}} \quad \text{and} \quad T_2 = \sigma\left(\frac{x}{L}-\delta\right)\sqrt{\frac{e^2V_0^2}{10h\kappa_0}}\ . \tag{4.42}$$

The obtained temperature profiles are visualized in Fig. 4.7 (right).

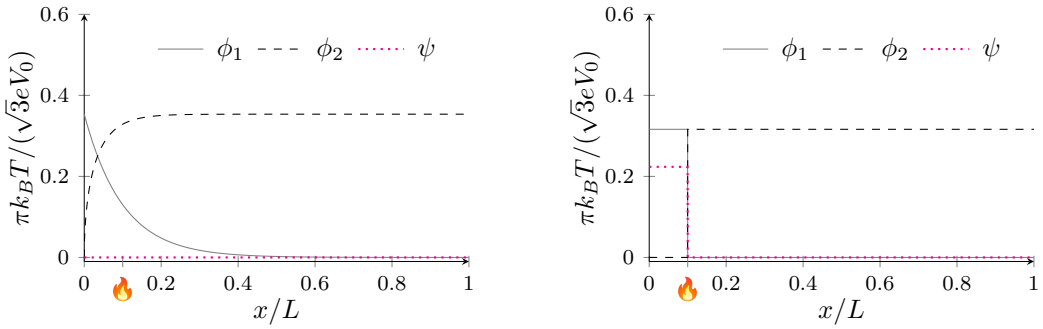

Figure 4.7: Comparison of the temperature profiles for ϕ_1, ϕ_2 and ψ in terms of x/L for an applied voltage bias of V_0 in the bare incoherent tunneling model (left) and in the adjusted case (right) for $\delta = 0.1$. The position of the *hotspot* is marked with the fire symbol.

In case of absent thermal equilibration the heat generated at the *hotspot* is thus transported back to the *noisespot* by ϕ_2 with the constant temperature T_2. Comparing the two plots in Fig. 4.7, the effect of the Majorana heat transport is small in this case but still desirable[11]. The corresponding noise kernel evaluates to

$$\Lambda(x) = 6\sqrt{\frac{6}{5}}\frac{eV_0\zeta(3)}{\pi^3}\ . \tag{4.43}$$

Using the current-voltage relation $I_0 = \frac{1}{2}\frac{e^2}{h}V_0$ to rewrite the noise (the computation is carried out in Sec. A.8), it takes the constant value

$$S^{exc} \approx 0.0637\frac{e^3}{h}V_0 = 0.1274eI_0 \approx 0.3953\ V_0 \cdot 10^{-30}\frac{\mathrm{A}^2}{\mathrm{Hz}\ \mu V}\ . \tag{4.44}$$

To account for some left over heat transport in all channels, the introduced extension to the incoherent tunneling model would have to be modified further. This could (e.g) be done by taking heat reflection at the contacts into account [55]. In general such an approach leads to

[11] The concept of heat division at the *hotspot* becomes more important when looking into the effect of heat reflection at the contacts.

a scenario with three channels of (very) different temperatures at the noise spot. Thus the non-equilibrium situation at the noise spot would have to be investigated further to obtain a solution.
The expected noise for the three viewed cases is computed numerically using the derived noise kernels. They are visualized using numerical integration techniques for increasing values of $1/\delta = L/l_{eq}^{C}$ in Fig. 4.8.

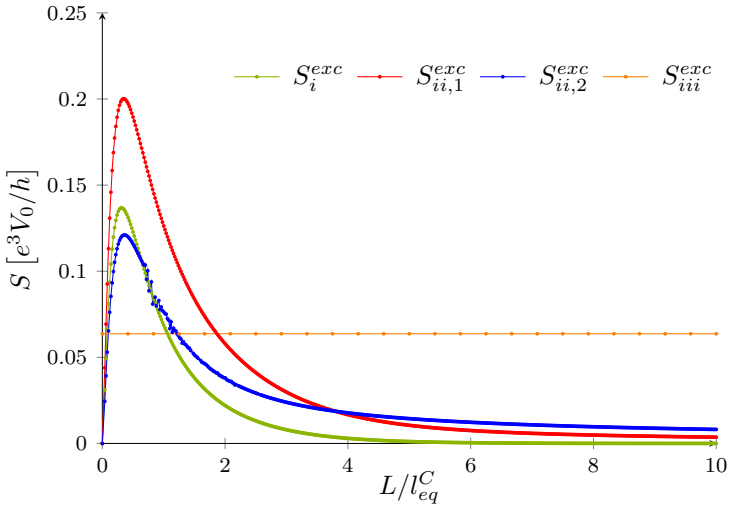

Figure 4.8: Numerically derived plots of the noise for an increasing ratio L/l_{eq}^{C} at the intermediate phPf-3 edge for the cases of very good thermal equilibration **(i)**, good thermal equilibration with $\alpha = 0.01$, $\beta = 0.5$ **(ii,1)** and $\alpha = 0.5$, $\beta = 0.01$ **(ii,2)** as well as for absent thermal equilibration **(iii)**.

5
Results and Conclusion

To compare the results of the incoherent tunneling model to experimental observations, the results from *Dutta, et al.* are summarized in Tab. 5.1. They measured the heat conductance [30] and noise [32] at the interface between the 5/2 edge and several integer ones in two different devices. The measured heat conductance of $G^Q_{2t} = 5/2\ \kappa$ at the bare $5/2-0$ edge eliminates the Pf edge from the list since it implies ballistic downstream (ds) heat transport with $G^Q_{2t} = 7/2\ \kappa$. Furthermore, the heat conductance at $5/2-3$ interface has been measured to be $G^Q_{2t} = 1/2\ \kappa$ which cannot be described using the aPf theory predicting $G^Q_{2t} = 3/2\ \kappa$. Additionally, the observation of noise at the $5/2-3$ interface is inexplicable with the aPf structure since the aPf-3 edge consists of co-propagating channels giving no opportunity for the generation of noise. Therefore, the observed heat conductance as well as the generation of noise at the $5/2-3$ interface point towards the phPf edge structure to describe the 5/2 edge best amongst the candidates.

Table 5.1: Comparison of experimental results for the charge (heat) conductance [30] and noise at different interfaces [32] to the theoretical prediction of the considered candidates. If the theoretical prediction matches the experimental result, the candidate is given a ✓(otherwise: ✗).

interface	$\lvert G_{2t}\rvert \left[\frac{e^2}{h}\right]$	$\lvert G^Q_{2t}\rvert\,[\kappa]$	Noise measured?	Agrees to 5/2 candidate		
				PHPf	APf	Pf
$5/2-0$	5/2	5/2	✓	✓	✓	✗
$5/2-1$	3/2	3/2	✓	✓	✓	✗
$5/2-2$	1/2	1/2	✓(only ds)	✓	✓	✗
$5/2-3$	1/2	1/2	✓(only us)	✓	✗	✓

Having justified the phPf edge to be the candidate of choice, the mechanisms that lead to equilibration of the transport at the phPf - 3 interface are reviewed next. Depending on the degree of equilibration (heat and charge), the edge structures are thought to show non-unique transport behaviour. Since the charge conductances have been measured to take the well equilibrated values, it is reasonable to assume that the charge transport equilibrates on smaller length scales than the heat transport. Under these assumptions, the two terminal heat conductance $G^Q_{2t}[\kappa]$ at the interface is found to show distinct plateaus at 5/2, 3/2 and 1/2 depending on the thermal equilibration length l_{ij} between pairs of the involved channels. This is as expected since all physical processes that take place on a similar length scale are thought to overlap. Therefore it gets more difficult to resolve their individual effects if the individual length scales get closer to another. In case of the heat equilibration of the 5/2 state, the plateau of $G^Q_{2t} = 3/2\ \kappa$ vanishes if the equilibration lengths of the two pairs of counter-propagating modes differ less. The existence of the plateaus for different pair-wise equilibration lengths also infers that an intermediate system might exist at the corresponding length scales leading to an observable change in the heat conductance.
The transitions between the predicted plateaus are described by possible interactions between the involved modes. Transition I is explained by charge tunneling between the ϕ_1 and ϕ_2 [1] and

[1] Even though, the Majorana carries no charge on its own, it is needed in the description of charge tunneling since it shares an electron with the 1/2 boson.

transition II by an effective heat interaction between the charge-neutral separated modes of the effective phPf-3. According to the different mechanisms of equilibration, the thermal equilibration lengths corresponding to transitions I and II are expected to show different temperature scaling. In particular the equilibration length of transition I scales as T^{-2} whereas the one of transition II scales as T^{-4}. The different temperature scalings of the thermal equilibration lengths also influence the temperature depending behaviour of the heat conductance which is visualized for arbitrarily chosen values of $l^I_{eq}(T)$ and $l^{II}_{eq}(T)$ in Fig. 5.1. In case of the prefactors taking the same value, the transitions vanish entirely and the heat conductance becomes $G^Q_{2t} = 1/2\ \kappa$. Because there is no reason for the prefactors in $l^i_{eq}(T)$ to be identical, a measurement at even lower temperatures is expected to reveal the theoretical plateau like structure of G^Q_{2t} at the interface.

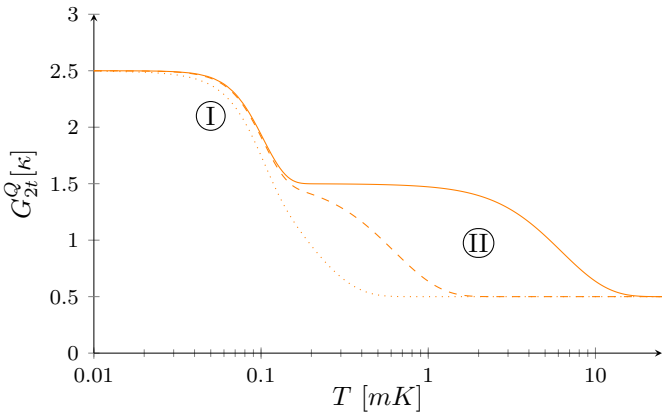

Figure 5.1: Temperature dependent equilibration of $G^Q_{2t}[\kappa]$ at the phPf-3 edge for different chosen heat equilibration lengths $l^I_{eq} \sim T^{-2} \cdot \{7 \cdot 10^{-5}, 7 \cdot 10^{-7}, 7 \cdot 10^{-8}\}$ (solid, dashed, dotted) and $l^{II}_{eq} \sim 10^{-16} \cdot T^{-4}$. Since these values were chosen arbitrarily, the temperature scale has to be considered with caution.

Since the equilibrated heat transport at the phPf-3 edge is along the direction of the charge transport, the generated noise is assumed to show the characteristic behaviour of the class $\nu_Q > 0$ (see Sec. 3.4). Due to the complexity of computation with three involved modes, the extreme cases of full and absent thermal equilibration have been used to give an idea about possible values of the noise at this interface. In case of very good thermal equilibration, the expected behaviour of exponentially vanishing noise for an increasing channel length L is approved numerically. For the opposite extreme of no thermal equilibration, the noise is expected to show length independant behaviour. Assuming that the charge transport is well equilibrated and thus $l^C_{eq} \ll L$[2], the noise is found to be within the region

$$\frac{S^{exc}}{V_0} \in \left(0, 0.0637\right] \frac{e^3}{h} \qquad \Leftrightarrow \qquad \frac{S^{exc}}{V_0} \in \left(0, 0.3953\right] \cdot 10^{-30} \frac{\mathrm{A}^2}{\mu V \mathrm{Hz}}$$

The noise measured in the experiment [32] is within this described region indicating the underlying edge structure to be consistent with the experiment.

[2] This refers to the region to the far right in Fig. 4.8.

6
Outlook

One possible step to investigate the structure of the 5/2 edge in more detail is to perform measurements of the noise and the heat conductance using the same device. It is then possible to compare the experimental results for noise and heat conductance to theoretical predictions depending on the degree of thermal equilibration. In such a scenario, two observables can be measured in the same device which gives the opportunity to estimate the heat and charge equilibration lengths.
In the following I'd like to further state some of the questions/problems that I did not tackle in this project but that could be included in a follow-up project on this topic

1. The (heat) transport in a system that is connected to macroscopic contacts always allows for some reflection at the contacts. Therefore the next step to look further into the heat transport along the edge would be to take this reflection into account in a setup like the one shown schematically in Fig. 6.1. [55]
2. To take the heat transport in Majorana channels into account it could furthermore be interesting to examine the transport in these channels in more detail. This includes to answer the question which physical process leads to the heat up of the Majorana channel if a system consisting of multiple modes is only biased by a voltage difference.
3. Relaxing the assumption of the edge to consist of a single edge structure throughout the entire edge, new transport scenarios could arise. The interplay between puddles of different edge structures along the edge allows for additional longitudinal interactions between different puddles. In general these interactions also lead to a finite reflection of charge and heat at the interfaces between puddles allowing for even more intricate descriptions of the noise at the edge. [86–90]

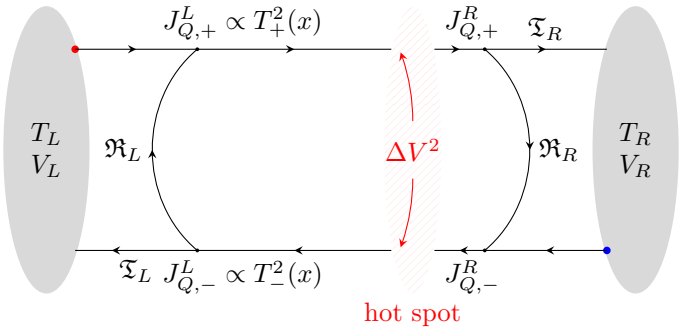

Figure 6.1: Schematic view of a model taking heat reflection at the contacts into account. Applying only a temperature bias, heat is reflected with $\mathfrak{R}_{L(R)}$ or transmitted with $\mathfrak{T}_{L(R)}$ at the corresponding contacts which leads in general to non-zero temperatures at the noise spot for all involved channels.

Bibliography

[1] M. Planck, "On an improvement of wien's equation for the spectrum", Ann. Physik 1, 719–721 1900.

[2] R. P. Feynman, "Space-Time Approach to Non-Relativistic Quantum Mechanics", Rev. Mod. Phys. 20, 367–387 1948.

[3] A. Altland and B. D. Simons, *Condensed Matter Field Theory* (Cambridge University Press, Cambridge, England, UK, Mar. 2010).

[4] P. Drude, "Zur Elektronentheorie der Metalle", Ann. Phys. 306, 566–613 1900.

[5] S. M. Girvin, "The Quantum Hall Effect: Novel Excitations and Broken Symmetries", arXiv, 10.48550/arXiv.cond-mat/9907002 1999.

[6] D. C. Tsui, H. L. Stormer, and A. C. Gossard, "Two-Dimensional Magnetotransport in the Extreme Quantum Limit", Phys. Rev. Lett. 48, 1559–1562 1982.

[7] D. Tong, *David tong: lectures on the quantum hall effect*, http://www.damtp.cam.ac.uk/user/tong/qhe.html, Accessed: 2022-03-15.

[8] Z. Papić and A. C. Balram, "Fractional quantum Hall effect in semiconductor systems", arXiv, 10.48550/arXiv.2205.03421 2022.

[9] K. von Klitzing, "The quantized hall effect", Rev. Mod. Phys. 58, 519–531 1986.

[10] P. W. Anderson, "Absence of Diffusion in Certain Random Lattices", Phys. Rev. 109, 1492–1505 1958.

[11] R. B. Laughlin, "Anomalous quantum hall effect: an incompressible quantum fluid with fractionally charged excitations", Phys. Rev. Lett. 50, 1395–1398 1983.

[12] B. I. Halperin, "Quantized hall conductance, current-carrying edge states, and the existence of extended states in a two-dimensional disordered potential", Phys. Rev. B 25, 2185–2190 1982.

[13] X.-G. Wen, "THEORY OF THE EDGE STATES IN FRACTIONAL QUANTUM HALL EFFECTS", Int. J. Mod. Phys B 06, 1711–1762 1992.

[14] J. M. Luttinger, "An Exactly Soluble Model of a Many-Fermion System", J. Math. Phys. 4, 1154–1162 1963.

[15] F. D. M. Haldane, "'luttinger liquid theory' of one-dimensional quantum fluids. i. properties of the luttinger model and their extension to the general 1d interacting spinless fermi gas", Journal of Physics C: Solid State Physics 14, 2585–2609 1981.

[16] F. D. M. Haldane, "Fractional Quantization of the Hall Effect: A Hierarchy of Incompressible Quantum Fluid States", Phys. Rev. Lett. 51, 605–608 1983.

[17] J. M. Leinaas and J. Myrheim, "On the theory of identical particles", Nuovo Cim. B 37, 1–23 1977.

[18] F. Wilczek, "Magnetic Flux, Angular Momentum, and Statistics", Phys. Rev. Lett. 48, 1144–1146 1982.

[19] Y.-S. Wu, "General Theory for Quantum Statistics in Two Dimensions", Phys. Rev. Lett. 52, 2103–2106 1984.

[20] G. A. Goldin, R. Menikoff, and D. H. Sharp, "Comments on "General Theory for Quantum Statistics in Two Dimensions"", Phys. Rev. Lett. 54, 603 1985.

[21] E. Witten, "Quantum field theory and the Jones polynomial", Commun. Math. Phys. 121, 351–399 1989.

[22] C. Nayak, S. H. Simon, A. Stern, M. Freedman, and S. Das Sarma, "Non-abelian anyons and topological quantum computation", Reviews of Modern Physics 80, 10.1103/revmodphys.80.1083 2008.

[23] V. Lahtinen and J. Pachos, "A short introduction to topological quantum computation", SciPost Physics 3, 10.21468/scipostphys.3.3.021 2017.

[24] A. Y. Kitaev, "Fault-tolerant quantum computation by anyons", Ann. Phys. 303, 2–30 2003.

[25]C. L. Kane and M. P. A. Fisher, "Quantized thermal transport in the fractional quantum Hall effect", Phys. Rev. B 55, 15832–15837 1997.
[26]R. A. Melcer, B. Dutta, C. Spånslätt, J. Park, A. D. Mirlin, and V. Umansky, "Absent thermal equilibration on fractional quantum Hall edges over macroscopic scale", Nat. Commun. 13, 1–7 2022.
[27]S. K. Srivastav, R. Kumar, C. Spånslätt, K. Watanabe, T. Taniguchi, A. D. Mirlin, Y. Gefen, and A. Das, "Determination of topological edge quantum numbers of fractional quantum Hall phases", arXiv, 10.48550/arXiv.2202.00490 2022.
[28]S. K. Srivastav, R. Kumar, C. Spånslätt, K. Watanabe, T. Taniguchi, A. D. Mirlin, Y. Gefen, and A. Das, "Vanishing Thermal Equilibration for Hole-Conjugate Fractional Quantum Hall States in Graphene", Phys. Rev. Lett. 126, 216803 2021.
[29]M. Banerjee, M. Heiblum, V. Umansky, D. E. Feldman, Y. Oreg, and A. Stern, "Observation of half-integer thermal hall conductance", en, Nature 559, 205–210 2018.
[30]B. Dutta, V. Umansky, M. Banerjee, and M. Heiblum, "Isolated ballistic non-abelian interface channel", 2021.
[31]R. Willett, J. P. Eisenstein, H. L. Störmer, D. C. Tsui, A. C. Gossard, and J. H. English, "Observation of an even-denominator quantum number in the fractional quantum Hall effect", Phys. Rev. Lett. 59, 1776–1779 1987.
[32]B. Dutta, W. Yang, R. Melcer, H. K. Kundu, M. Heiblum, V. Umansky, Y. Oreg, A. Stern, and D. Mross, "Distinguishing between non-abelian topological orders in a quantum hall system", Science 375, 193–197 2022.
[33]Y. Kitadono, M. Wakamatsu, L. Zou, and P. Zhang, "Role of guiding center in landau level system and mechanical and pseudo orbital angular momenta", International Journal of Modern Physics A 35, 10.1142/s0217751x20500967 2020.
[34]S. J. van Enk, "Angular momentum in the fractional quantum hall effect", American Journal of Physics 88, 10.1119/10.0000831 2020.
[35]O. Ciftja, "Detailed solution of the problem of landau states in a symmetric gauge", Eur. J. Phys. 41 2020.
[36]R. B. Laughlin, "Quantized hall conductivity in two dimensions", Phys. Rev. B 23, 5632–5633 1981.
[37]M. J. Clerk, "VIII. A dynamical theory of the electromagnetic field", Philos. Trans. R. Soc. Lond. 155, 459–512 1865.
[38]*The Nobel Prize in Physics 1998*, https://www.nobelprize.org/prizes/physics/1998/laughlin/lecture, [Online; accessed 28. Jun. 2022], June 2022.
[39]Y. Aharonov and D. Bohm, "Significance of Electromagnetic Potentials in the Quantum Theory", Phys. Rev. 115, 485–491 1959.
[40]M. Born and V. Fock, "Beweis des Adiabatensatzes", Z. Phys. 51, 165–180 1928.
[41]B. M. Victor, "Quantal phase factors accompanying adiabatic changes", Proc. R. Soc. Lond. A. 392, 45–57 1984.
[42]D. J. Thouless, M. Kohmoto, M. P. Nightingale, and M. den Nijs, "Quantized hall conductance in a two-dimensional periodic potential", Phys. Rev. Lett. 49, 405–408 1982.
[43]C. Kane, "Chapter 1 - topological band theory and the $\mathbb{Z}_2$ invariant", in *Topological insulators*, Vol. 6, edited by M. Franz and L. Molenkamp, Contemporary Concepts of Condensed Matter Science (Elsevier, 2013), 3–34.
[44]E. Miranda, "Introduction to bosonization", Braz. J. Phys. 33 2003.
[45]J. von Delft and H. Schoeller, "Bosonization for beginners - refermionization for experts", Annalen der Physik 7, 225–305 1998.
[46]A. Imambekov and L. I. Glazman, "Universal Theory of Nonlinear Luttinger Liquids", Science 323, 228–231 2009.
[47]X. G. Wen, "Gapless boundary excitations in the quantum hall states and in the chiral spin states", Phys. Rev. B 43, 11025–11036 1991.
[48]A. M. Chang, "Chiral luttinger liquids at the fractional quantum hall edge", Rev. Mod. Phys. 75, 1449–1505 2003.
[49]R. Floreanini and R. Jackiw, "Self-dual fields as charge-density solitons", Phys. Rev. Lett. 59, 1873–1876 1987.
[50]X.-G. Wen, "Topological orders and edge excitations in fractional quantum Hall states", Adv. Phys. 44, 405–473 1995.

[51]C. L. Kane and M. P. A. Fisher, "Impurity scattering and transport of fractional quantum Hall edge states", Phys. Rev. B 51, 13449–13466 1995.
[52]C. L. Kane, M. P. A. Fisher, and J. Polchinski, "Randomness at the edge: Theory of quantum Hall transport at filling $\nu = 2/3$", Phys. Rev. Lett. 72, 4129–4132 1994.
[53]C. Spånslätt, Y. Gefen, I. V. Gornyi, and D. G. Polyakov, "Contacts, equilibration, and interactions in fractional quantum Hall edge transport", Phys. Rev. B 104, 115416 2021.
[54]I. Protopopov, Y. Gefen, and A. Mirlin, "Transport in a disordered ν=2/3 fractional quantum hall junction", Annals of Physics 385, 287–327 2017.
[55]R. Kumar, S. K. Srivastav, C. Spånslätt, K. Watanabe, T. Taniguchi, Y. Gefen, A. D. Mirlin, and A. Das, "Observation of ballistic upstream modes at fractional quantum hall edges of graphene", Nat. Commun. 13, 213 2022.
[56]R. Landauer, "Electrical transport in open and closed systems", en, Z. Physik B - Condensed Matter 68, 217–228 1987.
[57]M. Büttiker, "Four-terminal phase-coherent conductance", Phys. Rev. Lett. 57, 1761–1764 1986.
[58]C. W. J. Beenakker, "Edge channels for the fractional quantum Hall effect", Phys. Rev. Lett. 64, 216–219 1990.
[59]A. H. MacDonald, "Edge states in the fractional-quantum-hall-effect regime", Phys. Rev. Lett. 64, 220–223 1990.
[60]Y. Cohen, Y. Ronen, W. Yang, D. Banitt, J. Park, M. Heiblum, A. D. Mirlin, Y. Gefen, and V. Umansky, "Synthesizing a ν=2/3 fractional quantum Hall effect edge state from counter-propagating ν=1 and ν=1/3 states", Nat. Commun. 10, 1–6 2019.
[61]A. Sommerfeld, "Zur Elektronentheorie der Metalle auf Grund der Fermischen Statistik", Z. Phys. 47, 1–32 1928.
[62]K. Schwab, E. A. Henriksen, J. M. Worlock, and M. L. Roukes, "Measurement of the quantum of thermal conductance", en, Nature 404, 974–977 2000.
[63]C. Wu, B. A. Bernevig, and S.-C. Zhang, "Helical Liquid and the Edge of Quantum Spin Hall Systems", Phys. Rev. Lett. 96, 106401 2006.
[64]G. Zhang, I. V. Gornyi, and C. Spånslätt, "Delta-T noise for weak tunneling in one-dimensional systems: Interactions versus quantum statistics", Phys. Rev. B 105, 195423 2022.
[65]C. Nosiglia, J. Park, B. Rosenow, and Y. Gefen, "Incoherent transport on the ν= 2/3 quantum hall edge", Physical Review B 98, 10.1103/physrevb.98.115408 2018.
[66]J. Park, A. D. Mirlin, B. Rosenow, and Y. Gefen, "Noise on complex quantum hall edges: chiral anomaly and heat diffusion", Physical Review B 99, 10.1103/physrevb.99.161302 2019.
[67]C. Spånslätt, J. Park, Y. Gefen, and A. D. Mirlin, "Topological classification of shot noise on fractional quantum hall edges", Physical Review Letters 123, 10.1103/physrevlett.123.137701 2019.
[68]J. Park, C. Spånslätt, Y. Gefen, and A. D. Mirlin, "Noise on the non-Abelian ν=5/2 Fractional Quantum Hall Edge", Phys. Rev. Lett. 125, 157702 2020.
[69]C. Spånslätt, J. Park, Y. Gefen, and A. D. Mirlin, "Conductance plateaus and shot noise in fractional quantum Hall point contacts", Phys. Rev. B 101, 075308 2020.
[70]H. Nyquist, "Thermal Agitation of Electric Charge in Conductors", Phys. Rev. 32, 110–113 1928.
[71]J. B. Johnson, "Thermal Agitation of Electricity in Conductors", Phys. Rev. 32, 97–109 1928.
[72]G. Moore and N. Read, "Nonabelions in the fractional quantum hall effect", Nucl. Phys. B 360, 362–396 1991.
[73]X. G. Wen, "Non-Abelian statistics in the fractional quantum Hall states", Phys. Rev. Lett. 66, 802–805 1991.
[74]N. Read and D. Green, "Paired states of fermions in two dimensions with breaking of parity and time-reversal symmetries and the fractional quantum Hall effect", Phys. Rev. B 61, 10267–10297 2000.
[75]L. Fidkowski, X. Chen, and A. Vishwanath, "Non-Abelian Topological Order on the Surface of a 3D Topological Superconductor from an Exactly Solved Model", Phys. Rev. X 3, 041016 2013.
[76]D. T. Son, "Is the Composite Fermion a Dirac Particle?", Phys. Rev. X 5, 031027 2015.

[77]P. T. Zucker and D. E. Feldman, "Stabilization of the Particle-Hole Pfaffian Order by Landau-Level Mixing and Impurities That Break Particle-Hole Symmetry", Phys. Rev. Lett. 117, 096802 2016.
[78]L. Antonić, J. Vučičević, and M. V. Milovanović, "Paired states at 5/2: Particle-hole Pfaffian and particle-hole symmetry breaking", Phys. Rev. B 98, 115107 2018.
[79]S.-S. Lee, S. Ryu, C. Nayak, and M. P. A. Fisher, "Particle-Hole Symmetry and the $\nu = \frac{5}{2}$ Quantum Hall State", Phys. Rev. Lett. 99, 236807 2007.
[80]M. Levin, B. I. Halperin, and B. Rosenow, "Particle-Hole Symmetry and the Pfaffian State", Phys. Rev. Lett. 99, 236806 2007.
[81]H. Asasi and M. Mulligan, "Partial equilibration of anti-pfaffian edge modes at ν=5/2", Phys. Rev. B 102, 205104 2020.
[82]K. K. W. Ma and D. E. Feldman, "Thermal equilibration on the edges of topological liquids", Phys. Rev. Lett. 125, 016801 2020.
[83]P. Di Francesco, P. Mathieu, and D. Sénéchal, *Conformal field theory*, Graduate texts in contemporary physics (Island Press, 1996).
[84]A. Cappelli, M. Huerta, and G. R. Zemba, "Thermal transport in chiral conformal theories and hierarchical quantum hall states", Nuclear Physics B 636, 568–582 2002.
[85]J. Rech, T. Jonckheere, B. Grémaud, and T. Martin, "Negative delta-t noise in the fractional quantum hall effect", Physical Review Letters 125, 10.1103/physrevlett.125.086801 2020.
[86]W. Zhu, D. N. Sheng, and K. Yang, "Topological Interface between Pfaffian and Anti-Pfaffian Order in ν=5/2 Quantum Hall Effect", Phys. Rev. Lett. 125, 146802 2020.
[87]D. F. Mross, Y. Oreg, A. Stern, G. Margalit, and M. Heiblum, "Theory of Disorder-Induced Half-Integer Thermal Hall Conductance", Phys. Rev. Lett. 121, 026801 2018.
[88]C. Wang, A. Vishwanath, and B. I. Halperin, "Topological order from disorder and the quantized Hall thermal metal: Possible applications to the $\nu = 5/2$ state", Phys. Rev. B 98, 045112 2018.
[89]B. Lian and J. Wang, "Theory of the disordered $\nu = \frac{5}{2}$ quantum thermal Hall state: Emergent symmetry and phase diagram", Phys. Rev. B 97, 165124 2018.
[90]P.-S. Hsin, Y.-H. Lin, N. M. Paquette, and J. Wang, "Effective field theory for fractional quantum Hall systems near $\nu = 5/2$", Phys. Rev. Res. 2, 043242 2020.
[91]H. Ebisu, N. Schiller, and Y. Oreg, "Fluctuations in Heat Current and Scaling Dimension", Phys. Rev. Lett. 128, 215901 2022.
[92]T. Martin, "Noise in mesoscopic physics", arXiv, 10.48550/arXiv.cond-mat/0501208 2005.

A
Additional Computations

A.1 General Identities

Expansion of a time-ordered exponential

$$\begin{aligned}\mathcal{T}\{e^{\int_0^t A(t')dt'}\} &\equiv \sum_{n=0}^{\infty}\frac{1}{n!}\int_0^t\dots\int_0^t \mathcal{T}\{A(t_1')\dots A(t_n')\}\,dt_1'\dots\,dt_n' \\ &\equiv \sum_{n=0}^{\infty}\int_0^t\dots\int_0^{t_{n-1}'} A(t_1')\dots A(t_n')\,dt_1'\dots\,dt_n' \end{aligned} \tag{A.1}$$

Definition of δ function by

$$\Big[\frac{1}{t_1-t_2-i\delta}-\frac{1}{t_1-t_2+i\delta}\Big]_{\delta\to 0^+} = 2\pi i\delta(t_1-t_2) \tag{A.2}$$

Action of δ function on functions $f(x)$ under the integral

$$\int_x \delta(x-y)f(x)\,dx = f(y) \tag{A.3}$$

$$\int_x \partial_x\delta(x-a)f(x)\,dx = -\int \partial_x f(x)\delta(x-y)\,dx = -\partial_y f(y) \tag{A.4}$$

A.2 Longitudinal Conductance in the Hall-cross

In general, four different well-defined longitudinal charge and heat conductances can be defined for the Hall-cross. It is, however, not very common to discuss longitudinal conductances in this setup. For a Hall-cross biased by a voltage ΔV and contact three connected to GND $V_3 = 0$, the longitudinal conductances can be defined by

$$G_{L,a} = \frac{I}{V_1-V_2} \qquad G_{L,b} = \frac{I}{V_2-V_3} \qquad G_{L,c} = \frac{I}{V_3-V_4} \qquad G_{L,d} = \frac{I}{V_4-V_1}$$

By the definition of $V_3 \equiv$ GND, it follows that $G_{L,a} = -G_{L,d}$ and $G_{L,b} = -G_{L,c}$. The conductances become for the considered cases

$\nu_+ \neq \nu_-$		
$G_{L,a} = \dfrac{G_+^2+G_-^2}{G_-}$	$G_{L,a} \overset{L\gg l}{\longrightarrow} \infty$	$G_{L,a} \overset{L\ll l}{\longrightarrow} \dfrac{\nu_+^2+\nu_-^2}{\nu_-}$
$G_{L,b} = \dfrac{G_+^2+G_-^2}{G_+}$	$G_{L,b} \overset{L\gg l}{\longrightarrow} \nu_1-\nu_2$	$G_{L,b} \overset{L\ll l}{\longrightarrow} \dfrac{\nu_+^2+\nu_-^2}{\nu_+}$
$\nu_+ = \nu_- = \nu$		
$G_{L,a} = G_{L,b} = \dfrac{2\nu^2}{\frac{L}{l}+\nu}$	$G_{L,a} \overset{L\gg l}{\longrightarrow} 0$	$G_{L,a} \overset{L\ll l}{\longrightarrow} 2\nu$

A.3 Conductances in the Diffusive Transport Regime

Analogous to the transport for $\nu_+(n_+) \neq \nu_-(n_-)$ it is possible to describe a downstream and upstream charge (heat) conductance in the diffusive transport regime (in units e^2/h and κ). This regime however, does not correspond to a proper quantum Hall state. The conductances take the following values:

$\nu_+ = \nu_- = \nu$		
Two terminal setup		
$G_{2t} = \dfrac{2\nu^2}{\frac{L}{l}+\nu}$	$G_{2t} \overset{L\gg l}{\longrightarrow} 0$	$G_{2t} \overset{L\ll l}{\longrightarrow} 2\nu$
Hall-cross		
$G_{2t} = \dfrac{\nu^2}{\frac{L}{l}+\nu}$ $G_H \to \infty$	$G_{2t} \overset{L\gg l}{\longrightarrow} 0$	$G_{2t} \overset{L\ll l}{\longrightarrow} \nu$
Hall-bar		
$G_{2t} = \dfrac{2\nu^2}{3\left(\frac{L}{l}+\nu\right)}$ $G_H \to \infty$	$G_{2t} \overset{L\gg l}{\longrightarrow} 0$	$G_{2t} \overset{L\ll l}{\longrightarrow} \frac{2}{3}\nu$
$G_L = \pm\dfrac{2\nu^2}{\frac{L}{l}+\nu}$	$G_L \overset{L\gg l}{\longrightarrow} 0$	$G_L \overset{L\ll l}{\longrightarrow} \pm 2\nu$
$n_+ = n_- = n$		
Two terminal setup		
$G^Q_{2t} = 2\dfrac{l^Q_{eq}}{l^Q_{eq}+\gamma L n} n$	$G^Q_{2t} \overset{L\gg l^Q_{eq}}{\longrightarrow} 0$	$G^Q_{2t} \overset{L\ll l^Q_{eq}}{\longrightarrow} 2n$
Hall-cross		
$G^Q_{2t} = \dfrac{n}{1+\frac{L}{l}n\gamma}$	$G^Q_{2t} \overset{L\gg l}{\longrightarrow} 0$	$G^Q_{2t} \overset{L\ll l}{\longrightarrow} n$
Hall-bar		
$G^Q_{2t} = \dfrac{2n}{3\left(1+\frac{L}{l}n\gamma\right)}$	$G^Q_{2t} \overset{L\gg l}{\longrightarrow} 0$	$G^Q_{2t} \overset{L\ll l}{\longrightarrow} \dfrac{2}{3}n$

A.4 Continuous Noise Coefficients

The continuous versions of the coefficients to the various noise contributions are defined by

$$A = \frac{(\nu_1-\nu_2)^2}{\left(\nu_2-\nu_1 e^{\frac{2L}{l^C_{eq}}}\right)^2} \qquad C = \frac{(\nu_1-\nu_2)^2 e^{\frac{2(L-x)}{l^C_{eq}}}}{\left(\nu_2-\nu_1 e^{\frac{2L}{l^C_{eq}}}\right)^2} \qquad D = \frac{\nu_2^2\left(e^{\frac{2L}{l^C_{eq}}}-1\right)^2}{\left(\nu_2-\nu_1 e^{\frac{2L}{l^C_{eq}}}\right)^2} \tag{A.5}$$

$$E = -\frac{\nu_2(\nu_1-\nu_2)\left(e^{\frac{2L}{l^C_{eq}}}-1\right)e^{\frac{2(L-x)}{l^C_{eq}}}}{\left(\nu_2-\nu_1 e^{\frac{2L}{l^C_{eq}}}\right)^2} \qquad F = \frac{(\nu_1-\nu_2)^2 e^{\frac{4(L-x)}{l^C_{eq}}}}{\left(\nu_1-\nu_2 e^{\frac{2L}{l^C_{eq}}}\right)^2} \tag{A.6}$$

In case of $L \gg l_{eq}^C$, they simplify to

$$A \to 0 \quad C \to 0 \quad D \to \left(\frac{\nu_2}{\nu_1}\right)^2 \quad E \to -\frac{\nu_2}{\nu_1^2}(\nu_1-\nu_2)e^{-\frac{2x}{l_{eq}^C}} \quad F \to \frac{(\nu_1-\nu_2)^2}{\nu_1^2}e^{-\frac{4x}{l_{eq}^C}} \tag{A.7}$$

A.5 Description of the Edge Theory

A.5.1 Equation of Motion

Given the action for a chiral bosonic mode S_ϕ connected to a contact S_V with χ, v and ν the chirality, velocity and fillling factor of the considered bosonic mode

$$S_\phi = -\frac{1}{4\pi\nu}\iint dx\,dt\,\left[\chi\partial_t\phi\partial_x\phi + v(\partial_x\phi)^2\right] \quad \text{and} \quad S_V = -\frac{\chi}{2\pi}\iint dx\,dt\,V(x)\partial_x\phi\ , \tag{A.8}$$

the total action $S_{tot} = S_\phi + S_V$ is minimized using the principle of stationary action :

$$\lim_{\epsilon\to 0}\frac{1}{\epsilon}\Big[S_{tot}[\phi+\epsilon\eta] - S_{tot}[\phi]\Big] = 0\ . \tag{A.9}$$

By the *algebraic limit theorem*, the limits are viewed one by one, starting with S_ϕ

$$\frac{1}{\epsilon}\Big[S_\phi[\phi+\epsilon\eta] - S_\phi[\phi]\Big] = -\frac{1}{4\pi\nu}\iint\limits_{t,x}\left(\chi\left(\partial_t\phi\partial_x\eta + \partial_t\eta\partial_x\phi + \epsilon\partial_t\eta\partial_x\eta\right) + v\left(2\partial_x\phi\partial_x\eta + \epsilon(\partial_x\eta)^2\right)\right)\ . \tag{A.10}$$

integrating terms 1,2 and 3 by parts (endpoints are fixed) and taking the limit gives

$$\lim_{\epsilon\to 0}\frac{1}{\epsilon}\Big[S_\phi[\phi+\epsilon\eta] - S_\phi[\phi]\Big] = \frac{1}{4\pi\nu}\iint\limits_{t,x}\Big[2\chi\partial_t\partial_x\phi + 2v\partial_x^2\phi\Big]\eta \overset{!}{=} 0\ . \tag{A.11}$$

The EOM for the chiral boson without attached contacts is thus given by

$$\chi\partial_t\partial_x\phi(x,t) + v\partial_x^2\phi(x,t) = 0\ . \tag{A.12}$$

A *left moving mode* $\phi(x,t) = \phi(x+vt)$ fulfills the EOM for $\chi = -1$, whereas for a *right moving mode* $\phi(x,t) = \phi(x-vt)$ solves the EOM for $\chi = +1$. In terms of the 1D charge density $\rho(x,t) = \frac{\chi}{2\pi}\partial_x\phi(x,t)$, this becomes

$$\partial_t\rho(x,t) + \chi v\partial_x\rho(x,t) = 0\ . \tag{A.13}$$

Viewing this as a continuity equation of the kind $\partial_t\rho + \partial_x I = 0$, the current I takes the form

$$\boxed{I(x,t) = \chi v\rho(x,t)}\ . \tag{A.14}$$

The variation of S_V, describing the additional contribution from the contact evaluates as

$$\frac{1}{\epsilon}\Big[S_V(\phi+\epsilon\eta) - S_V(\phi)\Big] = -\frac{\chi}{2\pi}\iint\limits_{t,x}V(x)\partial_x\eta = \frac{\chi}{2\pi}\iint\limits_{t,x}\partial_x V(x)\eta\ . \tag{A.15}$$

Therefore the equation of motion for the total action becomes

$$\lim_{\epsilon\to 0}\frac{1}{\epsilon}\Big[S_{tot}(\phi+\epsilon\eta) - S_{tot}(\phi)\Big] = \frac{1}{4\pi\nu}\iint\limits_{t,x}\Big[2\chi\partial_t\partial_x\phi + 2v\partial_x^2\phi + 2\nu\partial_x V\Big]\eta \overset{!}{=} 0\ . \tag{A.16}$$

Looking at the EOM wrt the charge density $\rho(x,t)$

$$\partial_t\rho + \chi\partial_x\left(v\rho + \nu V\right) = 0\ . \tag{A.17}$$

An additional "contact" term has been added. The current can now be described by

$$\boxed{I = \chi(v\rho + \nu V)}\ . \tag{A.18}$$

The net current carried by one mode connected to the potentials $V_1 = e\mu_1 > V_2 = e\mu_2$ becomes in units $\frac{e^2}{h}$

$$I_{net} = \chi\left(v\rho + \nu V_1 - (v\rho + \nu V_2)\right) = \chi\nu(V_1 - V_2)\ . \tag{A.19}$$

A.5.2 Derivation of $\phi_{-n}(t) = \phi^*(t)$

Looking at positive and negative n separately in the Fourier expansion of $\phi(x,t)$, one gets:

$$\phi(x,t) = \frac{1}{\sqrt{L}} \sum_{n=0}^{\infty} \left[\phi_n(t) e^{ik_n x} + \phi_{-n}(t) e^{-ik_n x}\right] . \tag{A.20}$$

Since $\phi(x,t)$ is a real valued field (particle, anti-particle argument), it follows for each Fourier-component

$$\mathrm{Im}\left\{\left[\mathrm{Re}\{\phi_n(t)\} + i\,\mathrm{Im}\{\phi_n(t)\}\right] e^{ik_n x} + \left[\mathrm{Re}\{\phi_{-n}(t)\} + i\,\mathrm{Im}\{\phi_{-n}(t)\}\right] e^{-ik_n x}\right\} \stackrel{!}{=} 0 \tag{A.21}$$

$$\Big(\mathrm{Re}\{\phi_n(t)\} - \mathrm{Re}\{\phi_{-n}(t)\}\Big)\sin(k_n x) + \Big(\mathrm{Im}\{\phi_n(t)\} + \mathrm{Im}\{\phi_{-n}(t)\}\Big)\cos(k_n x) = 0 . \tag{A.22}$$

Since $\sin(k_n x)$ and $\cos(k_n x)$ are in general not equal to zero and k_n is fixed for each n, this gives the solution

$$\mathrm{Re}\{\phi_n(t)\} = \mathrm{Re}\{\phi_{-n}(t)\} \quad \text{and} \quad \mathrm{Im}\{\phi_n(t)\} = -\,\mathrm{Im}\{\phi_{-n}(t)\} \quad \Rightarrow \quad \boxed{\phi_{-n}(t) = \phi_n^*(t)} \tag{A.23}$$

The same argument can be used to also show this relation for $\rho(x,t)$. Checking if $\phi(x,t) \in \mathbb{R}$:

$$\phi(x,t) = \frac{1}{\sqrt{L}} \sum_{n=0}^{\infty} \mathrm{Re}\{\phi_n(t)\}\left[e^{ik_n x} + e^{-ik_n x}\right] - \frac{1}{i}\,\mathrm{Im}\{\phi_n(t)\}\left[e^{ik_n x} - e^{-ik_n x}\right] \tag{A.24}$$

$$\phi(x,t) = \frac{2}{\sqrt{L}} \sum_{n=0}^{\infty} \mathrm{Re}\{\phi_n(t)\}\cos(k_n x) - \mathrm{Im}\{\phi_n(t)\}\sin(k_n x) \ \in \mathbb{R} \qquad \text{q.e.d} \tag{A.25}$$

A.5.3 Derivation of the Commutators between $\rho(x)$ and $\Psi_e^{(\dagger)}$, $\Psi_{qp}^{(\dagger)}$

For a well behaved function $f(B)$ the following identity is used

$$[A, f(B)] = f'(B)[A,B] \quad \text{if} \quad [[A,B],B] = 0 . \tag{A.26}$$

Since the commutator $[\rho(x), \phi(x')]$ is just a number the above identity can be used to obtain for the annihilation operator of the quasi particle Ψ_{qp} and the electron Ψ_e

$$[\rho(x), \Psi_{qp}(x')] = [\rho(x), e^{i\phi(x')}] = i e^{i\phi(x')}[\rho(x), \phi(x')] = -\nu \Psi_{qp}\delta(x-x') \quad \text{and} \tag{A.27}$$

$$[\rho(x), \Psi_e(x')] = [\rho(x), e^{im\phi(x')}] = \frac{i}{\nu} e^{im\phi(x')}[\rho(x), \phi(x')] = -\Psi_e \delta(x-x') . \tag{A.28}$$

Similarly, it follows for the commutators of the charge density and the creation operators of quasi-particles and electrons

$$[\rho(x), \Psi_{qp}^\dagger(x')] = [\rho(x), e^{-i\phi(x')}] = \nu \Psi_{qp}^\dagger \delta(x-x') \quad \text{and} \tag{A.29}$$

$$[\rho(x), \Psi_e^\dagger(x')] = [\rho(x), e^{-im\phi(x')}] = \Psi_e^\dagger \delta(x-x') . \tag{A.30}$$

Thus the creation and annihilation operators of the quasi-particles and electrons produce the correct charge.

A.6 Second order Correction to the Heat Current

Starting from the definition of the corrections to the heat current and by using the statistical independence of the chiral fields $[(\dots)_+, (\dots)_-] = 0$, the commutator of interest for the first order correction becomes

$$[\Gamma_0 O_-(t') O_+(t'), J_{Q,-}^{(0)}(\tilde{t})] = -\frac{\hbar v_-^2 \Gamma_0}{2\pi}[T_-(\tilde{t}), O_-(t')] O_+(t') . \tag{A.31}$$

The following OPEs are used to further simplify this expression [83]

$$T(z)O(z') \sim \frac{h_O O(z')}{(z-z')^2} + \frac{\partial_{z'} O(z')}{z-z'} + \dots \quad \text{and} \tag{A.32}$$

$$O(z)T(z') \sim \frac{h_O O(z)}{(z-z')^2} - \frac{\partial_z O(z)}{z-z'} + \dots \ . \tag{A.33}$$

Going back from imaginary to real time by $z - z' \to \delta + iv_-(t_1 - t_2)$ and by using Eq. (A.2) [91], the commutator becomes

$$[T(t_1), O(t_2)] = -\frac{2\pi i}{v_-^2}\delta(t_1-t_2)\partial_{t_2}O_-(t_2) + \frac{2\pi i d_-}{v_-^2}\partial_{t_1}\delta(t_1-t_2)O_-(t_2) \ , \tag{A.34}$$

where d_- denotes the conformal dimension of the operator O_-. The first order correction to the heat current is thus described by

$$J_Q^{(1)}(t) = -i\frac{v_-^2\Gamma_0}{2\pi}\int_{-\infty}^{t} dt' \Big[\frac{2\pi i d_-}{v_-^2}\partial_{\tilde{t}}\delta(\tilde{t}-t')O_-(t') - \frac{2\pi i}{v_+^2}\delta(\tilde{t}-t')\partial_{t'}O_-(t')\Big]O_+(t') \quad \text{and} \tag{A.35}$$

$$J_Q^{(1)}(t) = \Gamma_0\int_{-\infty}^{t} dt' \Big[d_-\partial_{\tilde{t}}\delta(\tilde{t}-t')O_-(t')O_+(t') - \delta(\tilde{t}-t')\partial_{t'}O_-(t')O_+(t')\Big] \ . \tag{A.36}$$

Performing the integration gives with the identities defined in Eqs. (A.3) and (A.4)

$$J_Q^{(1)}(t) = \Gamma_0\Big(d_-\partial_{\tilde{t}}\big(O_-(\tilde{t})O_+(\tilde{t})\big) - \big(\partial_{\tilde{t}}O_-(\tilde{t})\big)O_+(\tilde{t})\Big) \ . \tag{A.37}$$

Since the operators of the + and - fields are statistically independent, one finds a vanishing average of the first order correction

$$\langle J_Q^{(1)}(t)\rangle = 0 \ . \tag{A.38}$$

The second order correction is obtained by following a similar way

$$J_Q^{(2)}(t) = i^2\Gamma_0^2\int_{-\infty}^{\tilde{t}} dt''\big[O_-(t'')O_+(t''), d_-\partial_{\tilde{t}}\big(O_-(\tilde{t})O_+(\tilde{t})\big) - \big(\partial_{\tilde{t}}O_-(\tilde{t})\big)O_+(\tilde{t})\big] \quad \text{and} \tag{A.39}$$

$$J_Q^{(2)}(t) = -\Gamma_0^2\int_{-\infty}^{\tilde{t}} dt''\big(d_-(1) - (2)\big) \ . \tag{A.40}$$

Evaluating the commutator, the contributions (1) and (2) are computed to become

$$(1) = O_-(t'')O_+(t'')\partial_{\tilde{t}}\big(O_-(\tilde{t})O_+(\tilde{t})\big) - \partial_{\tilde{t}}\big(O_-(\tilde{t})O_+(\tilde{t})\big)O_-(t'')O_+(t'') \quad \text{and} \tag{A.41}$$

$$(2) = \big(\partial_{\tilde{t}}O_-(\tilde{t})\big)O_+(\tilde{t})O_-(t'')O_+(t'') - O_-(t'')O_+(t'')\big(\partial_{\tilde{t}}O_-(\tilde{t})\big)O_+(\tilde{t}) \ . \tag{A.42}$$

Expanding the derivative $\partial_{\tilde{t}}\big(O_-(\tilde{t})O_+(\tilde{t})\big)$ and using the commutation relations to rearrange some terms, one finds

$$(1) = \Big[O_-(t'')\big(\partial_{\tilde{t}}O_-(\tilde{t})\big)O_+(t'')O_+(\tilde{t}) + O_-(t'')O_-(\tilde{t})O_+(t'')\big(\partial_{\tilde{t}}O_+(\tilde{t})\big) \tag{A.43}$$

$$- \big(\partial_{\tilde{t}}O_-(\tilde{t})\big)O_-(t'')O_+(\tilde{t})O_+(t'') - O_-(\tilde{t})O_-(t'')\big(\partial_{\tilde{t}}O_+(\tilde{t})\big)O_+(t'')\Big] \ . \tag{A.44}$$

introducing the time difference $\tau = t'' - \tilde{t}$ and the Green's functions $G_{+(-)}(\tau) = \langle O_{+(-)}(\tau)O_{+(-)}(0)\rangle$, the corresponding averages become

$$\Big\langle(1)\Big\rangle = -\Big[\big(\partial_\tau G_-(\tau)\big)G_+(\tau) + G_-(\tau)\big(\partial_\tau G_+(\tau)\big) - \big(\partial_\tau G_-(-\tau)\big)G_+(-\tau) - G_-(-\tau)\big(\partial_\tau G_+(-\tau)\big)\Big] \ . \tag{A.45}$$

Noting that $G_i(\tau) = G_i(-\tau)$ and $\partial_\tau G_i(\tau) = -\partial_\tau G_i(-\tau)$ with $i \in \{+,-\}$, the resulting expressions simplify to

$$\Big\langle(1)\Big\rangle = -2d_-\partial_\tau\big(G_-(\tau)G_+(\tau)\big) \qquad \Big\langle(2)\Big\rangle = -\big(\partial_\tau G_-(-\tau)\big)G_+(-\tau) + \big(\partial_\tau G_-(\tau)\big)G_+(\tau) \ . \tag{A.46}$$

Performing the integration, only the contribution of (2) gives a non-zero result. The integration of $\langle(2)\rangle$ can further be simplified by

$$\int_{-\infty}^{\tilde{t}} \Big\langle (2) \Big\rangle \, d\tau = \int_{-\infty}^{\tilde{t}} \big(\partial_\tau G_-(\tau)\big) G_+(\tau) \, d\tau - \int_{-\infty}^{\tilde{t}} \big(\big(\partial_{\tau'} G_-(-\tau')\big) G_+(-\tau') \, d\tau' \ . \tag{A.47}$$

Using a transformation of variables $\tau' \to -\tau'$ in the second term, it follows

$$\langle J_Q^{(2)}(t)\rangle = \frac{\Gamma_0^2}{\hbar} \int_{-\infty}^{\infty} \big(\partial_\tau G_-(\tau)\big) G_+(\tau) \, d\tau \ . \tag{A.48}$$

The so found relations are in agreement with [91].

A.7 Computation of the Interaction Heat Current

In order to compute the finite temperature Greens' functions of the modes, a conformal transformation onto the cylinder $z(w) = \exp\left(2\pi i w/(\hbar\beta_{+(-)} v_{+(-)})\right)$ is performed. The Greens' function for the derivatives of the bosonic left-moving fields can be obtained by noting that they are primary fields and transform as [83]

$$G_-(w_1, w_2) = \langle \partial_{w_1}\phi(w_1)\partial_{w_2}\phi(w_2)\rangle = \left(\frac{dw}{dz}\right)_{w_1}^{-d_-} \left(\frac{dw}{dz}\right)_{w_2}^{-d_-} \langle \partial_{z_1}\phi(z_1)\partial_{z_2}\phi(z_2)\rangle \ . \tag{A.49}$$

Introducing $\alpha_- = \frac{2\pi i}{\hbar\beta_- v_-}$ and thus $z(w) = \exp(\alpha_- w)$ and by using the operator product expansion for the bosonic case $\langle \partial_{z_1}\phi(z_1)\partial_{z_2}\phi(z_2)\rangle \sim -\frac{\nu}{(z_1-z_2)^2}$, it follows

$$G_-(w_1, w_2) = -\nu\alpha_-^{2d_-} \left(\frac{e^{\alpha_- w_1} - e^{\alpha_- w_2}}{e^{\frac{\alpha_- d_-}{2} w_1} e^{\frac{\alpha_- d_-}{2} w_2}}\right)^{-2} \overset{d_-=1}{=} -\nu\alpha_-^2 \left(e^{\frac{\alpha_-}{2}(w_1-w_2)} - e^{-\frac{\alpha_-}{2}(w_1-w_2)}\right)^{-2} \tag{A.50}$$

$$= -\nu \left(\frac{\alpha_-}{2}\right)^2 \left(\sinh\left(\frac{\alpha_-}{2}(w_1 - w_2)\right)\right)^{-2} \ . \tag{A.51}$$

Setting $w_1 - w_2 = -iv_-\tau$ and re-introducing the cut off b from the bosonization result, one obtains the following expression for the ϕ modes' Greens' function

$$G_-(\tau) = -\frac{\nu}{b^2} \left(\frac{\pi i b/(\hbar v_-\beta_-)}{\sinh(\pi i/(\hbar v_-\beta_-)(b - iv_-\tau))}\right)^2 = -\frac{\nu}{b^2} \left(\frac{\pi b/(\hbar v_-\beta_-)}{\sin(\pi/(\hbar v_-\beta_-)(b - iv_-\tau))}\right)^2 \ , \tag{A.52}$$

$$\partial_\tau G_-(\tau) = \frac{2}{b^2} \left(\frac{i\nu\pi}{\hbar\beta_-}\right) \cot\left(\frac{\pi(b - iv_-\tau)}{\hbar v_-\beta_-}\right) \left(\frac{\pi b/(\hbar v_-\beta_-)}{\sin(\pi/(\hbar v_-\beta_-)(b - iv_-\tau))}\right)^2 \ . \tag{A.53}$$

To obtain the Greens' function of the right moving Majorana mode $G_+(\tau)$, the conformal transformation of the energy momentum tensor T_+ has to be considered

$$T(w) = \left(\frac{dw}{dz}\right)^{-2} \left[T(z) - \frac{c}{12}\{w; z\}\right] \overset{[83]\ (5.131)}{=} \left(\frac{dw}{dz}\right)^{-2} T(z) + \frac{c}{12}\{z; w\} \ , \tag{A.54}$$

where $\{z; w\}$ denotes the Schwarzian derivative. Using $\langle T(z)\rangle_{\text{plane}} = 0$, the Greens' function are found by

$$G_+(w_1, w_2) = \langle T(w_1)T(w_2)\rangle = \left(\frac{dw}{dz}\right)_{w_1}^{-2} \left(\frac{dw}{dz}\right)_{w_2}^{-2} \langle T(z_1)T(z_2)\rangle + \frac{c^2}{144}\{z; w\}_{w_1}\{z; w\}_{w_2} \ . \tag{A.55}$$

The Schwarzian becomes for the given transformation of the + mode

$$\{z; w\} = \left(\frac{\partial^3 z}{\partial w^3}\right)\left(\frac{\partial z}{\partial w}\right)^{-1} - \frac{3}{2}\left(\frac{\partial^2 z}{\partial w^2}\right)^2 \left(\frac{\partial z}{\partial w}\right)^{-2} = \frac{2\pi^2}{\hbar^2 v_+^2 \beta_+^2} \ . \tag{A.56}$$

Therefore the Greens' function become with the OPE of $T(z_1)T(z_2) \sim \frac{c}{2}\frac{1}{(z_1-z_2)^4}$

$$G_+(w_1,w_2) = \frac{c}{2}\frac{16\pi^4}{\hbar^4 v_+^4 \beta_+^4}\frac{e^{\frac{4\pi i}{\hbar v_+\beta_+}(w_1+w_2)}}{(z_1-z_2)^4} + \frac{c^2}{36}\left(\frac{\pi}{\hbar v_+\beta_+}\right)^4 . \tag{A.57}$$

Setting $\alpha_+ = \frac{2\pi i}{\hbar v_+\beta_+}$ and using the given transformation of z

$$G_+(w_1,w_2) = \frac{c}{2}\alpha_+^4\frac{e^{2\alpha_+(w_1+w_2)}}{(e^{\alpha_+ w_1}-e^{\alpha_+ w_2})^4} + \frac{c^2}{36}\left(\frac{\alpha_+}{2}\right)^4 = \frac{c}{2}\alpha_+^4\left(\frac{e^{\alpha_+ w_1}-e^{\alpha_+ w_2}}{e^{\frac{\alpha_+}{2}(w_1+w_2)}}\right)^{-4} + \frac{c^2}{36}\left(\frac{\alpha_+}{2}\right)^4 \tag{A.58}$$

$$= \frac{c}{2}\alpha_+^4\left(e^{\frac{\alpha_+}{2}(w_1-w_2)} - e^{-\frac{\alpha_+}{2}(w_1-w_2)}\right)^{-4} + \frac{c^2}{36}\left(\frac{\alpha_+}{2}\right)^4 \tag{A.59}$$

$$= \frac{c}{2}\left(\frac{\alpha_+}{2}\right)^4 \sinh\left(\frac{\alpha_+}{2}(w_1-w_2)\right)^{-4} + \frac{c^2}{36}\left(\frac{\alpha_+}{2}\right)^4 . \tag{A.60}$$

Putting back in the expression for α_+ as well as introducing the cut off b and setting $w_1 - w_2 = -iv_+\tau$, the final result becomes

$$G_+(\tau) = \frac{c}{2b^2}\left(\frac{\pi b/(\hbar v_+\beta_+)}{\sin(\pi/(\hbar v_+\beta_+)(b-iv_+\tau))}\right)^4 + \frac{c^2}{36}\left(\frac{\pi}{\hbar v_+\beta_+}\right)^4 . \tag{A.61}$$

The Greens' functions can now be used to compute the second order correction to the heat current. A variable shift of the form $\tau \to \tau + i\frac{b}{v_-} - i\frac{\hbar\beta_-}{2}$ is introduced to rearrange some terms in the integral. This shift is allowed since it does not exclude any of the poles. The second order correction to the heat current becomes with $\pm\infty^* = \pm\infty + i\frac{b}{v_-} - i\frac{\hbar\beta_-}{2}$ [92]

$$\langle J_Q^{(2)}(t)\rangle = -\frac{\Gamma_0^2 b^2\pi^7 c\nu}{18\hbar^7 v_-^2 v_+^4\beta_-^3\beta_+^4}\int_{-\infty^*}^{\infty^*} f(\tau)\,d\tau , \tag{A.62}$$

where $f(\tau)$ is described by

$$f(\tau) = \operatorname{sech}^2\left(\frac{\pi\tau}{\hbar\beta_-}\right)\tanh\left(\frac{\pi\tau}{\hbar\beta_-}\right)\left(c + 18b^2\csc^4\left(\frac{\pi\left(b - \frac{bv_+}{v_-} - \frac{\hbar v_+\beta_-}{2} - iv_+\tau\right)}{\hbar v_+\beta_+}\right)\right) . \tag{A.63}$$

Expanding this expression for small b while keeping terms up to leading order removes the b dependence from the argument. The integral limits are further switched back to $\pm\infty$. In the following, the dependency on the small temperature bias is examined up to order $\mathcal{O}(\Delta T)$. The local temperatures are defined by the temperatures of the reservoirs the modes emanate from, leading to $T_+ = T + \frac{\Delta T}{2}$ and $T_- = T - \frac{\Delta T}{2}$. Performing the expansion and transforming back into real time $\tau \to it$ gives

$$\langle J_Q^{(2)}(t)\rangle = \frac{2\Gamma_0^2 k_B^7\pi^8 T^6 c\nu}{\hbar^8 v_-^2 v_+^4}\Delta T\int_{-\infty}^{\infty}\operatorname{sech}^6\left(\frac{\pi k_B T}{\hbar}t\right)\tanh^2\left(\frac{\pi k_B T}{\hbar}t\right)dt \tag{A.64}$$

$$= \frac{32b^2 k_B^6\pi^7\Gamma_0^2 c\nu}{105\hbar^7 v_-^2 v_+^4}T^5\Delta T . \tag{A.65}$$

Therefore the correction to the heat conductance (resembling the "interaction conductance") becomes with $c = 1/2$, $\nu = 1/2$

$$G_{int}^Q = \frac{d}{d\Delta T}\langle J_Q^{(2)}\rangle = \frac{8b^2 k_B^4\pi^5\Gamma_0^2}{35\hbar^6 v_-^2 v_+^4}T^4\kappa . \tag{A.66}$$

A.8 Computation of the Noise Kernel $\Lambda(x)$

The final result for the noise kernel $\Lambda(x)$ is computed starting from the definition of the local noise and charge tunneling conductance in Eq. (4.30) and (4.31). Using the substitution $\omega_V = \frac{e\Delta V(x)\tau}{\hbar}$

it follows

$$S^{loc}(x) = 4\int_{-\infty}^{\infty} \cos(\omega_V \tau)\, \langle \mathcal{T}(\tau,0)\mathcal{T}^\dagger(0,0)\rangle \, d\tau \quad \text{and} \tag{A.67}$$

$$g^{loc}(x) = 2i\int_{-\infty}^{\infty} \tau \langle \mathcal{T}(\tau,0)\mathcal{T}^\dagger(0,0)\rangle \, d\tau \ . \tag{A.68}$$

The correlation function of the tunneling operators becomes for the desired edge structure

$$\langle \mathcal{T}(\tau,0)\mathcal{T}^\dagger(0,0)\rangle = \langle \psi(\tau,0)\psi(0,0)\rangle \langle e^{\frac{i}{\nu_1}\phi_1(\tau,0)} e^{\frac{i}{\nu_1}\phi_1(0,0)}\rangle \langle e^{\frac{i}{\nu_2}\phi_2(\tau,0)} e^{\frac{i}{\nu_2}\phi_2(0,0)}\rangle \tag{A.69}$$

and thus in terms of the modes Greens' functions

$$\langle \mathcal{T}(\tau,0)\mathcal{T}^\dagger(0,0)\rangle = \frac{\Gamma_0^2}{(2\pi b)^2} G_\psi(\tau,0) G_{\phi_1}(\tau,0) G_{\phi_2}^2(\tau,0) \ . \tag{A.70}$$

The Greens' functions are obtained by the known identities for the correlators of bosons and fermions in CFT (to be correct G_ϕ is actually e^{G_ϕ}, if G_ϕ is the bare bosonic correlator).

$$G_\psi = G_{\phi_1} = G_{\phi_2} = G_i = \frac{\pi b k_B T_i}{\hbar v_i} \csc\left(\frac{\pi k_B T_i}{\hbar v_i}(b - i v_i \tau)\right) \tag{A.71}$$

Using the definitions of the finite temperature Greens' functions, the temperatures are adjusted to meet the assumptions of the considered cases where $\alpha = l_{12}/L$ and $\beta = l_{23}/L$

case	assumptions	
(i)	$\alpha, \beta \ll 1$	$T_1(x) = T_2(x) = T_3(x)$
(ii)	$\alpha \ll \beta < 1$	$T_1(x) = T_2(x) = \kappa(x) T_3(x)$
	$1 > \alpha \gg \beta$	$T_1(x) = \kappa(x) T_2(x) = \kappa(x) T_3(x)$
(iii)	$\alpha, \beta \to \infty$	$T_1(x) = T_3(x) = 0$ and $T_2(x) = \sqrt{\frac{3}{\pi^2}}\frac{eV_0}{k_B}$

(A.72)

The correlator of interest is thus defined by different combinations of the modes' temperatures. Whenever temperatures are set to zero, the corresponding zero temperature Greens' function has been used. Depending on the given "reference temperature", the trick from the heat current computation is used once again. Assuming that everything is expressed in terms of T_1, the integrals for S^{loc} and g^{loc} are modified by introducing the shift $\{\tau' = \frac{\hbar\beta}{\pi}\tau - i\frac{\hbar}{k_B T_1} + i\frac{b}{v_1}\}$. Under the condition $\hbar v_1 \beta_1 > b$, there is no pole included in the contour and the integral boundaries can be switched back to $\pm\infty$ in both cases

$$\frac{\Gamma_0^2}{(2\pi b)^2}\int_{-\infty}^{\infty} f(\tau') G_\psi(\tau',0) G_{\phi_1}(\tau',0) G_{\phi_2}^2(\tau',0)\, d\tau \ , \tag{A.73}$$

where $f(\tau') \in \{\cos(\omega_V \tau'), \tau'\}$ for S^{loc} and g^{loc} respectively. The integrand is then expanded to leading order in the cut off b ($\mathcal{O}(b^2)$) for both expressions. In case of S^{loc}, it is further expanded for small applied voltage biases. For **(ii)**, the expressions are expanded around $\kappa = 1$ up to first order in κ additionally. Having done all these steps the final result is readily obtained for **(i)** and **(ii)**. For **(iii)** the noise kernel evaluates to ($\tau' \to \tau$)

$$\Lambda(x) = 2k_B T_2 \frac{\int_{-\infty}^{\infty} \frac{(\pi^2 - 4\tau^2)\mathrm{sech}^2(\tau)}{(\pi^2+4\tau^2)^2}\, d\tau}{\int_{-\infty}^{\infty} \frac{\mathrm{sech}^2(\tau)}{\pi^2+4\tau^2}\, d\tau} \ , \tag{A.74}$$

with the expressions of interest

$$S^{loc} = S_0 \int_{-\infty}^{\infty} \frac{(\pi^2 - 4\tau^2)}{(\pi^2+4\tau^2)^2 \cosh^2(\tau)}\, d\tau \quad \text{and} \quad g^{loc} = g_0 \int_{-\infty}^{\infty} \frac{1}{(\pi^2+4\tau^2)\cosh^2(\tau)}\, d\tau \ , \tag{A.75}$$

where S_0 and g_0 are constants that absorb the prefactors. Noting that $1/\cosh^2(\tau)$ is a meromorphic function with an infinite set of poles $\pm(2k+1)\frac{i\pi}{2}$, $k \in \mathbb{Z}_{\geq 0}$, it is rewritten using the *Mittag-Leffler's* theorem

$$\frac{1}{\cosh^2(\tau)} = -\sum_{k=0}^{\infty}\left[\frac{1}{\left(\tau - (2k+1)\frac{i\pi}{2}\right)^2} + \frac{1}{\left(\tau + (2k+1)\frac{i\pi}{2}\right)^2}\right] \ . \tag{A.76}$$

With this expression, the integrals for the two expressions of interest can be identified with the following integrals:

$$g^{loc}: \quad -\int_{\mathbb{R}} \frac{d\tau}{(\tau \pm z)^2(4\tau^2+\pi^2)}\, d\tau = \frac{2}{(\pi - 2iz)^2} \quad \text{and} \tag{A.77}$$

$$S^{loc}: \quad -\int_{\mathbb{R}} \frac{(\pi^2-4\tau^2)}{(\tau \pm z)^2(4\tau^2+\pi^2)}\, d\tau = \frac{4\pi}{(\pi - 2iz)^3}\ . \tag{A.78}$$

Identifying the similarity between z in Eqs. (A.77) and (A.78) and $(2k+1)\frac{i\pi}{2}$ in Eq. (A.76), by using the *Fubini-Tonelli* theorem to reverse the order of integration and summation and by inserting the series description of $\frac{1}{\cosh^2(\tau)}$, the solutions to the integrals become

$$g^{loc} = \frac{g_0}{\pi^2}\sum_{k=0}^{\infty}\frac{1}{(k+1)^2} = \frac{g_0}{\pi^2}\sum_{k=1}^{\infty}\frac{1}{k^2} = \frac{\zeta(2)}{\pi^2}g_0 = \frac{g_0}{6} \quad \text{and} \tag{A.79}$$

$$S^{loc} = \frac{S_0}{\pi^2}\sum_{k=1}^{\infty}\frac{1}{k^3} = \frac{\zeta(3)}{\pi^2}S_0 \approx 0.121794 S_0\ . \tag{A.80}$$

Recovering the prefactors S_0 and g_0, the noise kernel $\Lambda(x)$ is given by

$$\Lambda(x) = \frac{S^{loc}}{2g^{loc}} = \frac{12 k_B T_2 \zeta(3)}{\pi^2} = \sqrt{\frac{6}{5}}\frac{6eV_0\zeta(3)}{\pi^3}\ . \tag{A.81}$$

Under the assumption of very efficient charge equilibration ($L \gg l_{eq}^C$), the corresponding excess noise is computed as before by evaluating

$$S^{exc} = \lim_{L\gg l_{eq}^C}\left(\frac{4\nu_1\nu_2(\nu_1-\nu_2)}{l_{eq}^C\left(\nu_1-\nu_2 e^{-\frac{2L}{l_{eq}^C}}\right)^2}\int_0^L \Lambda(x) e^{-\frac{4x}{l_{eq}^C}}\, dx\right)\ . \tag{A.82}$$

The resulting expression for the excess noise $S_{V_0}^{exc}$ is given in units e^3V_0/h. Using the current-voltage relation

$$I_0 = GV_0\frac{e^2}{h} \quad \text{leads to} \quad S_{I_0}^{exc} = \frac{S_{V_0}^{exc}}{V_0}\frac{I_0}{G}\frac{h}{e^2}\ . \tag{A.83}$$

In case of the interface phPf-3, $G \overset{L\gg l_{eq}^C}{\longrightarrow} 1/2$. To connect to units used in [32] , $e \to 1.602\cdot 10^{-19} As$, $h \to 6.626\cdot 10^{-34} Js$ and $V_0 \to 10^{-6} V_{0,exp}$ are inserted in the noise expression instead. The noise is then given in units $10^{-30}A^2/(\mu V Hz)$.

A.9 HeatCond Module for Mathematica

This Module has been written to compute the two terminal heat conductance of edge structures for an applied temperature bias of ΔT with pairwise interactions between the involved modes. It converts inputs of the channels' chirality, heat conductance and specified pairwise equilibration lengths into the corresponding two terminal heat conductance. The given matrix M_T, is diagonalized by its eigenvalues λ_i and and eigenvectors $\vec{v}_i$ by

$$M_T = PDP^{-1}\ , \quad D = \mathrm{diag}(\{\lambda_i\}) \quad \text{and} \quad P = (\{\vec{v}_i\})^T\ . \tag{A.84}$$

The heat transport equation thus becomes

$$\partial_x\vec{T}(x) = M_T\vec{T}(x) = PDP^{-1}\vec{T}(x) \quad \Rightarrow \quad \partial_x P^{-1}\vec{T}(x) = DP^{-1}\vec{T}(x)\ . \tag{A.85}$$

Introducing a new temperature $\vec{T'}(x) = P^{-1}\vec{T}(x)$, the system takes the diagonal form

$$\partial_x\vec{T'}(x) = D\vec{T'}(x) \tag{A.86}$$

and is solved for the missing boundary conditions using standard methods. The final result is obtained by resubsting $\vec{T}(x)$. It becomes

$$\vec{T'}(L) = e^{DL}\vec{T'}(0) \quad \Rightarrow \quad \boxed{\vec{T}(L) = Pe^{DL}P^{-1}\vec{T}(0)}\ . \tag{A.87}$$

The code is attached in the electronic version of this thesis (https://odr.chalmers.se/).

A.10 Color-map of G^Q_{2t} for the intermediate phPf-3

Modelling the *hotspot* by heated contacts allows to compute (and measure) heat conductance and noise in the same setup. The thermal conductance G^Q_{2t} corresponding to an applied ΔT is visualized in the color-map below. It depends on the degree of equilibration between pairs of channels, defined by $\alpha = l_{12}/L$ and $\beta = l_{23}/L$. It follows in the corresponding limits:

1. Full thermal equilibration between channel one and two as well as between channel two and three
$$G^Q_{2t} \to 1/2\ \kappa \qquad \text{for} \quad \alpha \to 0 \qquad \text{and} \quad \beta \to 0$$
2. Absent thermal equilibration between channel one and two and full thermal equilibration between channel two and three
$$G^Q_{2t} \to 3/2\ \kappa \qquad \text{for} \quad \alpha \to \infty \qquad \text{and} \quad \beta \to 0$$
3. Absent thermal equilibration between channel one and two as well as between channel two and three
$$G^Q_{2t} \to 5/2\ \kappa \qquad \text{for} \quad \alpha \to \infty \qquad \text{and} \quad \beta \to \infty$$

In the limit $\alpha \to 0$ and $\beta \to \infty$, it can furthermore be seen that the equilibration between channel two and three ($\simeq \beta$) plays a minor role compared to the equilibration between channels one and two ($\simeq \alpha$).

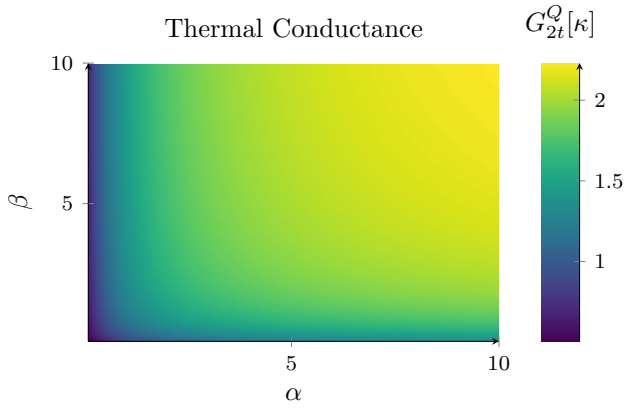

Figure A.1: Visualization of the thermal conductance G^Q_{2t} of the intermediate phPf-3 edge depending on α and β in the range $0 \leq \alpha, \beta \leq 10$.

DEPARTMENT OF MICRO AND NANOTECHNOLOGY
CHALMERS UNIVERSITY OF TECHNOLOGY
Gothenburg, Sweden
www.chalmers.se

CHALMERS
UNIVERSITY OF TECHNOLOGY